The Effect of an alkyl chain and β-diketonato-metal moiety on the photochromic behaviour of azobenzene compounds as materials for solar thermal fuels.

A dissertation submitted in partial fulfilment of the requirements for the degree of

Master of Science (Chemistry)

By

Witness Londi Bokhe

BSc Hons (Rhodes University)

Supervised by Dr N.F Molefe

Abstract

Scientists have been studying the development of renewable energy technologies in detail to create a sustainable energy supply. Among many new advanced material classes being researched recently are photo functional and photo responsive materials. These classes include azobenzene derivatives which are characterized by azo linkage (N=N) sandwiched by two phenyl rings. The *trans-to-cis* isomerization of azobenzene is a highly efficient and reversible process, making it an ideal candidate for solar thermal energy storage.

This research investigates the impact of alkyl chain modifications and the incorporation of a β-diketonato-copper(II) complex on azobenzene derivatives, aiming to optimize their performance as efficient components in solar thermal fuel cells (STFs). The study focuses on a comprehensive analysis of these materials' ability to capture, convert, store, and release solar energy for enhanced sustainability in renewable energy applications.

Experimental methodologies include synthesis of azobenzene derivatives with varying alkyl chain length, n (where n =8 & 10) and coordination of these compounds with a β-diketonato-copper(II) complex. Standard analytical techniques such as Nuclear Magnetic Resonance (^{1}H and ^{13}C NMR), Fourier Transform Infrared Spectroscopy (FTIR) and Ultraviolet/visible spectroscopy (UV/vis) were employed for chemical analysis of the synthesized material. Differential Scanning Calorimetry (DSC), Thermogravimetric Analysis (TGA), and Polarised Optical Microscope (POM) were used to study the thermal properties and morphology.

The photostationery states were determined using NMR spectroscopy and the kinetic parameters of the *cis-to-trans* relaxation process determined by a UV spectroscopy study. The *cis-to-trans* isomerisation had a longer half-life than the *trans-to-cis* isomerisation. The band gap of the isomers is within the range of semiconducting inorganic materials. DSC and POM thermograms showed that the compounds are liquid crystalline.

Finally, the study reports that the synthesised azobenzene derivatives show potential as material for solar thermal fuel cells because of their photo-isomerization ability. Furthermore, the synthesised compounds contribute to the advancement of sustainable and efficient solar energy utilization technologies, addressing the growing demand for clean energy solutions in the face of global environmental challenges. Because solar energy may be stored and used without causing direct emissions or pollution, they are considered clean energy. If solar thermal fuels

fulfil sustainability standards, they may qualify as green energy. This entails minimising adverse effects on the environment, using non-toxic chemicals and procedures.

Dedications

I am dedicating this dissertation to the following beloved people who have meant and continue to mean so much to me.

My mom, Kholofelo Mashigo and my father Lymon Bokhe.

My siblings, Lerato Bokhe and Nqobile Bokhe.

My grandmother, Dorah Manyike-Mashigo, although she is no longer of this world, her memories continue to regulate my life.

Acknowledgements

I want to acknowledge the support from all the beautiful people who made the completion of this work a success.

I would like to express my sincere gratitude to the following:

Dr Mpondi Molefe, my supervisor, without her thorough and supportive guidance, this work would not have been possible;

The Rhodes University Henderson scholarship for the financial support throughout my studies;

Dr Kabelo "KB" Ramollo for mentoring me and her thoughtful advice throughout my studies;

Professor RB Walker for allowing me to use his DSC instrument;

Professor Steffen Buttner for giving me access to use his polarizing microscope;

Professor John Mack for coaching me through TD-DFT calculations;

Professor Rosa Klein for her guidance and support throughout my studies;

Dr Baa Ebenezer for mentoring me and his thoughtful advice throughout my studies;

The Chemistry Department at Rhodes University; and the S3 and S4 lab members for being good collaborators;

My mother, Kholofelo Mashigo and my father, Lymon Bokhe for always being my cheerleaders and always believing in me;

My siblings: Lerato Bokhe, Nqobile Bokhe and Tshegofatso Mashigo;

My best friend: Kaisano "KG" Tauyakhale, for always being there for me making sure that throughout this journey, I'm still sane.

My unconditional friends: Bonani Vinindwa, Bongeka Ndwandwe, Urbain Ndagano, Kamogelo Mafokwane, Tsebang Matlapeng, and Bongeka Mgwengwe.

My mentor, Hlengiwe Zulu for helping me balance school and social life and being a shoulder to lean on.

Lastly, I give thanks to ALMIGHTY GOD, without whom the completion of this study would have been impossible. For his mercies, protection, provisions, sustenance, good health, and favour, I am highly grateful.

Table of Contents

Abstract ..... **ii**

Dedications ..... **iv**

Acknowledgements ..... **v**

List of figures ..... **ix**

List of Schemes ..... **xi**

List of tables ..... **xii**

List of abbreviations ..... **xiii**

Chapter 1: Introduction and aims of study. **1**

1.1 Introduction 1
1.2 Aim and Objectives 3
1.3 References 4

Chapter 2: Literature review **6**

2.1 Solar Thermal Fuels 6
2.1.1 Mechanism for Azobenzene (AZ) *trans-cis* Isomerization 7
2.1.2 Azobenzene – Based Solar Thermal Fuels 8
2.1.3 Azobenzene Derivatives as Materials for STFs. 10
2.1.4 Liquid Crystalline Azobenzene as Materials for STFs. 11
2.1.5 Synthesis of Azobenzene 17
2.2 Metallomesogens 18
2.4 References 20

Chapter 3: Synthesis, characterization, and photochemical studies **26**

3.1 Synthesis and characterization 26

3.1.1 Synthesis and characterisation of Ethyl (*E*)-4-((4-(alkyloxy) phenyl) diazenyl) benzoate……26

3.1.2 Synthesis and characterization of 2,4-dioxopentan-3-yl (*E*)-4-((4-(alkyloxy) phenyl) diazenyl) benzoate 29

3.1.3 Synthesis of *para*-substituted β-diketonato-Cu (II) complex..... 32

3.2 Photochromic Characterization 34

3.2.1 UV-Vis isomerization 36

3.2.2 Kinetic parameters for the trans-cis isomerization..... 41

3.2.3 Tauc plots and TD-DFT calculations..... 44

3.3 References 50

Chapter 4: Thermal properties and liquid crystals studies 53

4.3 Thermal stability by Thermogravimetric analysis (TGA)..... 53

4.2 Thermal analysis by DSC and POM 55

4.2.1 Alkyl chains compounds..... 55

4.2.2 β-diketonato-compounds..... 59

4.2.3 β-diketonato-Copper (II) complexes..... 63

4.3 References 67

Chapter 5: Experimental..... 70

5.1 Material 70

5. 2 Techniques and apparatus 70

5.2.1 Fourier Transform Infrared (FT-IR) spectroscopy..... 70

5.2.2 Nuclear Magnetic Resonance (NMR) spectroscopy 70

5.2.3 Mass Spectrometry..... 70

5.2.4 UV – Visible Spectroscopy..... 70

5.2.5 TD – DFT calculations..... 71

5.2.6 Thermogravimetric analysis..... 71

5.2.7 Melting point (M.p) and liquid crystals studies 71

5.3 Synthesis and Identification of all compounds.....71
5.3.1 Synthesis of ethyl (*trans*)-4-((4-hydroxyphenyl) diazenyl) benzoate.....72
5.3.2 Synthesis of Ethyl (*trans*)-4-((4-(alykloxy) phenyl) diazenyl) benzoate.....72
5.3.3 Synthesis of (*trans*)-4-((4-(alkyloxy) phenyl) diazenyl) benzoic acid.....73
5.3.4 Synthesis of 2,4-dioxopentan-3-yl (*E*)-4-((4-(alkyloxy) phenyl) diazenyl) benzoate.....74
5.3.5 Synthesis of *para*-substituted β-Cu (II).....76
5.4 References.....77

Chapter 6: Conclusion.....78

Appendix.....81

List of figures

Figure 1.1: Emerging technologies for capturing, converting, and storing solar energy.[6] (a) photovoltaics – credit: sunenergy1, available at: https://www.sunenergy1.com/ (date accessed: 27/12/2023) (b) artificial photosynthesis - Reprinted (adapted) with permission from RhightsLink, Copyright (2019) American Chemical Society. And (c) Solar thermal fuels - Licenses granted by RhightsLink, Copyright (2018) Royal Society of Chemistry. 3

Figure 2.1: different molecular photoswitches.[9] 7

Figure 2.2: Proposed mechanisms for the *trans* to *cis* isomerization of azobenzene[13] 8

Figure 2.3: A schematic depiction mechanism of the solar thermal conversion and storage method for azobenzene. The normal storage enthalpy of trans-to-cis isomerization is ΔH storage, while the energy barrier from *cis-to-trans* reversion is ΔEa.[20] 10

Figure 2.4: classification of liquid crystals.[27] 12

Figure 2.5: Calamitic liquid crystals classifications.[35] 13

Figure 2.6: A DSC schematic representation of a typical complex with liquid crystalline properties.[42] 14

Figure 2.7: A typical picture of a polarized microscopy showing the polarizer configuration (left) and alignment (right).[46] 15

Figure 2.8: different types of liquid crystals texture, pattern and packing arrangement visualised through polarized optical microscopy.[49] 16

Figure 2.9: Copper-containing beta-substituted metallomesogens.[62] 19

Figure 3.1: FTIR spectra of Ethyl (E)-4-((4-(alkyloxy) phenyl) diazenyl) benzoate. 27

Figure 3.2: ^{1}H NMR spectrum of Ethyl (E)-4-((4-(octyloxy) phenyl) diazenyl) benzoate . ..28

Figure 3.3: FTIR spectra of 2,4-dioxopentan-3-yl (E)-4-((4-(octyloxy) phenyl) diazenyl) benzoate 30

Figure 3.4: (a) ^{1}H and (b) ^{13}C NMR spectra of2,4-dioxopentan-3-yl (E)-4-((4-(alkyloxy) phenyl) diazenyl) benzoate. 31

Figure 3.5: ^{1}H NMR spectra of *para*-substituted β-diketonato-Cu (II) complex, compound 6a**.** 33

Figure 3.6: Mass spectrum of *para*-substituted β-diketonato-Cu (II) complex, compound 6a. 34

Figure 3.7: UV/Vis spectra of compound 3a in chloroform @365 nm (6W). 36

Figure 3.8: (a) Structures of the compound 3, 5 &6. (b) UV-Vis spectra of all synthesized compounds dissolved in $CHCl_3$. 37

Figure 3.9: ^{1}H NMR spectra of compound **3a** in $CHCl_3$-d, before irradiation (bottom spectra) *trans*-isomer and after 10 mins irradiation at 365 nm (top spectra) mixture of *trans*-and-*cis* isomers with the *cis* peaks shown by the black arrow. 38

Figure 4.1: Compounds **3a** (red), **5a** (green) and **6a** (purple) showing thermal decomposition. 54
Figure 4.2: Thermal degradation (TGA) of compound **3a**, **5a** and **6a** between 30 °C–900 °C at 10 °C per minute under nitrogen atmosphere. 55
Figure 4.3: DSC thermogram showing phase transitions and enthalpy stored in each peak of (A) compound **3a** and (B) compound **3b** (10 °C.min^{-1}). 57
Figure 4.4: POM textures of compound **3a**: while heating, (A) below 100 °C, Crystal; (B) between 100 °C to 110 °C, smectic A phase; and (C) after 110 °C, isotropic liquid; and when cooling (D) above 105 °C, isotropic liquid; (E) between 100 °C and 64 °C, nematic phase; and (F) below 64 °C, Crystal (10X magnification). 58
Figure 4.5: DSC thermogram showing phase transitions and enthalpy stored in each peak of compound **5a** (10 °C.min^{-1}). 60
Figure 4.6: DSC thermogram showing phase transitions and enthalpy stored in each peak of compound **5b** (10 °C.min^{-1}). 61
Figure 4.7: POM textures of compound **5b**: while cooling, (a) after 140 °C, Crystal; (b) between 110 °C to 135 °C, a mixture of smectic A and a nematic phase; and (c) below 80 °C, nematic phase (50X magnification). 62
Figure 4.8: DSC thermogram showing phase transitions and enthalpy stored in each peak of compound **6a** (10 °C.min^{-1}). 63
Figure 4. 9: POM textures of compound **6a**: while cooling, (A) below 49.07 °C, crystal solid phase and (B) above 79.77 °C, a mixture of smectic A and a nematic phase (50X magnification). 64
Figure 4.10: DSC thermogram showing phase transitions and enthalpy stored in each peak of compound **6b** (10 °C.min^{-1}). 65
Figure 4. 11: POM textures of compound **6b**: while cooling, (A) below 70.01 °C, crystal solid phase, (B) above 79.77 °C nematic droplets and (C) At 85.77 °C, an isotropic liquid was observed (50X magnification). 65

List of Schemes

Scheme 2.1: A scheme illustrating the synthesis of compound 1-3 by varying the aryl groups.[53] 17

Scheme 3.3: Synthesis of Ethyl (E)-4-((4-(alkyloxy) phenyl) diazenyl) benzoate .[2].....26

Scheme 3.4: synthesis of 2,4-dioxopentan-3-yl (E)-4-((4-(alkyloxy) phenyl) diazenyl) benzoate.[3,4].....29

Scheme 3.5: Synthesis of *para* substituted β-diketonato Cu (II) complexes.[5].....32

List of tables

Table 3.1: Calculation of the trans and cis isomer content from integration (%) after being exposed to UV light (365 nm) for 10 mins.....40
Table 3.2: *trans* and *cis* content (%) after UV irradiation from ^{1}H NMR integrals.....41
Table 3.3: *Trans-cis* (forward) and *cis-trans* (reverse) conversion rate constant (K_{obs} in s^{-1}) and half-life and the activation energy (ΔE_a in $J.mol^{-1}$) of all synthesized compounds.....43
Table 3.4: Band gap energies obtained by experimentally by Tauc plots for the synthesised compounds.....48

Table 4.1: Summary of compound **3a** and **3b** phase transitions and peak enthalpy and energy density from DSC and POM at 10 °C min^{-1}.....59
Table 4.2: Summary of compound **5a** and **5b** phase transitions and peak enthalpy and energy density from DSC (for the first cycle) and POM at 10 °C min^{-1}.....62
Table 4.3: Summary of compound **6a** and **6b** phase transitions and peak enthalpy and energy density from DSC (for the second cycle for 6a) and POM at 10 °C min^{-1}.....66

List of abbreviations

amu	Atomic mass unit
AZ	Azobenzene
β	Beta
C	Carbon
$CHCl_3$ / $CDCl_3$	Chloroform / deuterated chloroform
C=C	Alkene
CO_2	Carbon dioxide
cm	centimetre
CNT	Carbon nanotubes
CNNC	Carbon-nitrogen-nitrogen-carbon
CLCs	Cholesteric liquid crystals
Cr	crystal
CuO	Cupric oxide
Cu_2O	Cuprous oxide
$CuCl_2.2H_2O$	copper(II) chloride dihydrate
°C	Degrees Celsius
d	Doublet
dd	Doublet of doublet
DMSO	Dimethyl sulfoxide
DNA	Deoxyribonucleic acid
DSC	Differential Scanning Calorimetry
E	*Cis* isomer
ΔEa	Activation energy
ED	Energy density
Eg	Band gap energy
EJ	Exajoule
EtOH	Ethanol
eV	Electron volts
FTIR	Fourier transform infrared
γ	Gamma
ΔH	Enthalpy

Hg	Mercury
Hacac	Acetyl acetone
H	proton
h	Planck's constant
HOMO	Highest Occupied Molecular Orbital
HCL	Hydrochloric acid
Hz	Hertz
I	Isotropic liquid
J	Joule
J/mol	Joule per mole
J/g	Joule Per Gram
K_b	Rate constant
KJ/mol	kilojoules per mole
Kg/mol	kilogram per mole
KI	Potassium iodide
KOH	Potassium hydroxide
K_2CO_3	Potassium carbonate
LCs	Liquid crystals
LUMO	Lowest unoccupied molecular orbital
M	Molarity
m	Mass
mL	Millilitre
MHz	megahertz
m/z	Mass-charge ratio
mJ/s	Megajoule per second
mW	Milliwatt
Min	Minutes
MO	Molecular orbitals
M.P	Melting points
MS	Mass Spectrometry
$MgSO_4$	Magnesium sulfate
N	Nematic
$NaNO_2$	Sodium nitrite

N=N	Azo bond
NBD	Norbornadiene
nm	nanometre
NMR	Nuclear magnetic resonance
O	Oxygen
π	pi
%	Percentage
PCLT	photochemical crystal-liquid transition
POM	Polarizing Optical Microscopy
PV	Photovoltaic
ppm	Parts per million
QC	Quadricyclane
q	Heat
R	Gas constant
S	Seconds
Sm	Smectic
STFs	Solar thermal fuels
T	Temperature
t	Time
$t_{1/2}$	Half-time
TEA	Triethanolamine
Tg	Glass transition
TGA	Thermogravimetric analysis
THF	Tetrahydrofuran
UV/Vis	Ultraviolet–visible spectroscopy
λ	Wavelength
W	Watt
W h/Kg	Watt hour / kilogram
Z	*trans* isomer

Chapter 1: Introduction and aims of study.

1.1 Introduction

The world's population is increasing significantly, which leads to the high demand in energy.[1] The energy resources are depleting fast to meet the growing population's energy needs. For instance, the energy crisis in South Africa is the result of a complex interplay of aging infrastructure, financial mismanagement, corruption, policy challenges, and an over-reliance on coal. South Africa's heavy reliance on coal for electricity generation makes it vulnerable to supply issues and environmental regulations.[2,3] However, environmental problems such as acid rain, global warming, air pollution and climate change are a result of burning fossil fuels.[4,5]

Development of renewable and sustainable energy technologies is currently the main driving force in meeting the required energy demand of the world's population.[1,6] Sustainable energy can be provided by renewable energy sources such as biomass, wind, sun, hydropower, and geothermal energy.[7] The most rich and limitless of these is the sun, which has been used to advance innovative technologies that can capture, store, and convert solar energy.[6–8] According to literature, the sun sends approximately 430 exajoules (EJ), of energy to the earth per hour.[9] This figure is equivalent to the estimated annual world energy consumption of 583.9 EJ, which indicates that a significant quantity of energy may be captured if appropriate conversion and storage technologies can be created.[10]

Effective solar energy harvesting is severely hindered by the uneven and seasonal nature of sun exposure around the world.[11] The unpredictability of sunshine demands the creation of effective systems for capturing, storing, and converting it into energy to provide a steady and dependable energy source. [11,12]A good illustration of this problem is to contrast Africa, which experiences more sunlight, with Europe, which experiences harsh winters and fewer summer days.[11,13] Several European countries, including Sweden, Norway, and Finland, have long winter solstice leading to longer nights and shorter days. The lowered solar irradiation and shorter daylight hours make it difficult to produce electricity continuously. This seasonality emphasises the need for technology that can store solar energy during times of abundance, turn it into useable energy when needed, and capture solar energy when it's accessible. [11,13]In contrast, In contrast, several African nations, including those in South Africa and equatorial countries (such as Ethiopia, Republic of Congo, and Kenya etc.), enjoy year-round access to plenty of sunlight. Even with this benefit, there are still seasonal especially during spring and summer (September to February) with the highest solar irradiance and daily changes in the

amount of sunlight received, necessitating the use of efficient energy conversion and storage technology to ensure a steady supply of energy.[11,13] Even in areas with comparatively constant sunlight, the need for reliable solar energy storage technologies is critical because energy use can vary or peak at specific periods. [11,12,14] To combat the irregular sun exposure in these areas, energy storage technologies need to be implemented. Photovoltaics (PV), artificial photosynthesis, and solar thermal fuels (STFs) are the main examples of innovative technologies that yield abundant solar energy necessary for a sustainable world.[6] These processes directly convert solar heat into energy. Photovoltaic (PV) conversion is the direct conversion of sunlight into electricity without any heat engine (**Figure 1.1a**). PV is problematic in that it requires different materials for photon collection, photon conversion to electrons, and storage of those electrons in an external battery.[15] Artificial photosynthesis in **Figure 1.1b** imitates natural photosynthesis, but it includes a bed reactor enzyme which fix CO_2. Hydrogen gas is used to fuel this bed reactor.[16,17] However, artificial photosynthesis has major drawbacks as hydrogen production emits greenhouse gas which leads to climate change.[17]

Solar thermal fuels (STFs) on the other hand uses chemical bonds as photoactive materials to collect, convert, store and releases energy (**Figure 1.1c**).[18] By storing solar energy for eventual conversion during hours of maximum sunlight, these materials offer a way around the geographical restrictions on solar exposure.[19] Although azobenzene derivatives exhibit enormous potential for use as solar thermal fuels (STFs), one significant obstacle is the lack of an ideal STF that satisfies every requirement for peak performance.[20] Even though the current azobenzene-based materials have favourable photoisomerization properties, they frequently lack some essential components that are required for effective solar energy absorption, storage, and release.[21,22] The lack of understanding in this area provides strong support for the need for more research. Tackling the issues with azobenzene-based STFs is critical to the advancement of the field and the development of effective solar energy technologies as efforts around the world increase to shift to sustainable and renewable energy sources.

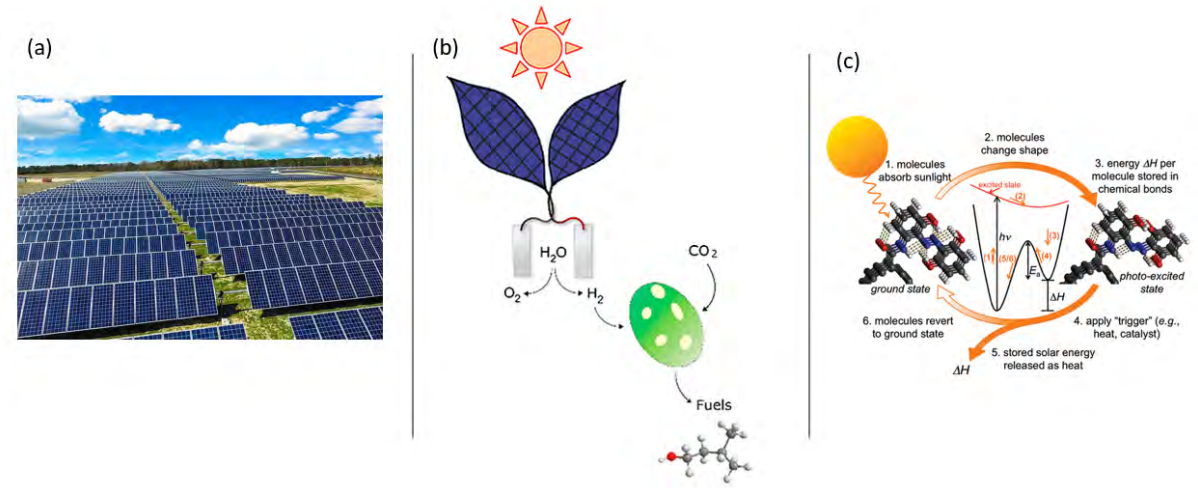

Figure 1.1: Emerging technologies for capturing, converting, and storing solar energy.[6] (a) photovoltaics – credit: sunenergy1, available at: https://www.sunenergy1.com/ (date accessed: 27/12/2023) (b) artificial photosynthesis - Reprinted (adapted) with permission from RhightsLink, Copyright (2019) American Chemical Society. And (c) Solar thermal fuels - Licenses granted by RhightsLink, Copyright (2018) Royal Society of Chemistry.

1.2 Aim and Objectives

The aim of this work was to synthesise and characterise liquid crystalline azobenzene derivatives with alkyl chain length (n) where n=8 and 10, coordinated with a β-diketonato-copper(II) metal as efficient solar thermal fuel cells that can capture, convert, store, and release solar energy.

Objectives are as follows:

- Synthesis of Liquid crystalline Azobenzene with various alkyl length chains where n = 8 & 10. varying the chain length for different liquid crystals properties
- Addition of a beta-diketone & coordinating a metal (Copper (II))
- Confirm structures using NMR and IR spectroscopy.
- Photochromic effect using ultraviolet-visible spectrometry.
- Determine phase transition of liquid crystals using polarizing optical microscopy (POM)
- Measure solar thermal energy storage using Differential Scanning Calorimeter (DSC)
- Calculate Energy storage half-life and energy density (ED).

1.3 References

1. Kannan, N. & Vakeesan, D. Solar energy for future world: - A review. *Renewable and Sustainable Energy Reviews* vol. 62 1092–1105 Preprint at https://doi.org/10.1016/j.rser.2016.05.022 (2016).
2. Spracklen, T. South Africa's energy crisis: Sustainable solutions. *Transactions of the Royal Society of South Africa* **62**, 38–40 (2007).
3. Lawrence, A. Energy decentralization in South Africa: Why past failure points to future success. *Renewable and Sustainable Energy Reviews* **120**, (2020).
4. Sampaio, P. G. V. & González, M. O. A. Photovoltaic solar energy: Conceptual framework. *Renewable and Sustainable Energy Reviews* vol. 74 590–601 Preprint at https://doi.org/10.1016/j.rser.2017.02.081 (2017).
5. Peng, J., Lu, L. & Yang, H. Review on life cycle assessment of energy payback and greenhouse gas emission of solar photovoltaic systems. *Renewable and Sustainable Energy Reviews* vol. 19 255–274 Preprint at https://doi.org/10.1016/j.rser.2012.11.035 (2013).
6. Dong, L., Feng, Y., Wang, L. & Feng, W. Azobenzene-based solar thermal fuels: design, properties, and applications. *Chemical Society Reviews* vol. 47 7339–7368 Preprint at https://doi.org/10.1039/c8cs00470f (2018).
7. Herzog, A.V., Lipman, T.E., Edwards, J.L., & Kammen, D.M. Renewable Energy: A Viable Choice. *Environment: Science and Policy for Sustainable Development*, **43**, 20–8 (2001).
8. Jaiswal, K. K. *et al.* Renewable and sustainable clean energy development and impact on social, economic, and environmental health. *Energy Nexus* vol. 7 Preprint at https://doi.org/10.1016/j.nexus.2022.100118 (2022).
9. Kucharski, T. J., Tian, Y., Akbulatov, S. & Boulatov, R. Chemical solutions for the closed-cycle storage of solar energy. *Energy and Environmental Science* vol. 4 4449–4472 Preprint at https://doi.org/10.1039/c1ee01861b (2011).
10. BP. *Statistical Review of World Energy. https://www.bp.com/content/dam/bp/business-sites/en/global/corporate/pdfs/energy-economics/statistical-review/bp-stats-review-2022-full-report.pdf. (Accessed date: November 2022).*
11. Archer, C. L. & Jacobson, M. Z. Spatial and temporal distributions of U.S. winds and wind power at 80 m derived from measurements. *Journal of Geophysical Research: Atmospheres* **108**, (2003).
12. O'Donnell, E. H. & Glassman, L. W. Author Wasn't Convincing On Why Regulators Shouldn't Reduce Investors' Burden. *Electricity Journal* **22**, 1–3 (2009).
13. Kim, Y. *et al.* The effect of rear surface polishing to the performance of thin crystalline silicon solar cells. *Solar Energy* **85**, 1085–1090 (2011).
14. Liu, H. & Liang, D. A review of clean energy innovation and technology transfer in China. *Renewable and Sustainable Energy Reviews* **18**, 486–498 (2013).

15. Xu, Y. *et al.* Strategies for Efficient Charge Separation and Transfer in Artificial Photosynthesis of Solar Fuels. *ChemSusChem* vol. 10 4277–4305 Preprint at https://doi.org/10.1002/cssc.201701598 (2017).

16. Barber, J. & Tran, P. D. From natural to artificial photosynthesis. *J R Soc Interface* **10**, (2013).

17. Lee, K. M. *et al.* Recent Advances in Electro-Optic Response of Polymer-Stabilized Cholesteric Liquid Crystals. *Materials* vol. 16 Preprint at https://doi.org/10.3390/ma16062248 (2023).

18. Jungbluth, N., Stucki, M., Frischknecht, R. & Tuchschmid, M. *Photovoltaics*. www.ipcrystalclear.info (2009).

19. Wu, S. & Butt, H. J. Solar-Thermal Energy Conversion and Storage Using Photoresponsive Azobenzene-Containing Polymers. *Macromol Rapid Commun* **41**, (2020).

20. Zhang, B., Feng, Y. & Feng, W. Azobenzene-Based Solar Thermal Fuels: A Review. *Nanomicro Lett* **14**, (2022).

21. Merritt, I. C. D., Jacquemin, D. & Vacher, M. cis→transphotoisomerisation of azobenzene: a fresh theoretical look. *Physical Chemistry Chemical Physics* **23**, 19155–19165 (2021).

22. Kolpak, A. M. & Grossman, J. C. Azobenzene-functionalized carbon nanotubes as high-energy density solar thermal fuels. *Nano Lett* **11**, 3156–3162 (2011).

Chapter 2: Literature review

2.1 Solar Thermal Fuels

Solar thermal fuels (STFs) are a recent type of innovative technology that uses chemical bonds of photoactive materials to collect and store solar energy and later release it as heat.[1,2] STFs should be excited with wavelengths (230-280 nm) that are near to the spectrum of sunlight to make greater use of solar energy. The excitation range of STFs should be red - shifted to the visible light area to focus the content of the specific sunlight wavelength in the spectrum that is required for activating STFs.[3] Conjugate alkene and azo bonds (C=C and N=N respectively) have high photochemical activity and are red shifted as they are typically excited at near-solar wavelengths, which makes them suitable STFs.[2] The energy-storage of STFs has enticing benefits in that they are rechargeable, renewable, clean, eco-friendly, and produce required energy in the form of heat.[1,4] In addition, for a molecule to be considered an efficient STF it should; have no photon competition during photo isomerization and back-conversion, have high quantum yield, match solar spectrum, cost less, have high energy density and power density, long half-life, and exhibit a large energy storage capacity.[1]

Prior research on potential solar thermal fuels has demonstrated promise and numerous difficulties in achieving the necessary characteristics such as quantum yield, energy storage and cyclability.[5,6] For instance, norbornadiene (NBD) (**Figure 2.1a**), which has a high energy density of 89 kJ/mol, demonstrated excellent potential. However, low quantum yield and poor solar spectrum matching are two consistent challenges of NBD energy storage systems, consequently resulting in a reduced solar energy utilisation rate. According to recent research, tetracarbonyl-diruthenium (Fulvalene, **Figure 2.1b**) has great cyclability and a respectable gravimetric energy density (30.6 Wh/kg), but its potential is constrained by its low storage density and the usage of pricey ruthenium.[6] Azobenzene (AZ) (**Figure 2.1c**) molecules are in the limelight of research in the field of STFs due to its emergence as a “star” material. When exposed to near-UV light, azobenzene undergoes trans (E) – *cis* (Z) isomerization.[7] This reversible isomerization between the *trans* and *cis* configurations is the most intriguing feature of the molecule. Pure azobenzene can absorb UV light (365 nm) to transform solar energy into latent chemical energy and release heat through *cis*-to-*trans* isomerization.[8]

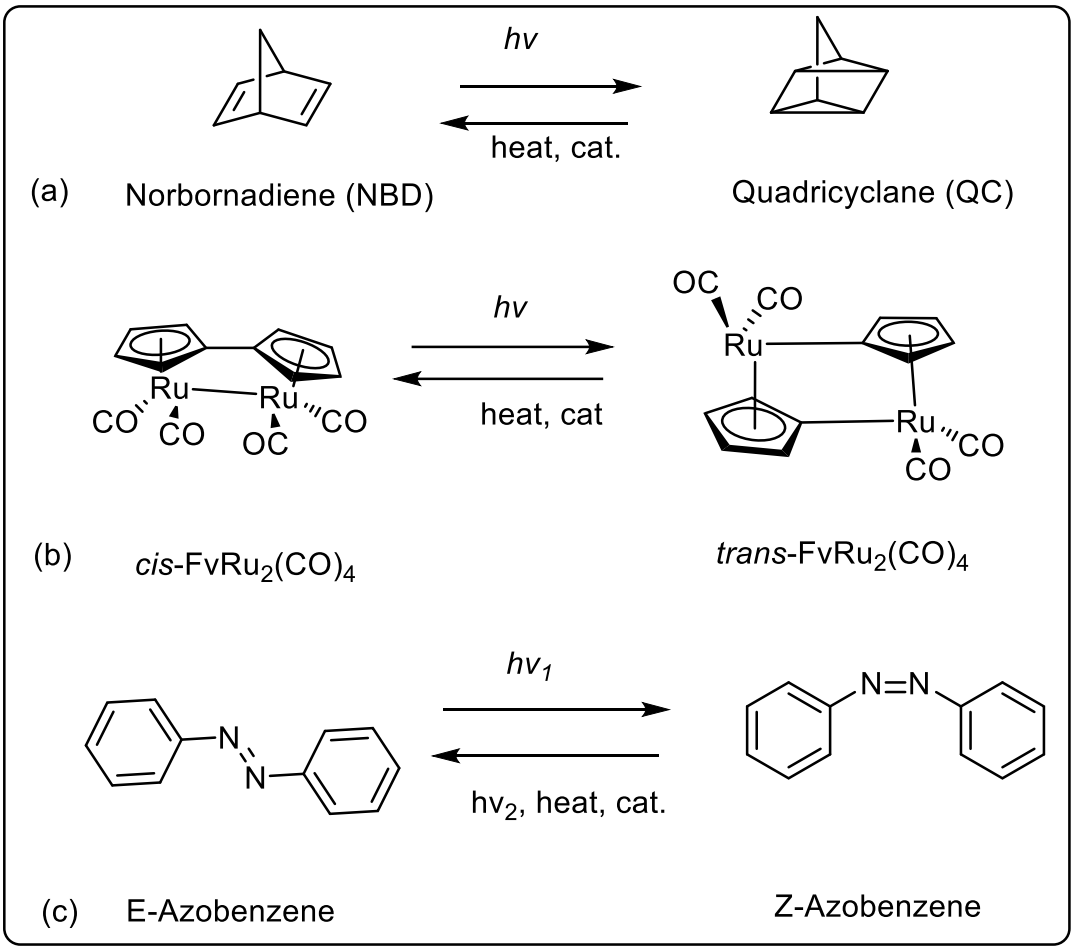

Figure 2.1: different molecular photoswitches.[9]

2.1.1 Mechanism for Azobenzene (AZ) *trans-cis* Isomerization

Numerous research groups have focused on the *E-to-Z* isomerization and have suggested a variety of potential isomerization processes (**Figure 2.2**). Rotation and inversion are the two pathways that are most usually encountered.[10] While the inversion approach produces a semi-linear structure by increasing one of the two NNC angles to 180°, the rotational pathway includes twisting around the core NN link.[11] As potential paths for the photoisomerization of azobenzene, other mixed processes have also been suggested, such as the concerted inversion or the inversion-assisted rotation. Inversion-assisted rotation includes simultaneous increases in the CNNC dihedral angle and NNC angles, while concerted inversion entails both NNC bond angles increasing to 180° and producing a linear transition state.[12] According to more recent research,[10,12] the pedal-like action of the azo nitrogen will dominate isomerization.

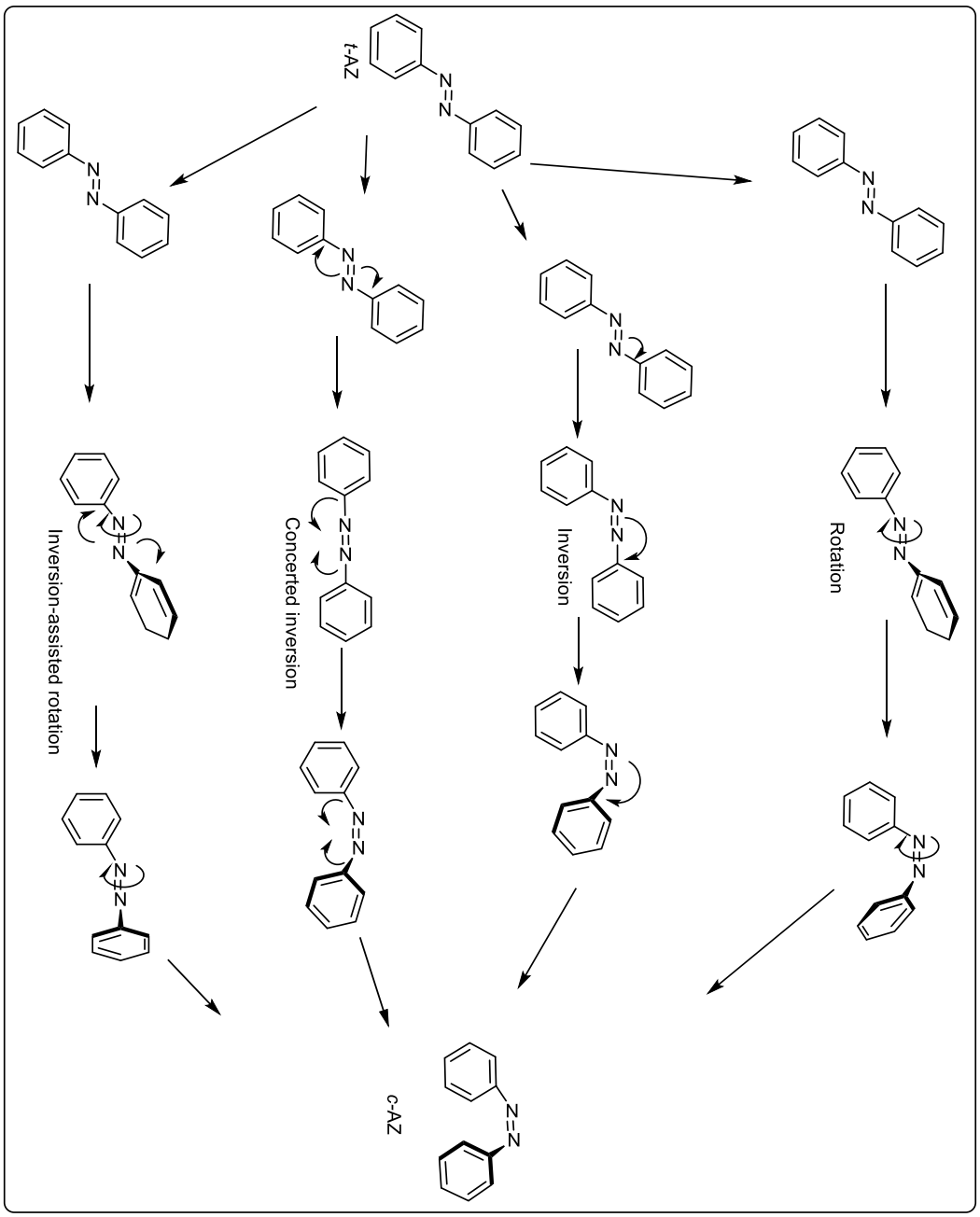

Figure 2.2: Proposed mechanisms for the *trans-to-cis* isomerization of azobenzene[13]

2.1.2 Azobenzene – Based Solar Thermal Fuels

STFs store solar energy through a photochemical conversion process known as photochromism - the reversible transition of a chemical unit between two forms, resulting in distinct absorption spectra, caused by electromagnetic light absorption in one or both directions.[14] The *trans-cis* photo-isomerization is by far the most studied photochemical process.[15] Azobenzene undergoes said isomerization, normally evidenced by significant quantum yields between the *trans* and *cis* states. The strong absorption observed in ultraviolet-visible (UV-Vis)

spectroscopy of azobenzene is due to π – conjugation which is evident in **Figure 2.3**. Consequently, UV-Vis spectra of the *trans*-azobenzene typically display a distinct π–π* shift at around 320 nm, while the *cis*-azobenzene displays a distinct n–π* band at 440 nm.[15] Photoisomerization is one of azobenzene's attractive properties which eases reduction of its surplus energy via regulation of its molecular configuration.[16] Other activities, such as radiation-less/radiative transitions, vibration relaxation, and energy transfer quenching, are frequently present together with this shift.[16,17] As a result, azobenzene is among the best choices to be used as STFs. *Trans* azobenzene often has high heat stability, but it can isomerize to the cis conformer when exposed to UV light. Solar energy is stored in the metastable cis isomer of azobenzene because its energy level (275 kJ.kg-1) is approximately 50 kJ.mol^{-1} greater than that of the *trans* isomer.[2,18]

This phenomenon is depicted in **Figure 2.3** below, where the mechanism of closed-system energy storage of STFs based on azobenzene photoswitches is outlined. Firstly, at normal temperature, the azobenzene molecules are in the *trans* conformation (which exists in either a solid or liquid form), which is often referred to as the ground state or low-energy state. Upon UV exposure (365 nm), the *trans*-azobenzene molecule (in its ground state) picks up photon energy and changes into an excited state, or the intermediate state.[1,17,19] A few picoseconds after entering the photoexcited state, the azobenzene molecule undergoes a conformational shift, making it very unstable. A few molecules may switch back to the initially stable *trans*-isomer during ineffective relaxation while the majority of photoexcited azobenzene molecules transform to the *cis* isomer.[1] Solar energy is stored in chemical bonds in the new state, referred to as the metastable state, also known as the high-energy state. An external trigger, such as heat or visible light, is often employed to overcome the energy barrier (ΔEa.) to access this stored energy in azobenzene molecules.[1,2] The molecule returns to its natural shape as the stored solar energy is subsequently released as heat.

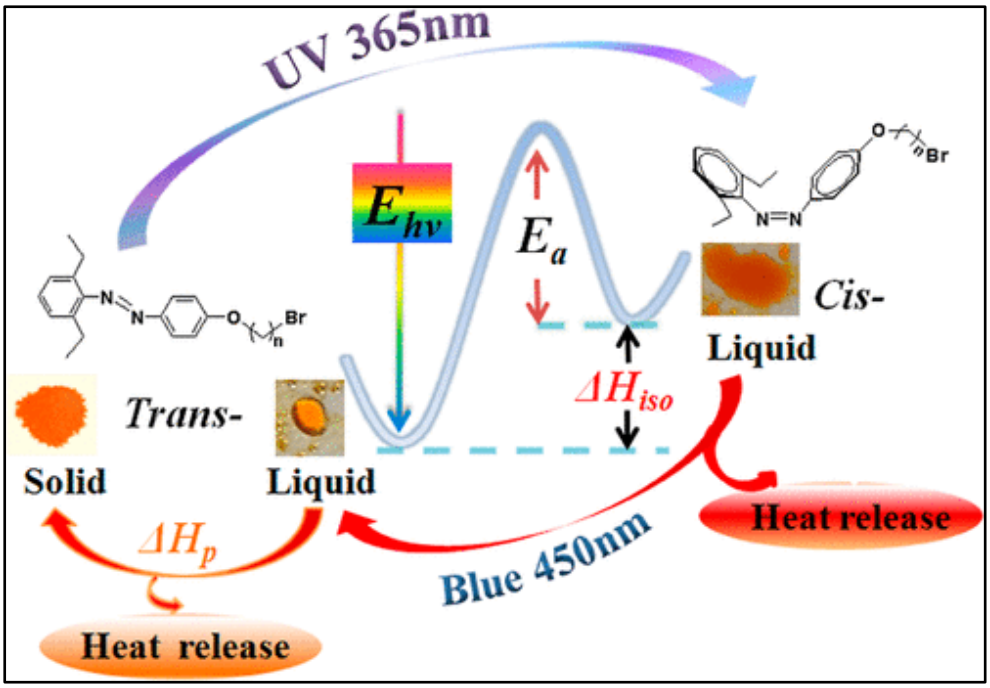

Figure 2.3: A schematic depiction mechanism of the solar thermal conversion and storage method for azobenzene. The normal storage enthalpy of *trans-to-cis* isomerization is ΔH storage, while the energy barrier from *cis*-to-*trans* reversion is ΔEa.[20]

2.1.3 Azobenzene Derivatives as Materials for STFs.

Due to their benefits of simpler synthesis, cheaper cost, and less degradation than other photoswitchable compounds, AZ derivatives are ubiquitous candidates for STFs.[2] Recent research has shown that AZ-based STFs have the potential to increase their energy density, energy storage half-life, and solar energy conversion efficiency. By covalently connecting AZ derivatives to carbon nanotube (CNT) templates, Grossman and colleagues created a hybrid nanostructure that showed how the steric strain imposed by the CNT templates aided in lengthening the STFs' energy density and energy-storage half-life.[21] To increase the solid-state STFs' ability to store energy, they also included conformal electroplating, layer-by-layer crosslinking, and spin coating.[6,22] In an unrelated study, Feng and colleagues discovered that, when grafting AZ derivatives onto graphene templates, the high grafting density and the optimised hydrogen bonding considerably increased the energy-storage capacity.[23] Kimizuka and colleagues developed a solvent-free STF utilising a liquid AZ derivative and demonstrating the energy-storage capabilities of photoliquefiable ionic crystals.[24]

The photochemical crystal-liquid transition (PCLT) theory for azobenzene optical switches has been continually refined in recent years.[2] The following is a general outline of the entire process: After overcoming the molecular stacking interaction of the crystal to liquid phase

transition, azo molecules spontaneously absorb heat from the environment to execute *trans-cis* photoisomerization.[2] Through the *cis-trans* isomerization and crystallisation of trans isomers in the liquid phase. The process of cis liquid phase to trans crystal transition (by external triggers, such as light irradiation or heating) allows the stored energy to be released in the form of chemical and crystallisation enthalpy (ΔH_{isom} and ΔH_{cryst}).[2] Through this technique, photon energy and ambient heat may be simultaneously stored and released as high-temperature heat as needed. Due to the synergistic effects of the two types of energy, the ambient heat that is accumulated in the liquid of low-melting point metastable isomers during photochemical melting can be released as high-temperature heat during the recrystallization of the high-melting point parent isomers, and the energy capacity they offer is higher than that of conventional solar/thermal energy storage systems that exclusively depend on molecular photoisomerization or phase transitions.[2]

2.1.4 Liquid Crystalline Azobenzene as Materials for STFs.

In today's world, liquid crystal (LC), the most popular and significant material, has a wide range of uses in common devices like displays, optical equipment, sensors, data storage and transmission.[25] Numerous azobenzene liquid crystal compounds have been created and synthesised, and much research has been done on their liquid crystalline self-assembly behaviour and the link between structure and property. Liquid crystals (LCs) are partly ordered, anisotropic fluids that display low-dimensional positional order along their long molecule axes or molecular centres of mass.[26,27] Liquid crystals are materials that have the characteristics of both liquids and solids.[26]They may be divided into two primary categories: thermotropic liquid crystals, which are created by changing the temperature of a liquid, and lyotropic liquid crystals, which are created by dissolving a molecule in certain solvents (**Figure 2.4**) which are further sub-divided based on their particle arrangement.[27] They differ from liquids and solids in that they have distinct molecular configurations. Since Friedrich Reinitzer discovered LCs in 1888, chemists, physicists, biologists, and engineers have become interested in them.[28,29] Liquid crystals have been thoroughly investigated and have uses in a variety of industries, including medicine, cosmetics, science, engineering, and gadget technology[28–30]

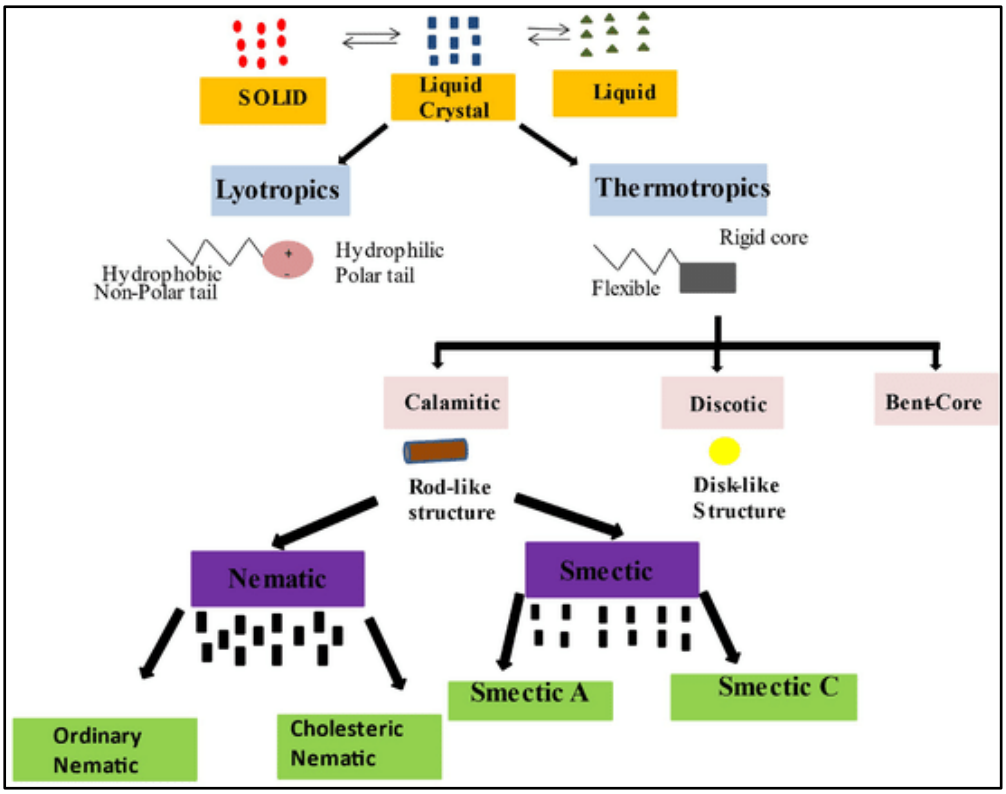

Figure 2.4: classification of liquid crystals.[27]

The calamitic or rod-shaped organic molecules no longer have positional order in a nematic phase, but they cause them to align to provide long-range directional order with their long axes generally parallel (**Figure 2.5a**). Consequently, the molecules still maintain their long-range directional order even though they are primarily free to flow and have centres of mass that are randomly dispersed, much as in a liquid. Nematics are often uniaxial in character. They only have one longer and preferred axis; the other two are equal (and may be roughly modelled as cylinders or rods). However, certain liquid crystals are also biaxial nematics, which means they create orientations with a secondary axis in addition to their long axis.[31] The molecules in smectic crystals are tilted away from the normal layer in the smectic C phase (**Figure 2.5c**), but they are aligned with it in the smectic A phase (**Figure 2.5b**). Since these phases are liquid, they exist between the layers. There are more distinct smectic phases, and they are all distinguished by various types and intensities of positional and directional order.[32]

Cholesteric liquid crystals (CLCs) are molecules that can self-assemble into helicoidal superstructures with circularly polarised reflection (**Figure 2.5d**).[33] Potential use of CLCs in a variety of technologies, including reflecting displays, tenable lasers, optical storage, colour

filters, and smart windows, has been investigated. When exposed to outside stimuli like electric fields, heat, and light, they can display dynamic optical reactions.[33,34]

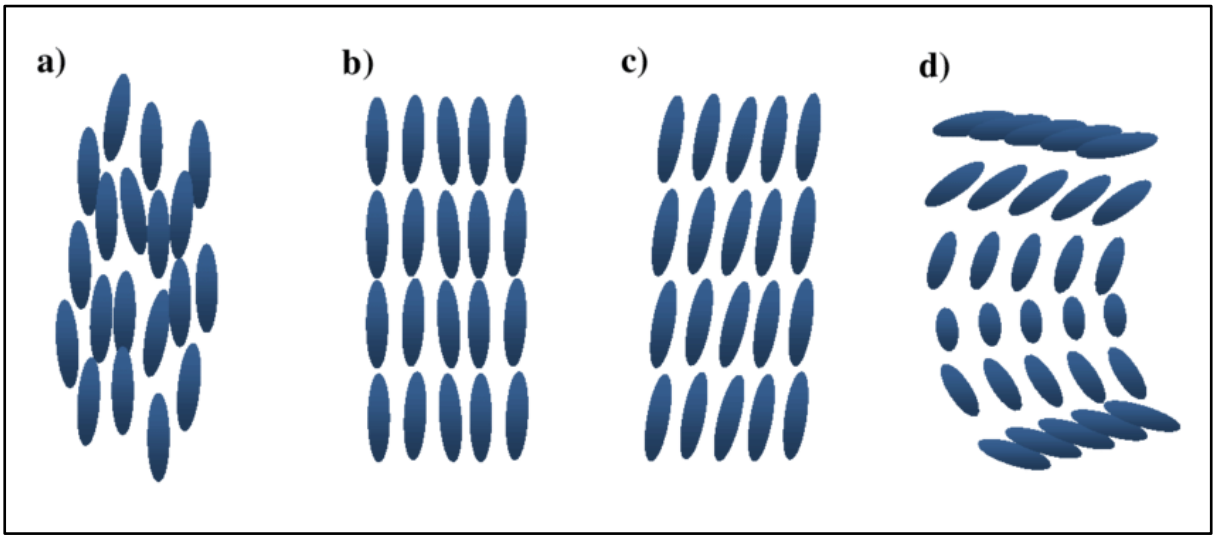

Figure 2.5: Calamitic liquid crystals classifications.[35]

Differential scanning calorimetry (DSC) is the most common thermal analysis method used to study properties of materials as they change with temperature. The principle behind this technique is to heat or cool a sample while comparing it to an inert reference to learn about thermal changes in the sample.[36] The fluctuation of energy allows for the quantitative discovery and quantification of thermal transitions occurring in the sample as well as characterization of the material for a variety of thermal events, including transitions, melting, and crystallisation. The primary attribute measured by DSC is heat flow as a function of temperature or time, which is often expressed in units of mW or mJ/s. The representation of the heat flow curve uses two separate convections, one of which is exothermic and moves upward while the other is endothermic with the peak pointing down.[36] By integrating the peak related to a particular thermal phenomenon, the DSC curve may be used to determine the enthalpies of transitions (**Figure 2.6**).[37,38] Phase transitions in liquid crystals are studied using the differential scanning calorimetry (DSC) method.[39,40] It determines the heat flow connected to these transitions and provides details on the material's thermal characteristics. The study of liquid crystalline systems, which includes substances like octyl-cyanobiphenyl (8CB), chiral smectic C mixes, and different thermotropic liquid crystals, frequently makes use of DSC.[41] It has been used to ascertain these materials' phase identities, transition temperatures, and enthalpies (**Figure 2.6**).

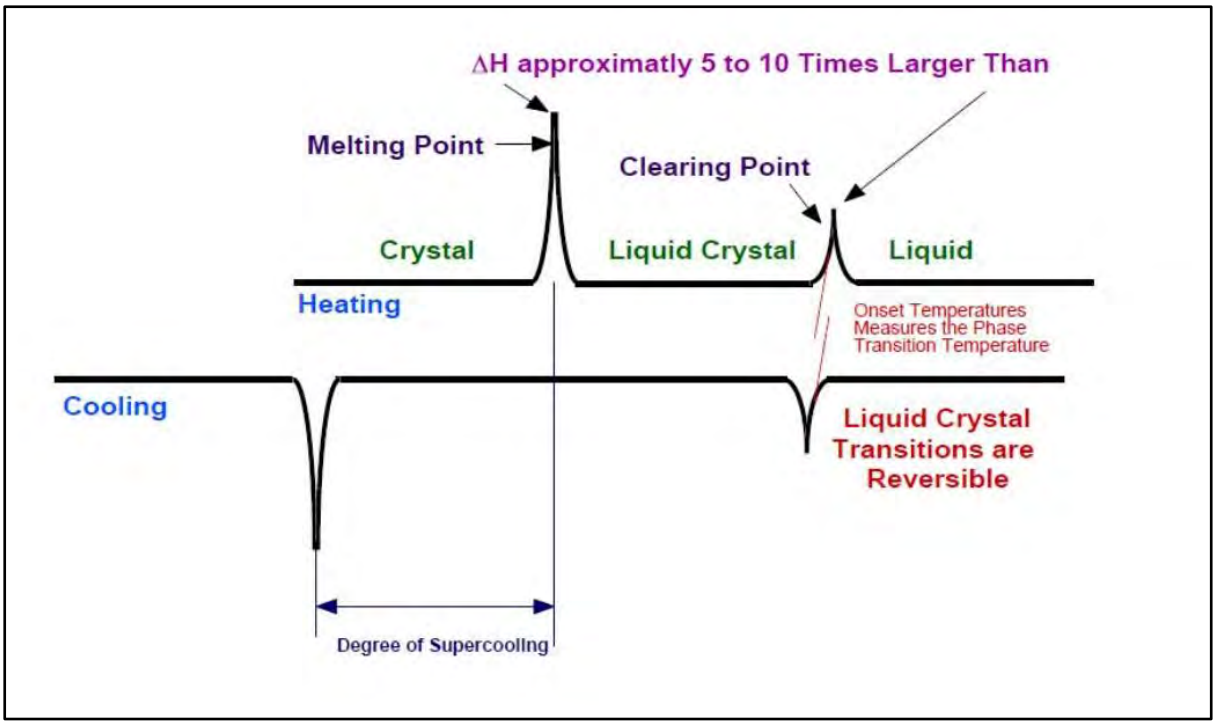

Figure 2.6: A DSC schematic representation of a typical complex with liquid crystalline properties.[42]

A liquid crystal phase has a distinctive texture, and POM is the technique of choice for determining the phase of a liquid crystal sample. There are two polarising filters in a polarising optical microscope.[43] Although it may typically be rotated through 360 degrees, the polarizer (**Figure 2.7)** is often placed below the specimen stage with its suitable vibration direction set in the east-west direction.[43] The analyser may be rotated 360 degrees but is typically oriented north – south (**Figure 2.7**, right). As a result, the polarizer shown in **Figure 2.7** (left) and analyser are often perpendicular to one another and in the optical path. In other terms, they are crossed, and the eyepiece has a black field of view.[43–45] In contrast, LCs typically appear bright when viewed between crossed polarizers because the polarised light makes an angle of 0 and 90 degrees with the liquid crystal's director, which is why the insertion of isotropic material has no effect on this. The optical textures were captured using the standard 10X magnification for both the ocular (eyepiece) and objective lenses, yielding a final magnification of 100X.[43,45]

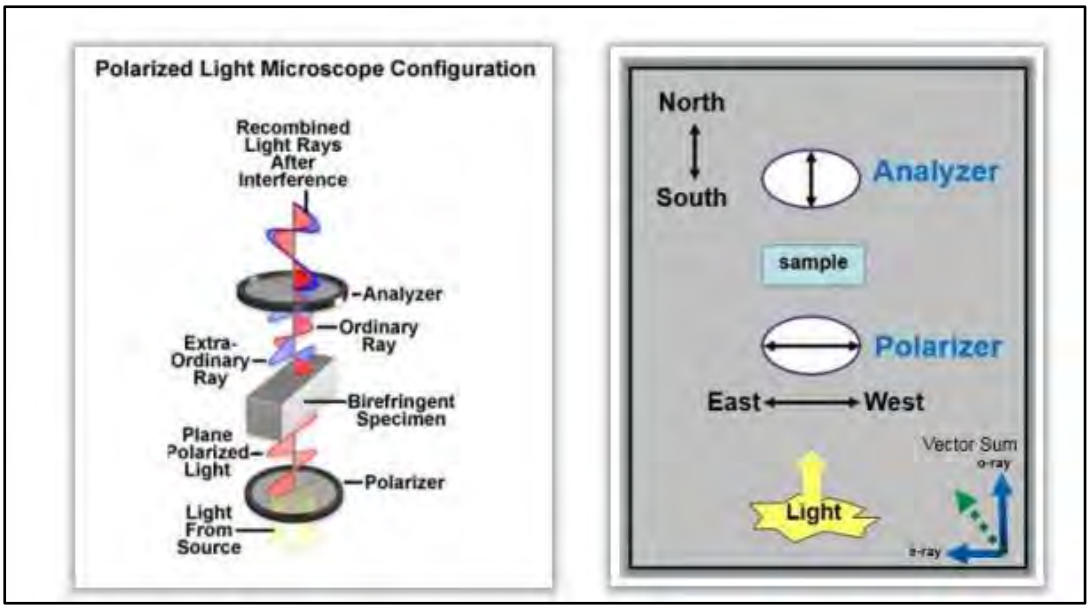

Figure 2.7: A typical picture of a polarized microscopy showing the polarizer configuration (left) and alignment (right).[46]

Although DSC is used as a practical instrument for observing phase transitions of liquid crystals during the heating and cooling cycle, POM – employed with a hot stage is used to visually observe the phase transitions properties such as texture, colour, and patterns/packing of the liquid crystal.[47] As mentioned earlier that liquid crystals exist in different mesophases namely: nematic, cholesteric, smectic and columnar. **Figure 2.8** below shows how the mesophases appear when visualized in POM distinguished by the difference in their packing arrangement and texture. Nematics: (a) A nematic film with surface point defects has a Schlieren texture. (b) A thin, isotropic layer of nematic material. (c) Nematic texture resembling thread. The Greek word for the "thread" that may be seen in these textures is nematic. (d) The texture of cholesteric fingerprints. The helical structure of the cholesteric phase, with the helical axis in the plane of the substrate, is what causes the line pattern. (e) When seen between crossed polarizers, a short-pitch cholesteric liquid crystal with Grandjean or standing helix texture. The distinction in rotatory power resulting from domains with various cholesteric pitches is what causes the vibrant colours. Near the smectic A phase, when the pitch sharply diverges with falling temperature, this pattern develops during fast cooling. (f) In a magnetic field, long-range orientation of cholesteric liquid crystalline DNA mesophases. (g, h) A chiral smectic A liquid crystal's focal conic texture. (i) A chiral smectic C liquid crystal's focal conic texture. Hexagonal columnar phase in (j) with characteristic spherulitic texture. (k)

The liquid crystal's rectangular phase, hexagonal columnar liquid-crystalline phase, abbreviated (l).[48]

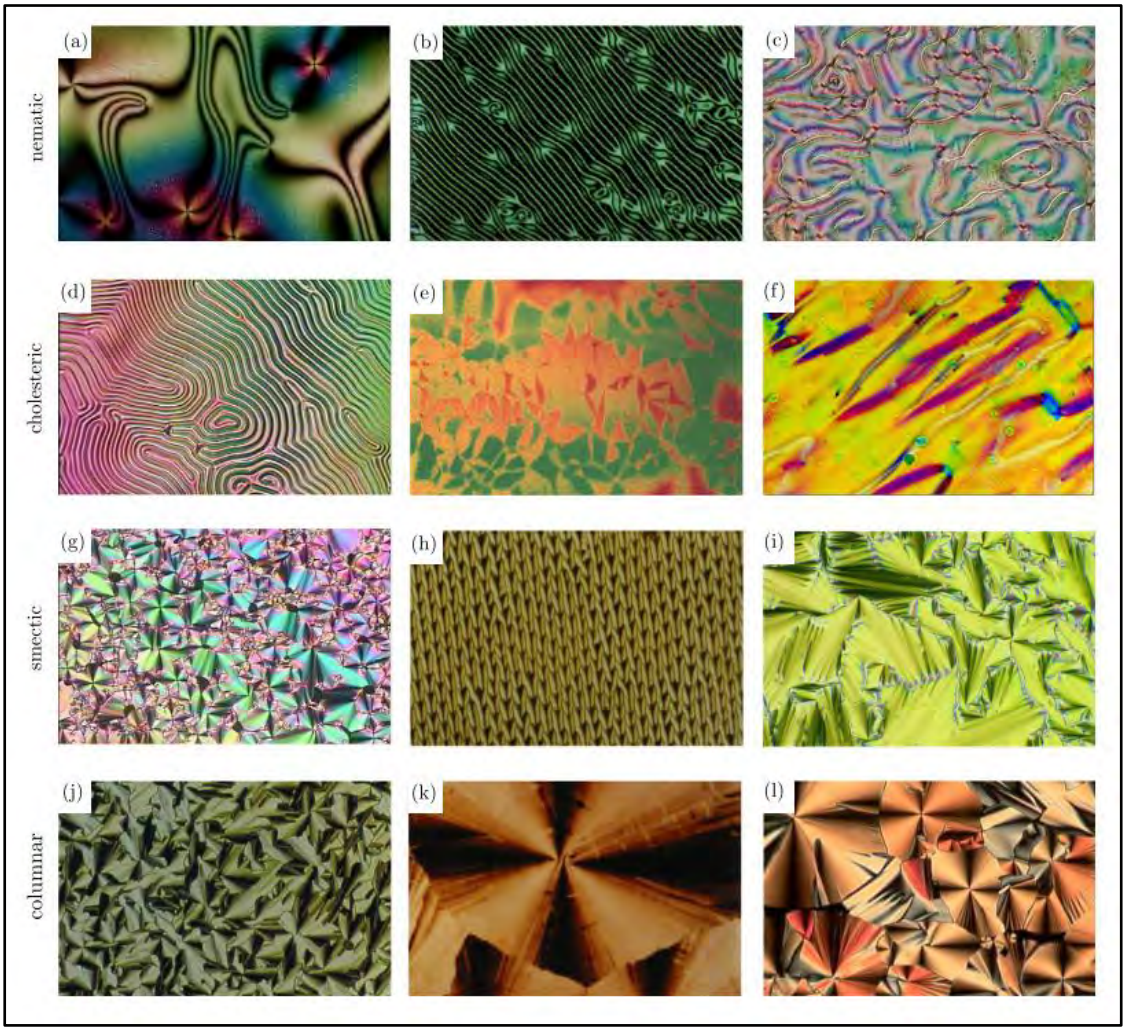

Figure 2.8: different types of liquid crystals texture, pattern and packing arrangement visualised through polarized optical microscopy.[49]

The combination of liquid crystallinity, photoresponsivity, and reactivity in the azobenzene-containing liquid crystal draws a lot of interest.[25] Their potential for creating intelligent, photo-driven soft materials is increasing. Thermal behaviour often regulates the phase transitions of common rod-like LC molecules.[50,51] Long-range crystal order and fluid mobility, such as birefringence, fluidity, and alignment modification by external fields, are what give LC phases their outstanding features. LC polymers are well-known polymer substances that combine the mesogenic groups' ability to self-organize into the ordered structure of LC phases with certain common polymer features.[50,51] For instance, these polymers in the LC state and may be ordered by electric or magnetic fields when they are above the glass transition temperature (Tg).[51] As

the system cools below Tg, it converts into glass by heat, producing anisotropic glasses. As a result, the material is suited for storage devices and optical applications.[51] Phase behaviour and phase transition have been photo-controlled using rod-shaped LC molecules containing azobenzene. The *trans-cis* isomerization of azobenzene is stimulated by heat or light, and this process results in the concentration of *cis* isomers, which results in the phase transition from the LC phase to the isotropic phase.[52]

2.1.5 Synthesis of Azobenzene

Scheme 2.1 above exemplifies a newly developed class of solid-state azobenzene derivatives with bulky aromatic groups with the aim of improving energy density and thermal stability. Bulkier functionalization on Azobenzene scaffold maintains the amorphous state at higher temperatures and improves the photostationery phase of the solid-state molecule, thereby allowing the *trans-cis* isomerization rate to be faster.[54]

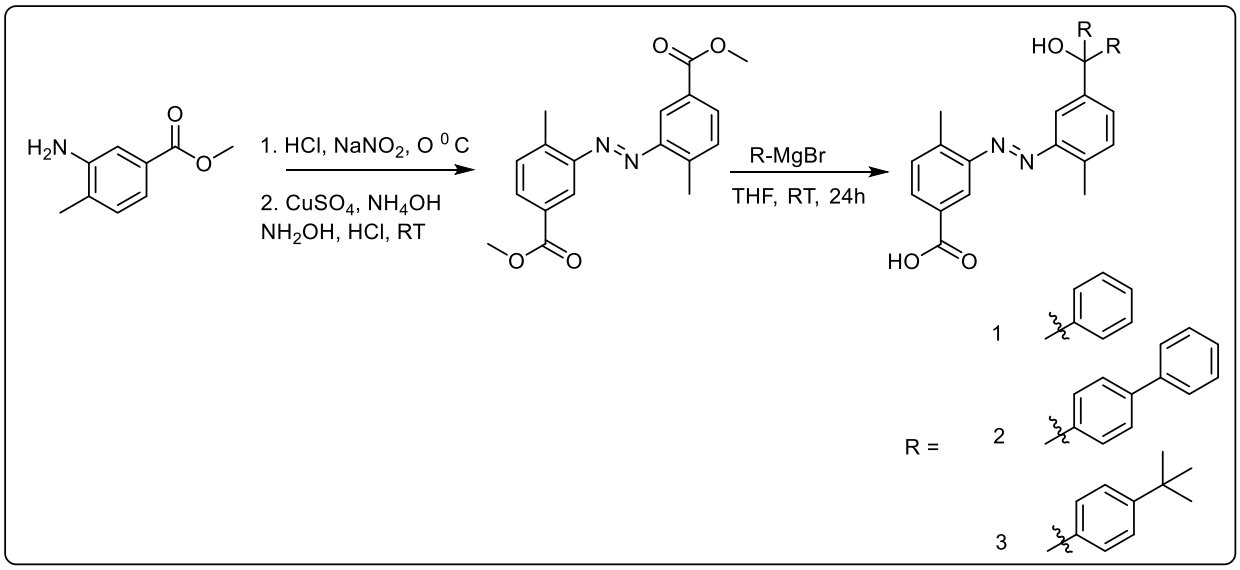

Scheme 2.1: A scheme illustrating the synthesis of compound 1-3 by varying the aryl groups.[53]

According to Cho et.al., When compared to the previously reported azobenzene-functionalized polymer, functionalizing azobenzene with bulky aromatic groups results in high energy storage per molecule (nearly 90 kJ/mol), which translates to an improvement in solid-state energy storage density of over 30%.[6] This further promotes excellent solid-state film formation. Breaking the molecule's planarity has a significant impact on solar thermal fuel properties and provides insight into future options for structural engineering of molecules to enable thermally stable and switchable STF thin films.[6] Cho and associates were able to simultaneously

synthesise small molecule films that have improved charging and cycling capabilities as well as higher energy density.[6]

2.2 Metallomesogens

Transition metal complexes with liquid crystalline ligands are known as metallomesogens (a class of mesogens). Mesogenic compounds containing metals can be classified as either standard inorganic coordination complexes or organometallic coordination complexes.[55,56] Adding a metal centre may change many physical characteristics, there is now a lot of interest in the synthesis and characterisation of liquid crystalline solids incorporating metal atoms.[57–59] Dielectric anisotropy and birefringence are two characteristics that should be affected by the addition of an electron-dense metal centre. Since metals display a surprising diversity of geometries in addition to the linear, trigonal, or tetrahedral arrangements seen by carbon, there is enormous potential for these metallomesogens.[59,60] The addition of metals creates the possibility of new physical characteristics for the liquid crystals as every metal ion has a huge and polarizable electron density, many of which contain unpaired electrons and are strongly coloured. Transition metal centres can impart unique optical, magnetic, and electrical characteristics, which is why liquid-crystalline materials containing these centres are garnering special interest.[57–61]

The first liquid crystal containing a metal was described by Vorlander in 1910.[62] He found that the traditional lamellar phases typical of soaps were generated by the alkali-metal carboxylates, $R(CH_2)nC(O)ONa$.[57,62] He also discovered that the diarylmercury Schiff bases $(RC_6H_4CH=NC_6H_4)_2Hg$ produce smectic phases later, in 1923. Malthete and Billard synthesised the smectic ferrocenyl Schiff bases in 1976, Skoulios and his associates characterised several alkali and alkaline earth salts of carboxylic acids with ordered mesophases. The mesogenic nickel and platinum dithiolene were initially discovered by Giroud and Muller-Westerhoff in 1977, and they were the ones who started looking for innovative substances for electronic, optoelectronic, and related applications among these compounds, which are known as advanced materials.

One of the main areas of study in the subject is copper containing metallomesogens; all those that show liquid crystalline nature are Cu(II) with ligand atoms largely arranged in a square planar pattern around the metal. It was discovered that many of the earliest ones to be described had discotic stages.[59,60,62] Nevertheless, there have also been a lot of calamitic copper mesogens

created, and these complexes offer some fascinating metallomesogens chemistry and physics. This is especially true due to the paramagnetism that is generated by the copper(II) (d^9) centre, which can have practical potential uses. [57,62] The discotic nature of the copper beta-diketonato (**Figure 2.9a**) was shown by early research. Miihlberger and Haase found that the cyclohexyl phenyl complex in **Figure 2.9b** (R = alkyl) were nematic monotropic. β-diketone (1, 3-diketone) ligand comprises of two carbonyls separated by one γ- carbon. The protons on the α-carbon are acidic and are easily detachable with a weak base.[63] β-diketone undergoes keto-enol tautomerism.[63] Together with the metal ion, the diketonato ligands form a six-membered chelate ring. Acetyl acetone (Hacac) is the most common diketone. All other diketones are thought to have originated from Hacac where the methyl group is substituted. The kind of substituents influences the energy level of the ligand's location, which improves the photophysical characteristics of the associated metal complexes.[63]

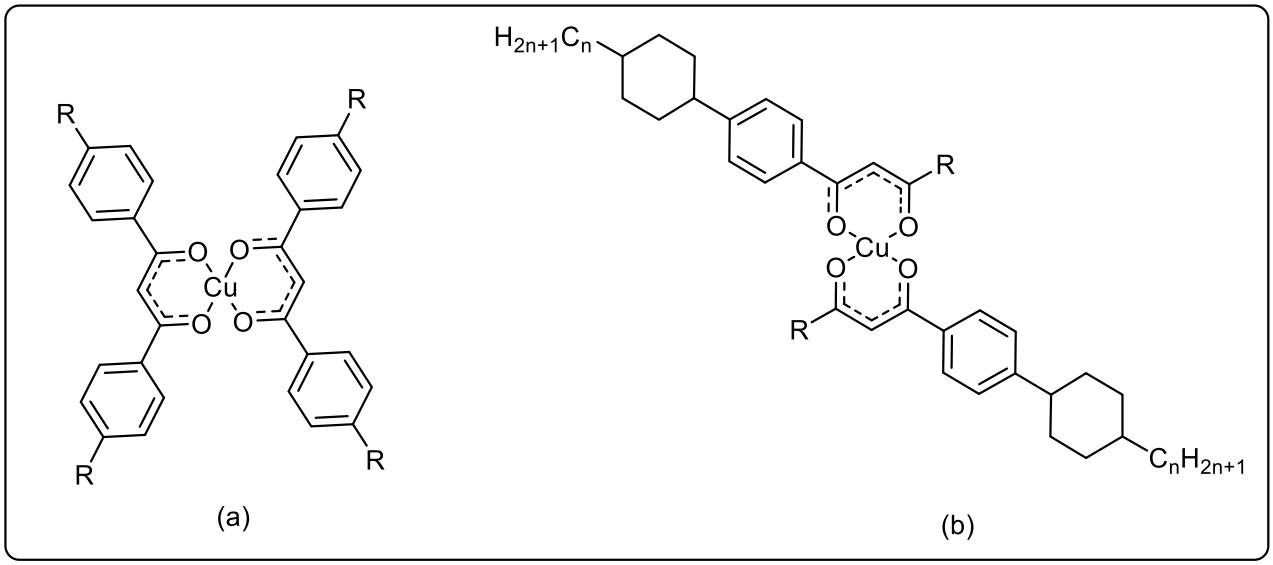

Figure 2.9: Copper-containing beta-substituted metallomesogens.[62]

2.4 References

1. Dong, L., Feng, Y., Wang, L. & Feng, W. Azobenzene-based solar thermal fuels: design, properties, and applications. *Chemical Society Reviews* vol. 47 7339–7368 Preprint at https://doi.org/10.1039/c8cs00470f (2018).
2. Zhang, B., Feng, Y. & Feng, W. Azobenzene-Based Solar Thermal Fuels: A Review. *Nanomicro Lett* **14**, (2022).
3. Hong, J., Xu, C., Deng, B., Gao, Y., Zhu, X., Zhang, X., & Zhang, Y. Photothermal Chemistry Based on Solar Energy: From Synergistic Effects to Practical Applications. *Advanced Science* vol. 9 Preprint at https://doi.org/10.1002/advs.202103926 (2022).
4. Hu, J., Huang, S., Yu, M. & Yu, H. Flexible Solar Thermal Fuel Devices: Composites of Fabric and a Photoliquefiable Azobenzene Derivative. *Adv Energy Mater* **9**, (2019).
5. Philippopoulos, C.; Economou, D.; Economou, C.; and Marangozis, J. *Industrial & Engineering Chemistry Product Research and Development* **1983** *22* (4), 627-633. DOI: 10.1021/i300012a021
6. Martins, G. F., Cardoso, B. de P., Galamba, N. & Cabral, B. J. C. Solar-Thermal Fuels and the Role of Carbon Nanomaterials: A Perspective with Emphasis on the Azobenzene System. *Energy and Fuels* vol. 37 1731–1756 Preprint at https://doi.org/10.1021/acs.energyfuels.2c03677 (2023).
7. Cho, E. N., Zhitomirsky, D., Han, G. G. D., Liu, Y. & Grossman, J. C. Molecularly Engineered Azobenzene Derivatives for High Energy Density Solid-State Solar Thermal Fuels. *ACS Appl Mater Interfaces* **9**, 8679–8687 (2017).
8. Marturano, V., Ambrogi, V., Bandeira, N. A. G., Tylkowski, B., Giamberini, M., & Cerruti, P. Modeling of azobenzene-based compounds. *Physical Sciences Reviews* vol. 2 Preprint at https://doi.org/10.1515/psr-2017-0138 (2019).
9. Szymański, W., Beierle, J. M., Kistemaker, H. A. V., Velema, W. A. & Feringa, B. L. Reversible photocontrol of biological systems by the incorporation of molecular photoswitches. *Chemical Reviews* vol. 113 6114–6178 Preprint at https://doi.org/10.1021/cr300179f (2013).
10. Dong, L., Feng, Y., Wang, L. & Feng, W. Azobenzene-based solar thermal fuels: design, properties, and applications. *Chem Soc Rev* **47**, 7339–7368 (2018).

11. García-Amorós, J. & Velasco, D. Recent advances towards azobenzene-based lightdriven real-time information-transmitting materials. *Beilstein Journal of Organic Chemistry* vol. 8 Preprint at https://doi.org/10.3762/bjoc.8.113 (2012).
12. Konieczkowska, J., Wasiak, A., Sobolewska, A., Bartkiewicz, S., Małecki, J. G., & Schab-Balcerzak, E. Kinetics of the dark cis–trans isomerization of azobenzene and azo pyridine derivatives in ethanol and chloroform solutions. *J Photochem Photobiol A Chem* **444**, (2023).
13. Liu, Z. F., Morigaki, K., Enomoto, T., Hashimoto, K., & Fujishima, A. Kinetic studies on the thermal cis-trans isomerization of an azo compound in the assembled monolayer film. *The Journal of Physical Chemistry* **96,** 1875-1880 (1992).
14. Konieczkowska, J.; Wasiak, A.; Sobolewska, A.; Bartkiewicz, S.; Małecki, J. G.; & Schab-Balcerzak, E. Kinetics of the dark cis–trans isomerization of azobenzene and azo pyridine derivatives in ethanol and chloroform solutions. *Journal of Photochemistry and Photobiology A: Chemistry*, 114979 (2023).
15. Fu, S. & Zhao, Y. Orientation of Azobenzene Mesogens in Side-Chain Liquid Crystalline Polymers: Interplay between Effects of Mechanical Stretching, Photoisomerization and Thermal Annealing. *Macromolecules* **48**, 5088–5098 (2015).
16. Bouas-Laurent, H. & Dürr, H. International union of pure and applied chemistry organic chemistry division commission on photochemistry* organic photochromism (iupac technical report) organic photochromism (iupac technical report*)*. *Pure Appl. Chem* vol. 73 (2001).
17. Yang, Y., Huang, S., Ma, Y., Yi, J., Jiang, Y., Chang, X., & Li, Q. Liquid and Photoliquefiable Azobenzene Derivatives for Solvent-free Molecular Solar Thermal Fuels. *ACS Appl Mater Interfaces* **14**, 35623–35634 (2022).
18. Merritt, I. C. D., Jacquemin, D. & Vacher, M. cis→transphotoisomerisation of azobenzene: a fresh theoretical look. *Physical Chemistry Chemical Physics* **23**, 19155–19165 (2021).
19. Dong, L., Chen, Y., Zhai, F., Tang, L., Gao, W., Tang, J., ... & Feng, W. Azobenzene-based solar thermal energy storage enhanced by gold nanoparticles for rapid, optically triggered heat release at room temperature. *J Mater Chem A Mater* **8**, 18668–18676 (2020).
20. Miao, Z. C., Zhang, Y. M., Zhao, Y. Z. & Wang, D. Azobenzene liquid crystals with high birefringence and their effect of trans-cis photoisomerization on selective reflection. *Molecular Crystals and Liquid Crystals* **582**, 98–106 (2013).

21. Kolpak, A. M. & Grossman, J. C. Azobenzene-functionalized carbon nanotubes as high-energy density solar thermal fuels. *Nano Lett* **11**, 3156–3162 (2011).
22. Zhitomirsky, D. & Grossman, J. C. Conformal Electroplating of Azobenzene-Based Solar Thermal Fuels onto Large-Area, and Fiber Geometries. *ACS Appl Mater Interfaces* **8**, 26319–26325 (2016).
23. Feng, W., Luo, W. & Feng, Y. Photo-responsive carbon nanomaterials functionalized by azobenzene moieties: Structures, properties, and application. *Nanoscale* vol. 4 6118–6134 Preprint at https://doi.org/10.1039/c2nr31505j (2012).
24. Masutani, K., Morikawa, M. A. & Kimizuka, N. A liquid azobenzene derivative as a solvent-free solar thermal fuel. *Chemical Communications* **50**, 15803–15806 (2014).
25. Wang, Q., Chen, H., Xing, H., Deng, Y., Luo, Z. W., & Xie, H. L. (2021). long rod-like liquid crystal containing azobenzene and the applications in phase-transition regulation and orientation of nematic liquid crystal. *Crystals (Basel)* **11**, (2021).
26. Tyagi, Y. Liquid crystals: An approach to different state of matter. *The Pharma Innovation Journal* **7**, 540–545 (2018).
27. Bala, R., Sindhu, R. K., Kaundle, B., Madaan, R. & Cavalu, S. The prospective of liquid crystals in nano formulations for drug delivery systems. *J Mol Struct* **1245**, (2021).
28. Bhowmik, P. K. Special issue editorial: Current advances in liquid crystals. *Molecules* vol. 26 Preprint at https://doi.org/10.3390/molecules26123713 (2021).
29. Jasiurkowska-Delaporte, M. & Kolek, Ł. Nematic liquid crystals. *Crystals* vol. 11 Preprint at https://doi.org/10.3390/cryst11040381 (2021).
30. Dierking, I. Nanomaterials in liquid crystals. *Nanomaterials* vol. 8 Preprint at https://doi.org/10.3390/nano8070453 (2018).
31. Shen, Y. & Dierking, I. Perspectives in liquid-crystal-aided nanotechnology and nanoscience. *Applied Sciences (Switzerland)* vol. 9 Preprint at https://doi.org/10.3390/app9122512 (2019).
32. Yu, H. & Ikeda, T. Photocontrollable liquid-crystalline actuators. *Advanced Materials* **23**, 2149–2180 (2011).
33. Wu, Z., Ji, C., Zhao, X., Han, Y., Müllen, K., Pan, K., & Yin, M. Green-Light-Triggered Phase Transition of Azobenzene Derivatives toward Reversible Adhesives. *J Am Chem Soc* **141**, 7385–7390 (2019).
34. Zhang, B., Feng, Y. & Feng, W. Azobenzene-Based Solar Thermal Fuels: A Review. *Nanomicro Lett* **14**, (2022).

35. Gonzalez, A., Kengmana, E. S., Fonseca, M. V. & Han, G. G. D. Solid-state photoswitching molecules: structural design for isomerization in condensed phase. *Materials Today Advances* vol. 6 Preprint at https://doi.org/10.1016/j.mtadv.2020.100058 (2020).
36. Serrano, J. L. Metallomesogens: Synthesis, Properties, and Applications. Metallomesogens: Synthesis, Properties, and Applications. *John Wiley & Sons.* doi:10.1002/9783527615094 (2007).
37. Gharanjig, H., Gharanjig, K., Hosseinnezhad, M. & Jafari, S. M. Differential scanning calorimetry (DSC) of nanoencapsulated food ingredients. in *Characterization of Nanoencapsulated Food Ingredients* 295–346 (Elsevier, 2020). doi:10.1016/B978-0-12-815667-4.00010-9.
38. Pijpers, M. F. J. & Mathot, V. B. F. Optimization of instrument response and resolution of standard- and high-speed power compensation DSC: Benefits for the study of crystallization, melting and thermal fractionation. *J Therm Anal Calorim* **93**, 319–327 (2008).
39. Chiyindiko, E., Stuurman, N. F., Langner, E. H. G. & Conradie, J. Electrochemical behaviour of bis(β-diketonato)copper(II) complexes containing γ-substituted β-diketones. *Journal of Electroanalytical Chemistry* **860**, (2020).
40. Löwen, H. A phase-field-crystal model for liquid crystals. *Journal of Physics Condensed Matter* **22**, (2010).
41. Simula, T. "Liquid Time Crystals." *arXiv preprint arXiv:2202.05407* (2022).
42. Lisetski, L., Bulavin, L. & Lebovka, N. Effects of Dispersed Carbon Nanotubes and Emerging Supramolecular Structures on Phase Transitions in Liquid Crystals: Physico-Chemical Aspects. *Liquids* **3**, 246–277 (2023).
43. Han, J., Zhang, L. F. & Wan, W. Synthesis and liquid crystal behaviours of 2,4-dioxo-3-pentyl 4-decyloxy cinnamate rhodium(I) complexes. *Chin J Chem* **21**, 1521–1524 (2003).
44. Purdes, A. J., Liu, Z. F., Morigaki, K., Enomoto, T., Hashimoto, K., & Fujishima, A. Kinetic studies on the thermal cis-trans isomerization of an azo compound in the assembled monolayer film. *The Journal of Physical Chemistry* **96**, 1875-1880 (1992).
45. Frandsen, A. F. *NASA Work Experience* (No. KSC-E-DAA-TN24465) (2015).
46. Corradini, M. G. & Julian McClements, D. Microscopy | Food applications. in *Encyclopedia of Analytical Science* 47–56 (Elsevier, 2019). doi:10.1016/B978-0-12-409547-2.14314-8.

47. Frandsen, A. F. *Polarized light microscopy* (No. KSC-E-DAA-TN37401) (2016).
48. Levit, S. L. *et al.* Color Space Transformation-Based Algorithm for Evaluation of Thermochromic Behavior of Cholesteric Liquid Crystals Using Polarized Light Microscopy. *ACS Omega* **5**, 7149–7157 (2020).
49. Andrienko, D. Introduction to liquid crystals. *Journal of Molecular Liquids*, *267*, 520-541 (2018).
50. Collings, P. J., & Goodby, J. W. Introduction to liquid crystals: chemistry and physics. *Crc Press* (2019).
51. Espinet, P., Esteruelas, M. A., Oro, L. A., Serrano, J. L. & Sola, E. Transition metal liquid crystals: advanced materials within the reach of the coordination chemist. *Coord Chem Rev* **117**, 215–274 (1992).
52. Espinet, P., Esteruelas, M. A., Oro, L. A., Serrano, J. L. & Sola, E. Transition metal liquid crystals: advanced materials within the reach of the coordination chemist. *Coord Chem Rev* **117**, 215–274 (1992).
53. Lai, C. Liquid crystalline properties of bis (salicylaldiminato) copper (II) complexes: the first columnar discotics derived from salicylaldimine Schiff bases. *Journal of Materials Chemistry* **8**, 599–602 (1998).
54. Mim, A., Enamullah, M., Haque, I., Mohabbat, A. & Janiak, C. Synthesis, molecular structure, mesomorphism and DFT/TD-DFT calculations of square-planar bis[1-((p-tolylimino)methyl)naphthalen-2-olato-κ2N,O]nickel and copper(II) complexes. *J Mol Struct* **1291**, 135669 (2023).
55. Hakemi, H. & Hakemi, H. Metallomesogen Mixtures as Potential Materials for Application in Liquid Crystal Devices. *Journal of Materials and Polymer Science* **2**, 4–8 (2022).
56. Hudson, S. A., & Maitlis, P. M. Calamitic metallomesogens: metal-containing liquid crystals with rodlike shapes. *Chemical Reviews* **93**, 861–885 (1993).
57. Chiyindiko, E., Stuurman, N. F., Langner, E. H. G. & Conradie, J. Electrochemical behaviour of bis(β-diketonato)copper(II) complexes containing γ-substituted β-diketones. *Journal of Electroanalytical Chemistry* **860**, (2020).
58. Yogeshvar Tyagi. Liquid crystals: An approach to different state of matter. *The Pharma Innovation Journal* **7**, 540–545 (2018).
59. Ogiwara, Y., Iwata, N. & Furumi, S. Dominant Factors Affecting Rheological Properties of Cellulose Derivatives Forming Thermotropic Cholesteric Liquid Crystals with Visible Reflection. *Int J Mol Sci* **24**, (2023).

60. Lee, K. M., Marsh, Z. M., Crenshaw, E. P., Tohgha, U. N., Ambulo, C. P., Wolf, S. M., ... & Godman, N. P. Recent Advances in Electro-Optic Response of Polymer-Stabilized Cholesteric Liquid Crystals. *Materials* vol. 16 Preprint at https://doi.org/10.3390/ma16062248 (2023).
61. Gharanjig, H., Gharanjig, K., Hosseinnezhad, M. & Jafari, S. M. Differential scanning calorimetry (DSC) of nanoencapsulated food ingredients. in *Characterization of Nanoencapsulated Food Ingredients* 295–346 (Elsevier, 2020). doi:10.1016/B978-0-12-815667-4.00010-9.
62. Pijpers, M. F. J. & Mathot, V. B. F. Optimization of instrument response and resolution of standard- and high-speed power compensation DSC: Benefits for the study of crystallization, melting and thermal fractionation. *J Therm Anal Calorim* **93**, 319–327 (2008).
63. Löwen, H. A phase-field-crystal model for liquid crystals. *Journal of Physics Condensed Matter* **22**, (2010).
64. Lisetski, L., Bulavin, L. & Lebovka, N. Effects of Dispersed Carbon Nanotubes and Emerging Supramolecular Structures on Phase Transitions in Liquid Crystals: Physico-Chemical Aspects. *Liquids* **3**, 246–277 (2023).

Chapter 3: Synthesis, characterization, and photochemical studies

Azobenzene is the most researched photochromic molecule and because of its simple synthesis processes, superior processability, great thermal and chemical stability, it appears to be a promising photo-switcher.[1] Nevertheless, the reversible isomerisation of the double bond between the *trans* and *cis* configurations is the most intriguing feature of azobenzene molecules as it drives the geometry of the molecule to change, this process is called "photoisomerization".[1,2] The aim of this chapter was to synthesise azobenzene ligands, by firstly varying the alkyl length, n (where n = 8 & 10), functionalize the ligands with a β-diketone and lastly, the β-diketonato compounds were coordinated with copper (II) to form *para*-substituted β-diketonato-Cu(II) complexes. Nuclear Magnetic Resonance (NMR), Fourier transform infrared (FTIR) spectroscopy and mass spectrometry (MS) were used to confirm the structure of the synthesized compounds. Photochromic studies by UV-Vis spectroscopy, and TD-DFT to evaluate the compounds' efficiency as solar thermal fuels was achieved.

3.1 Synthesis and characterization

3.1.1 Synthesis and characterisation of Ethyl (*E*)-4-((4-(alkyloxy) phenyl) diazenyl) benzoate

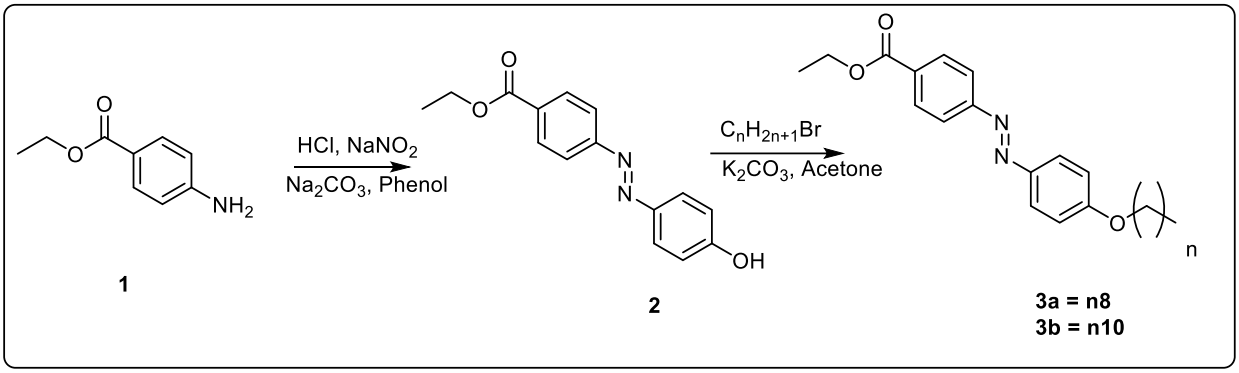

Scheme 3.1: Synthesis of Ethyl (*E*)-4-((4-(alkyloxy) phenyl) diazenyl) benzoate .[2]

The azobenzene precursor, compound **2** was synthesized via the diazotization reaction of Ethyl 4-aminobenzoate (**1**), carried out under strong acidic conditions, and subsequently reacted with phenol. The reaction was carried out at low temperatures (0–5 °C) for 3 hours to form a yellow

crude product with a percentage yield of 76.89%. Compounds **3a** and **3b** were synthesized by the addition of the alkyl chain under argon atmosphere with a dropwise addition of 1-bromoalkyl chain (n=8&10) and was left to reflux overnight. The reaction was extracted with dichloromethane (DCM) and recrystallized in ethanol which resulted in an orange powder with a percentage yield of 48% and 46.5% for **3a** and **3b** respectively (**Scheme 3.1**).

The FTIR Spectroscopy as shown in **Figure 3.1** confirms the functional groups present in compound **3a** and **3b.** The results show that the compounds have the same functional groups with the only difference in the C-H stretch absorption intensity, alkyl chain, n (where n = 8 for **3a** and n = 10 for **3b**). The absorption band at 2919 cm^{-1} and 2851 cm^{-1} represent both the symmetrical and unsymmetrical CH_2 stretch of the alkyl chain respectively. We observe that as the alkyl chain length increases, the intensity of the absorption band increases which distinguishes the compounds. The absorption band at 1710 cm^{-1} represents the carbonyl group and N=N is attributed by the absorption band at 1500 cm^{-1}.

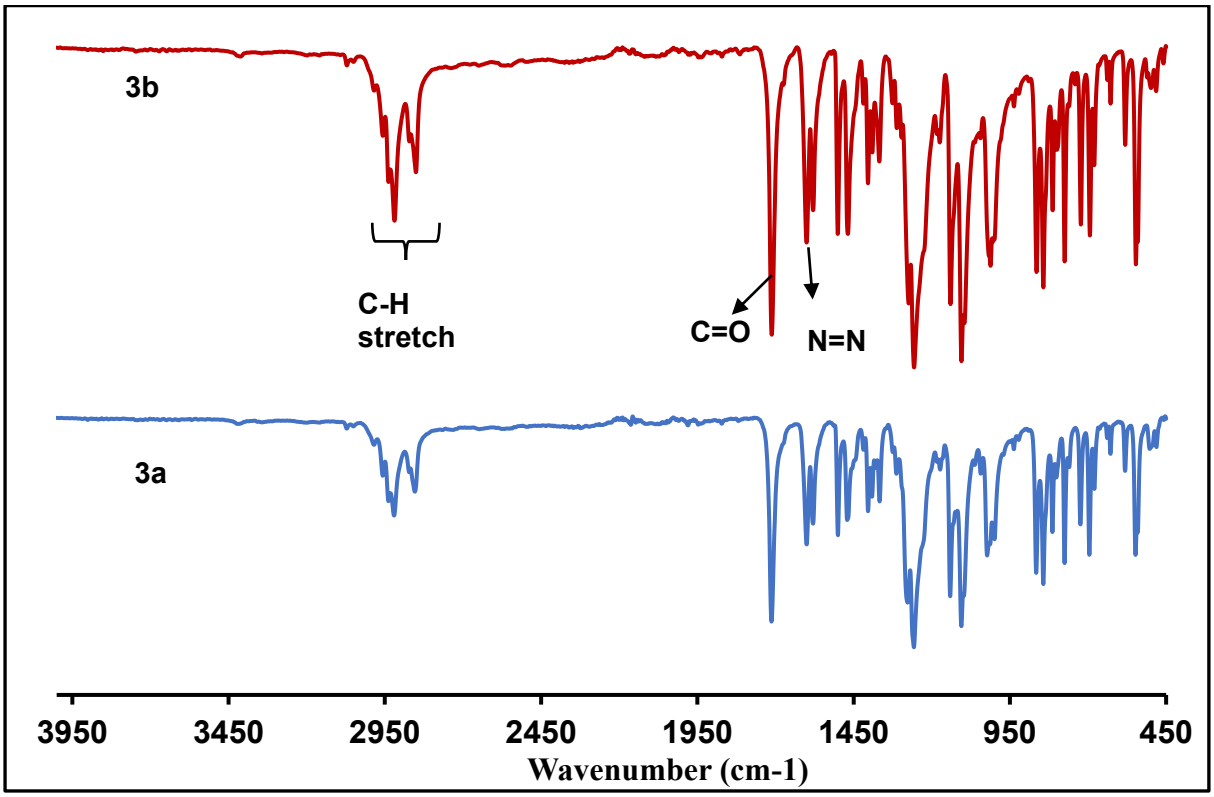

Figure 3.1: FTIR spectra of Ethyl (E)-4-((4-(alkyloxy) phenyl) diazenyl) benzoate.

The ^{1}H NMR spectroscopy was used to confirm the structure of compound **3a** and **3b**. The results show that the compounds have the same proton spectrum with the only difference in the hydrogens of the alkyl chains, n (where n = 8 for **3a** and n = 10 for **3b**). The ^{1}H NMR spectrum of compound **3a** shown in **Figure 3.2** is used as an example. The chemical shifts around 7.24-8.43 ppm corresponds to the azobenzene aromatic rings. The alkyl chain and the CH_3 groups correspond to the chemical shifts around 1.13-2.09 ppm.

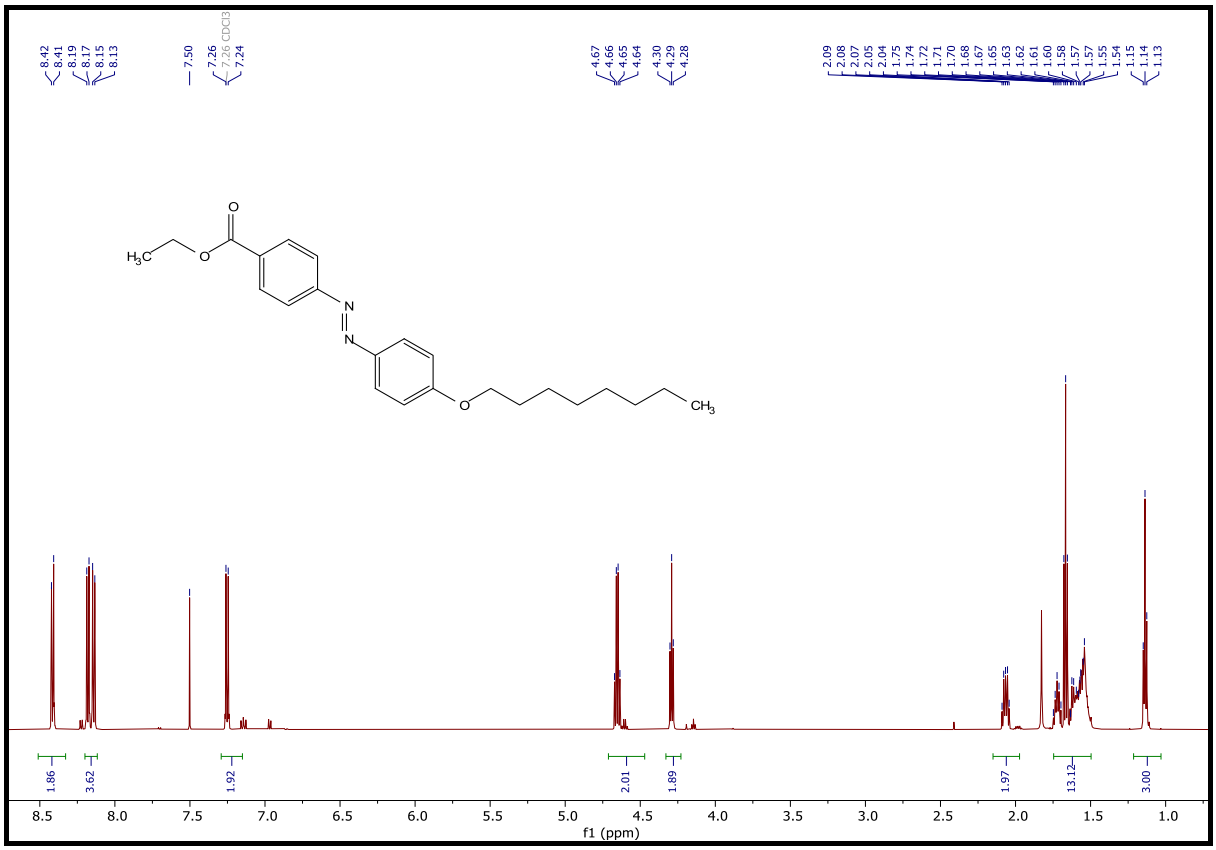

Figure 3.2: ^{1}H NMR spectrum of Ethyl (E)-4-((4-(octyloxy) phenyl) diazenyl) benzoate .

3.1.2 Synthesis and characterization of 2,4-dioxopentan-3-yl (*E*)-4-((4-(alkyloxy) phenyl) diazenyl) benzoate

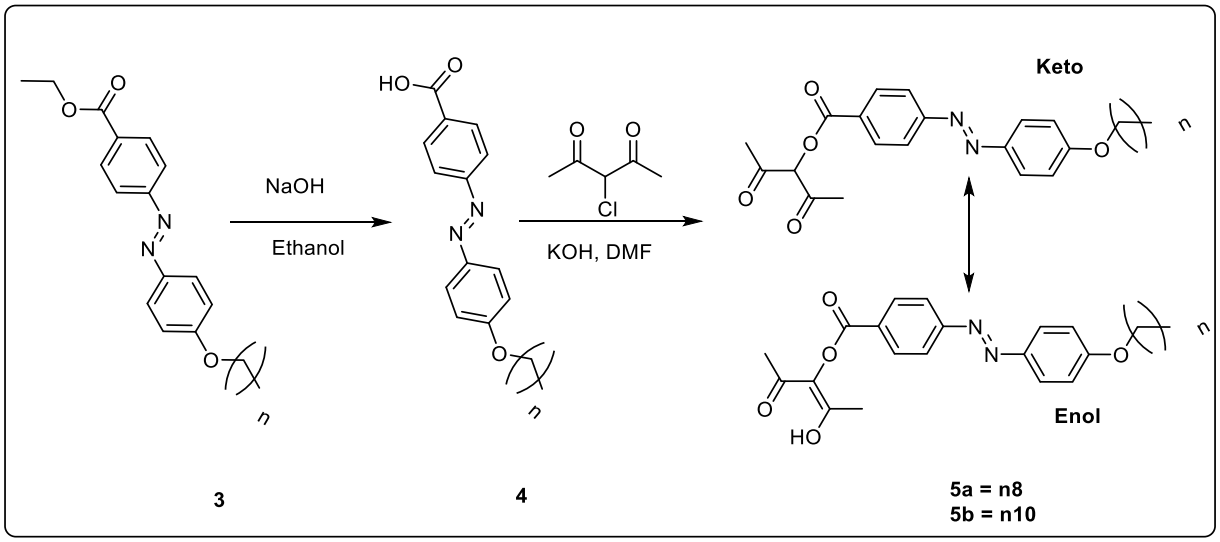

Scheme 3.2: synthesis of 2,4-dioxopentan-3-yl (*E*)-4-((4-(alkyloxy) phenyl) diazenyl) benzoate.[3,4]

The *para*-substituted β-diketones were synthesized using Ethyl (*E*)-4-((4-(alkyloxy) phenyl) diazenyl) benzoate (**3**) which was synthesized in **Scheme 3.2** as a starting material. Firstly, hydrolysis of an ester (**3**) to carboxylic acid (**4**) reaction was completed, (**4**) was followed by functionalization with 3-chloro-2,4-pentanedione. The reaction was conducted under a nitrogen gas atmosphere. The resulted mixture was extracted three times with chloroform to give a brown-orange product (**5**) with a percentage yield of 20% and 30,5% for compound **5a** and **5b** respectively (**Scheme 3.3**).

The spectroscopic characterization, both FTIR and ^{1}H NMR show that the -diketone underwent keto-enol tautomerization thereby forming two products (keto and enol form). The results show that the compounds have the same functional groups with the only difference in the C-H stretch absorption intensity, alkyl chain, n (where n = 8 for **5a** and n = 10 for **5b**), for example, compound **5a** in **Figure 3.3** has an absorption band at 3659 cm^{-1} assigned to the OH group of the enolic form and the absorption band at 1715 cm^{-1} correspond to the carbonyl group.

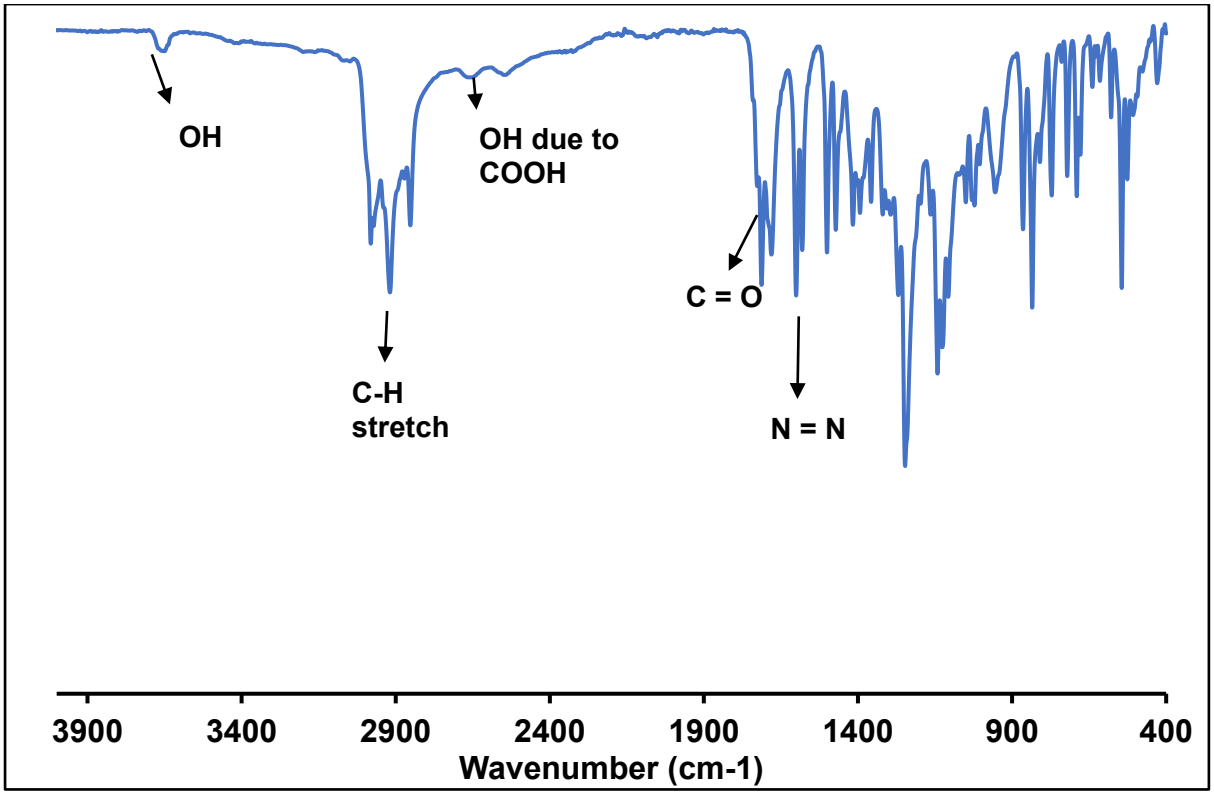

Figure 3.3: FTIR spectra of 2,4-dioxopentan-3-yl (E)-4-((4-(octyloxy) phenyl) diazenyl) benzoate .

The ^{1}H NMR spectroscopy was used to confirm the structure of compound **5.** The results show that the compounds have the same proton spectrum with the only difference in the hydrogens (by integration) of the alkyl chains, n (where n = 8 for **5a** and n = 10 for **5b**). ^{1}H and ^{13}C NMR spectra of these para-substituted β-diketones are shown in **Figure 3.4** below. In the ^{1}H NMR spectrum (a) the peak corresponding to the enol OH proton appears at 14.5 ppm, and a corresponding singlet signal for the two methyl groups resonates at 2.09 ppm. For the ketone, the diketo-sandwiched CH proton resonates at 5.75 ppm, and the accompanying keto-methyl protons at 2.45 ppm. The ^{13}C NMR spectrum (b) confirms the functionalization of the β-diketones with the CO carbon resonating at 199.0 ppm, and the COO- carbon evident at 164.51 ppm (with another signal at 184.96 ppm assigned to the tautomer enol's COH carbon).

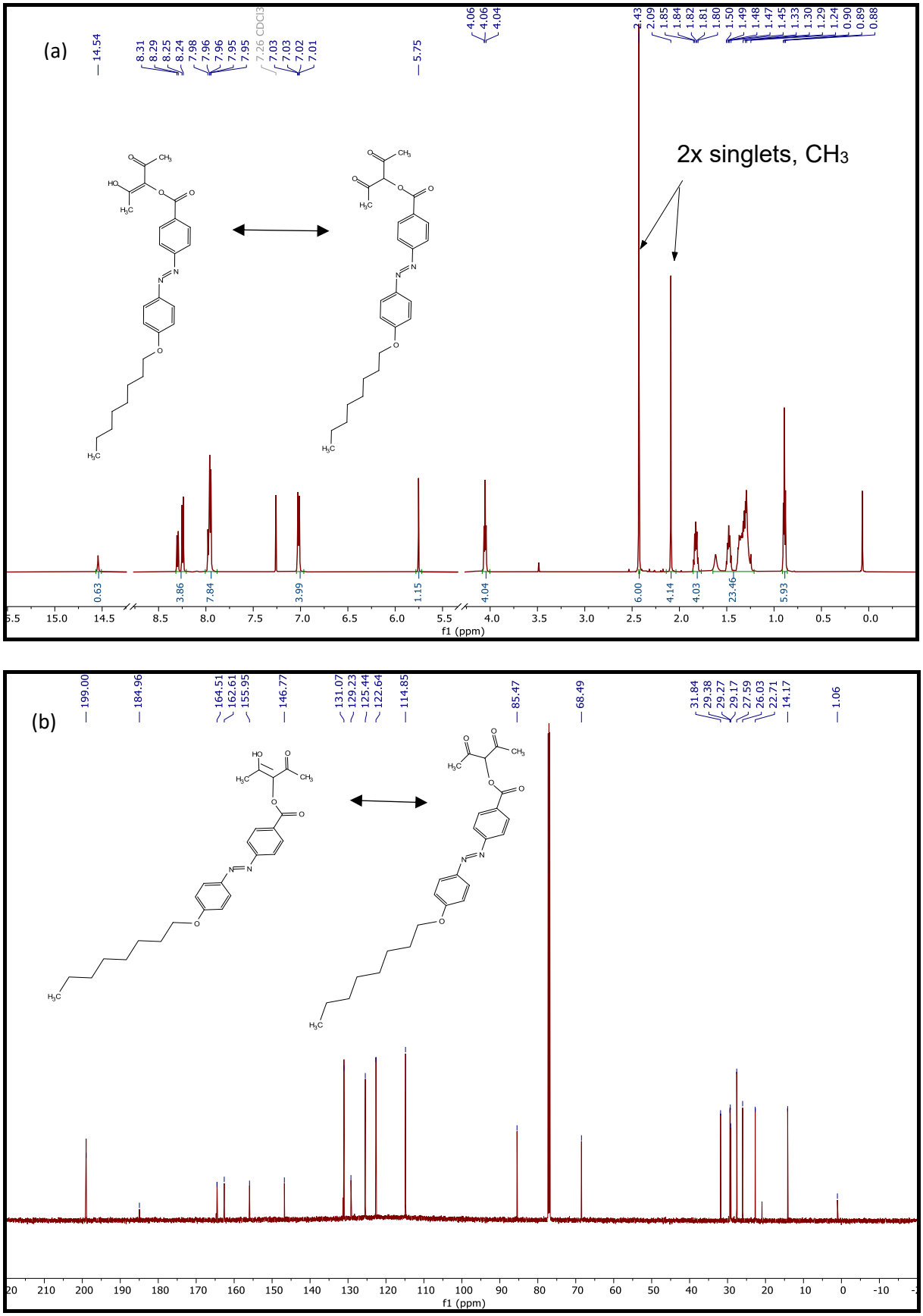

Figure 3.4: (a) ^{1}H and (b) ^{13}C NMR spectra of 2,4-dioxopentan-3-yl (E)-4-((4-(alkyloxy) phenyl) diazenyl) benzoate.

3.1.3 Synthesis of para-substituted β-diketonato-Cu (II) complex

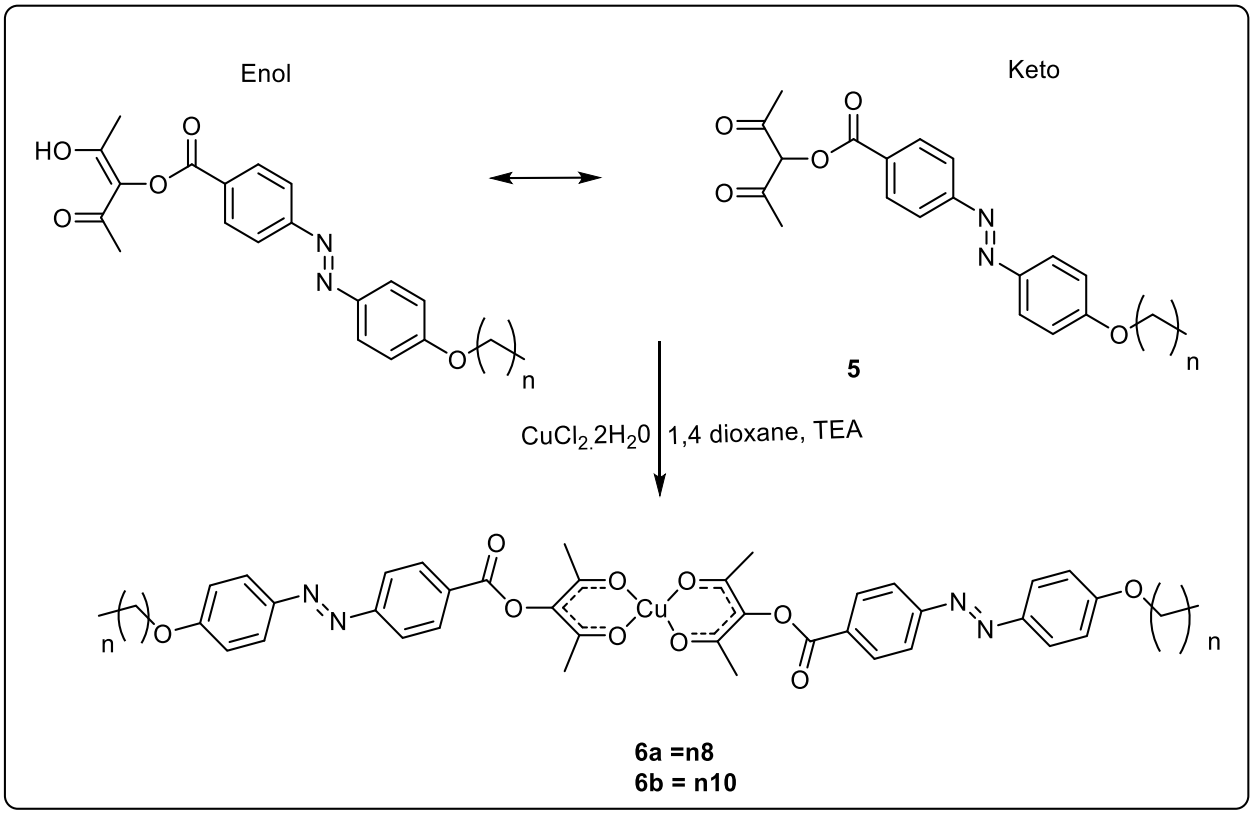

Scheme 3.3: Synthesis of *para* substituted β-diketonato Cu (II) complexes.[5]

As depicted in **Scheme 3.3** above, the *para*-substituted β-diketonato-Cu(II) complex was synthesized by reaction of copper(II) chloride dihydrate and diazo precursor **5** at room temperature. The resulting crude mixture was dissolved in THF and poured into methanol to form a precipitate which was dried and resulted in a green-brown powder (with a percentage yield of 32.54% (**6a**) and 31.87% (**6b**)). Upon complexation, ^{1}H NMR spectroscopy of copper(II) complex **6a** shows a general downfield-shift of proton signals belonging to the annotated metalacyclic CH hydrogens (see **Figure 3.5** below). As is typical for transition metal complexes, the isolated copper(II) complex is stabilized by synergic *sigma*- and *pi*-donation of electrons, from the ligand and metal, respectively.[6,7] Consequently, the general pull of electron clouds away from the ligand substituents (towards the copper atom center) deshields the substituents' hydrogen and carbon atoms, causing them to resonate at higher ^{1}H and ^{13}C NMR frequencies than in their free ligand form. This is evident as ligand **5**'s diketo-sandwiched CH proton shifted from 5.75 ppm (**Figure 3.4**) to 5.99 ppm upon complexation (**Figure 3.5**).

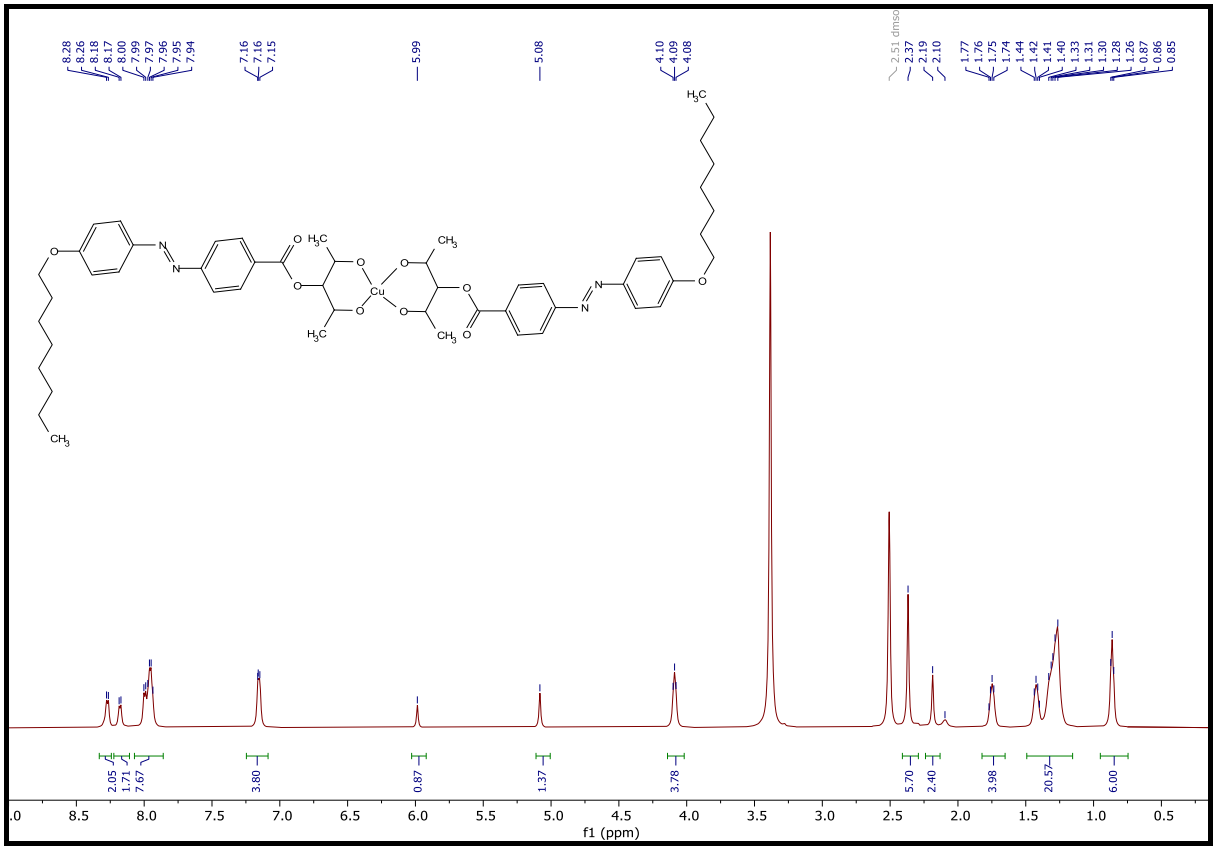

Figure 3.5: ^{1}H NMR spectra of para-substituted -diketonato-Cu (II) complex, compound 6a**.**

Mass spectrometry was then employed to confirm the formation of the product. The calculated mass is 965.38 amu. This mass is consistent with the parent peak obtained at 965.52 m/z shown in **Figure 3.6**.

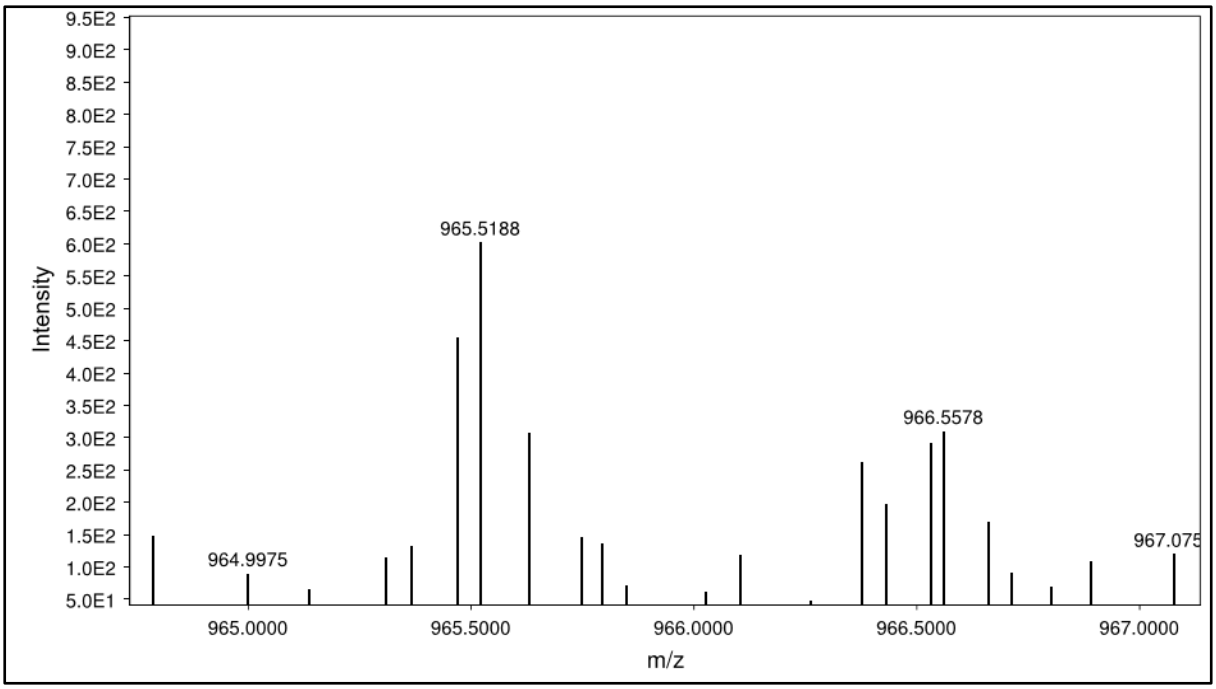

Figure 3.6: Mass spectrum of para-substituted -diketonato-Cu (II) complex, compound 6a.

3.2 Photochromic Characterization

Liquid crystals incorporating azobenzene moiety undergoes *trans-cis* photoisomerization when irradiated by UV light (320-380 nm) and *cis-trans* photoisomerization when exposed to visible light (380-420 nm) or heat.[8,9] Upon irradiation, it is stated that the thermal *cis-to-trans* isomerization take place by either in-plane inversion, out-of-plane rotation around the N=N double bond, or a mixture of both, depending on the polarity of the solvent and the location and kind of substituents.[9–12] The amount of time the sample is exposed to radiation before the kinetic measurements has no impact on the *cis* isomer concentration or the kinetics of the thermal *cis-to-trans* isomerization of substituted azobenzene.[13] Ideally, effective STFs should, in general, satisfy the following set of requirements:[14] (i) Sunlight spectrum match: the low-energy isomer's absorption should coincide with the solar emission's most intense region. (ii) High storage energy capacity: Preferably, there should be as much of an energy differential between the high- and low-energy isomers in relation to the molecular weight or volume. (iii) High quantum yield: there should be a high efficiency in the photoinduced conversion to the high-energy isomer. (iv) Avoid photon competition: Since light can trigger the processes of photoisomerization and back-conversion in most photoactive compounds, photon rivalry between two isomers should be avoided. (v) Stability over the long run: the ground state energy

landscape's back-conversion barrier should be high enough to allow for long-term storage and the photoactive materials should exhibit strong cyclability performance.[14]

All the synthesized compounds were exposed to UV-Visible light to explore their suitability as solar thermal fuels by calculating their half-life, rate constants for the *cis-trans* isomerization, activation energy, *cis* content, and band gap energies (band gap energy is required to study if the compounds are semi-conductors). The *cis* % content was determined by ^{1}H NMR and calculated using the equation:

The *cis %* content was determined by ^{1}H NMR and calculated using the equation 3.1:[15]

$Cis\ \% = \frac{Acis}{Atrans+Acis} \times 100\%$, Where A is the peak integral area…….(3.1)

The observed first-order rate constants, k_{obs}, were obtained by plotting ln(Ainf − At) vs. time data according to the first-order kinetic equation 3.2:[13]

$\ln(A\infty - A_t) = -K_{obs} \times t + \ln(A\infty - A_0)$……(3.2)

Where A_t is the absorbance of the compound at a time, A∞ is the absorbance at time infinity and A_0 is the absorbance at zero seconds.

The half-life of the *cis-trans* isomerization was calculated using equation 3.3:

$t_{1/2} = \ln(2) / k$, where k is the rate constant……(3.3)

The activation energy of the synthesized compounds was calculated using the equation 3.4:

$\Delta Ea = -RT \ln \frac{h \ln 2}{t_{\frac{1}{2}}\ Kb\ T}$ ……(3.4)

Where R=gas constant, h=Planck's constant, T=temperature, $t_{1/2}$=half-life and K_b is the Boltzmann constant.

3.2.1 UV-Vis isomerization

The synthesised compounds were dissolved in chloroform, at room temperature to monitor their photoresponsive nature. As seen for the azobenzene in **Figure 3.7**, using compound **3a** as an example, the absorption of the ground state, *trans* azobenzene includes two distinct bands. **Figure 3.7** displays the data for the compound 3a transitioning from the *trans* dominating isomer (t = 0) to the *cis* isomer over time (t = 3 min).

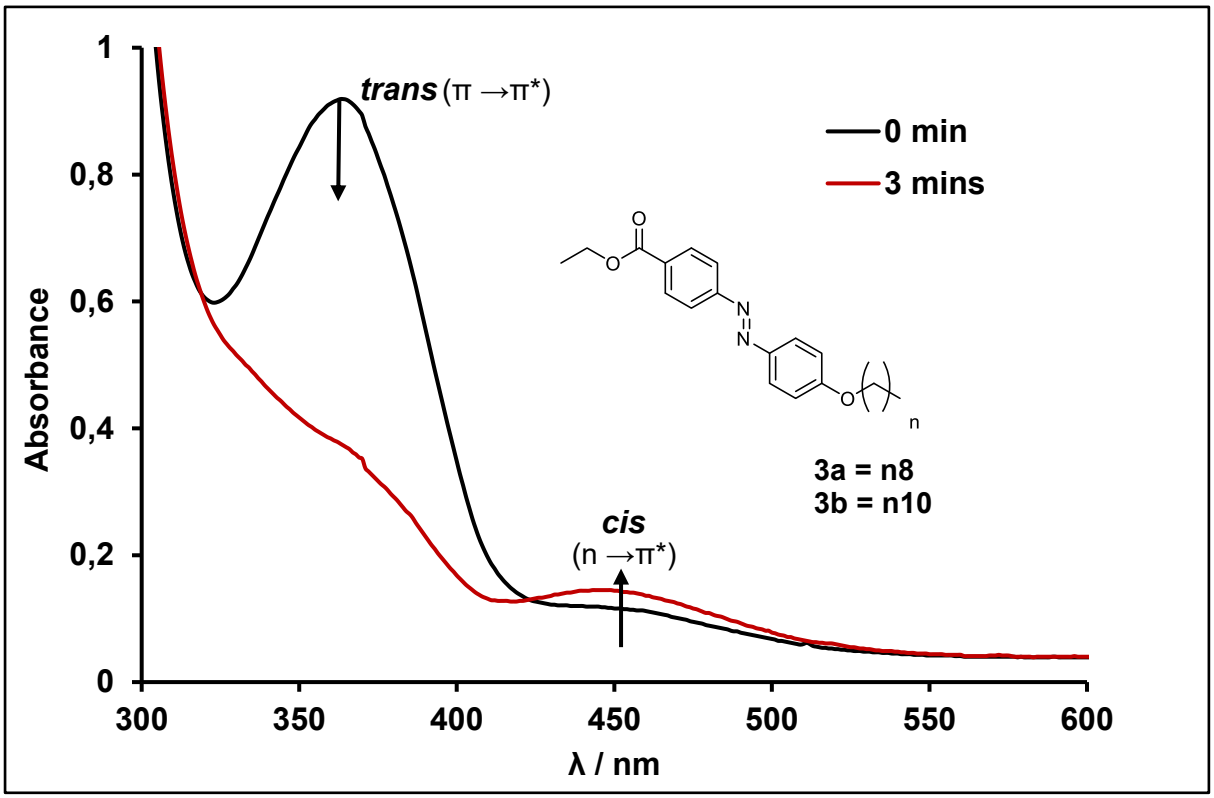

Figure 3.7: UV/Vis spectra of compound 3a in chloroform @365 nm (6W).

The black spectrum (at 0 min) is typically the most intense and occurs around 360-365 nm, meaning that it is a *trans* isomer (π →π*). The red spectrum (at 3 mins) is weaker and typically appears around 440–460 nm, showing that the compound isomerised into a *cis* isomer (n →π*). The symmetry-allowed π →π* transition is represented by the initial absorbance of 0.9, whereas the symmetry-forbidden n →π* transition is represented by the latter band with an absorbance of 0.1. As the time of exposure is increased, the band intensity decreases at 360-365 nm and increase at 440-460 nm. The n → π* transition is banned; hence its intensity will always be lower than the π → π* transition. The absorption of the π→ π* transition gets less and that of the n → π* transition grows greater as the fraction of *cis* form increases. In summary, irradiation at 365 nm promotes conversion of the *trans* to *cis* isomerisation. On the

other hand, exposure to radiation in the n → π* band, which is around 440 nm, promotes the conversion of *cis* to *trans* isomerisation.

All the synthesized compounds shown in **Figure 3.8** were dissolved in chloroform at room temperature without being exposed to UV light to see if all the compounds absorbed at the same wavelength. Literature suggests that the N=N bond is the most active, allowing free rotation of the molecule for isomerization to occur hence the wavelength absorption of the compounds shown no significant difference.[1,16]

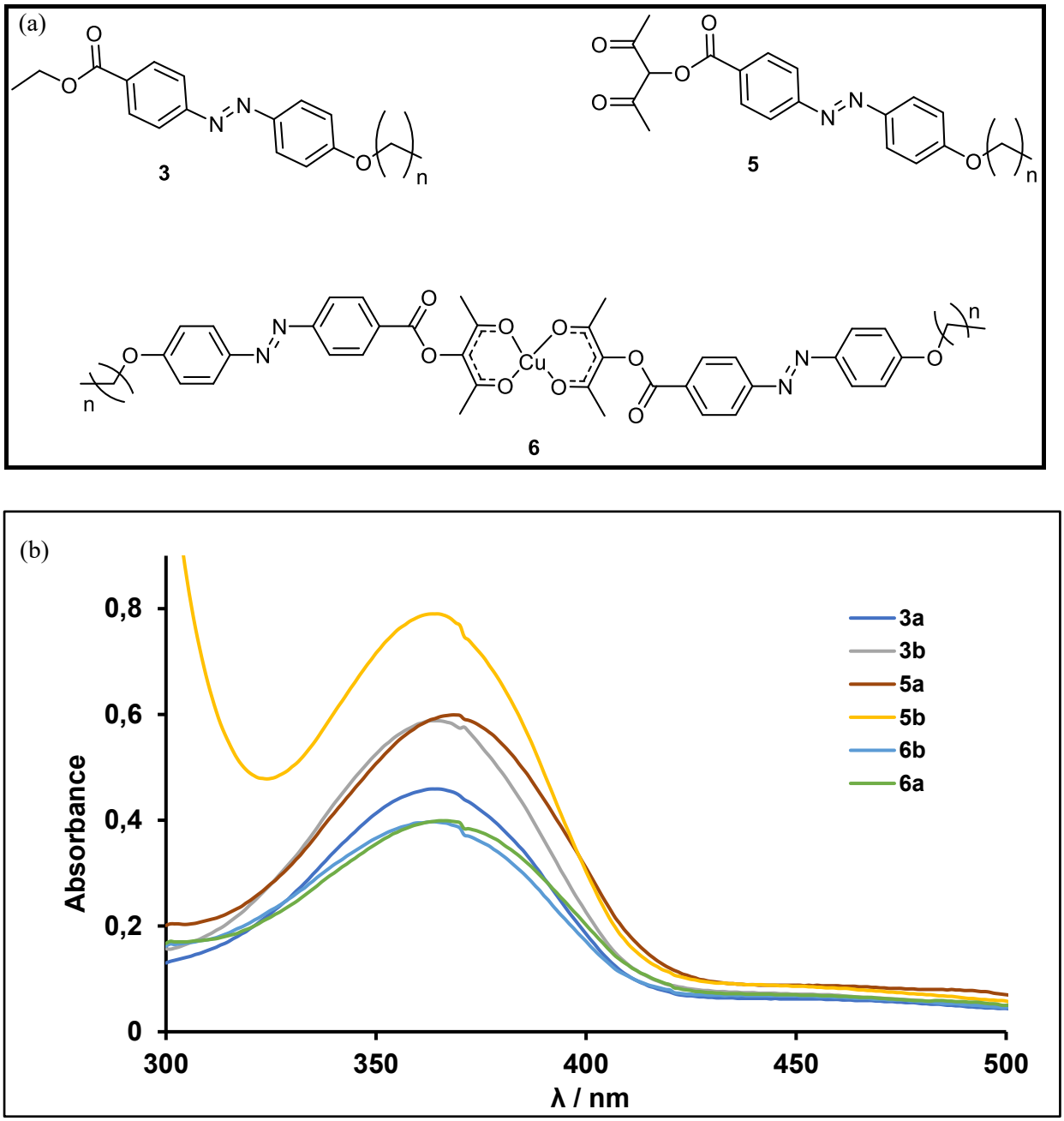

Figure 3.8: (a) Structures of the compound 3, 5 & 6. (b) UV-Vis spectra of all synthesized compounds dissolved in $CHCl_3$.

The photoisomerization from *cis* % content was determined by ^{1}H NMR spectroscopy. The samples were irradiated at 365 nm to alter the *trans* to *cis* photoisomerization (**Figure 3.9**).^{1}H NMR spectra of compound 3a in $CHCl_3$-d, before irradiation (bottom spectra) *trans*-isomer and after 10 mins irradiation at 365 nm (top spectra) mixture of *trans*-and-*cis* isomers with the *cis* peaks shown by the black arrow. The red letters A, B and C represent the aromatic hydrogens in the *trans* spectra (bottom), whereas the black letters D, E, F, G, H, and I represent the aromatic hydrogens of the *cis* spectra (top) To determine the *cis* content, the relative integration signal assigned to both isomers in the aromatic region were examined and signals in other regions overlap. In this case, H and I were not included in the analysis because the overlap of the alkyl chain of both isomers.

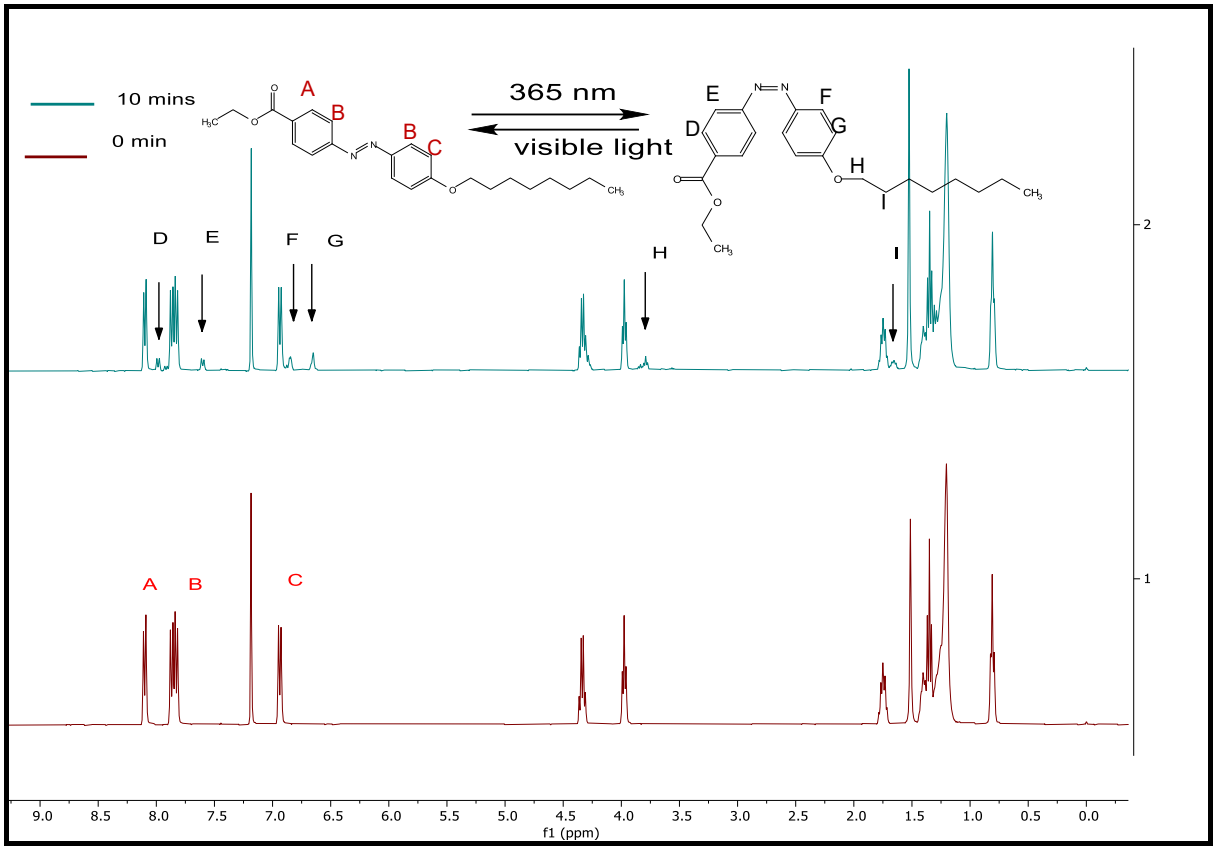

Figure 3.9: ^{1}H NMR spectra of compound **3a** in $CHCl_3$-d, before irradiation (bottom spectra) *trans*-isomer and after 10 mins irradiation at 365 nm (top spectra) mixture of *trans*-and-*cis* isomers with the *cis* peaks shown by the black arrow.

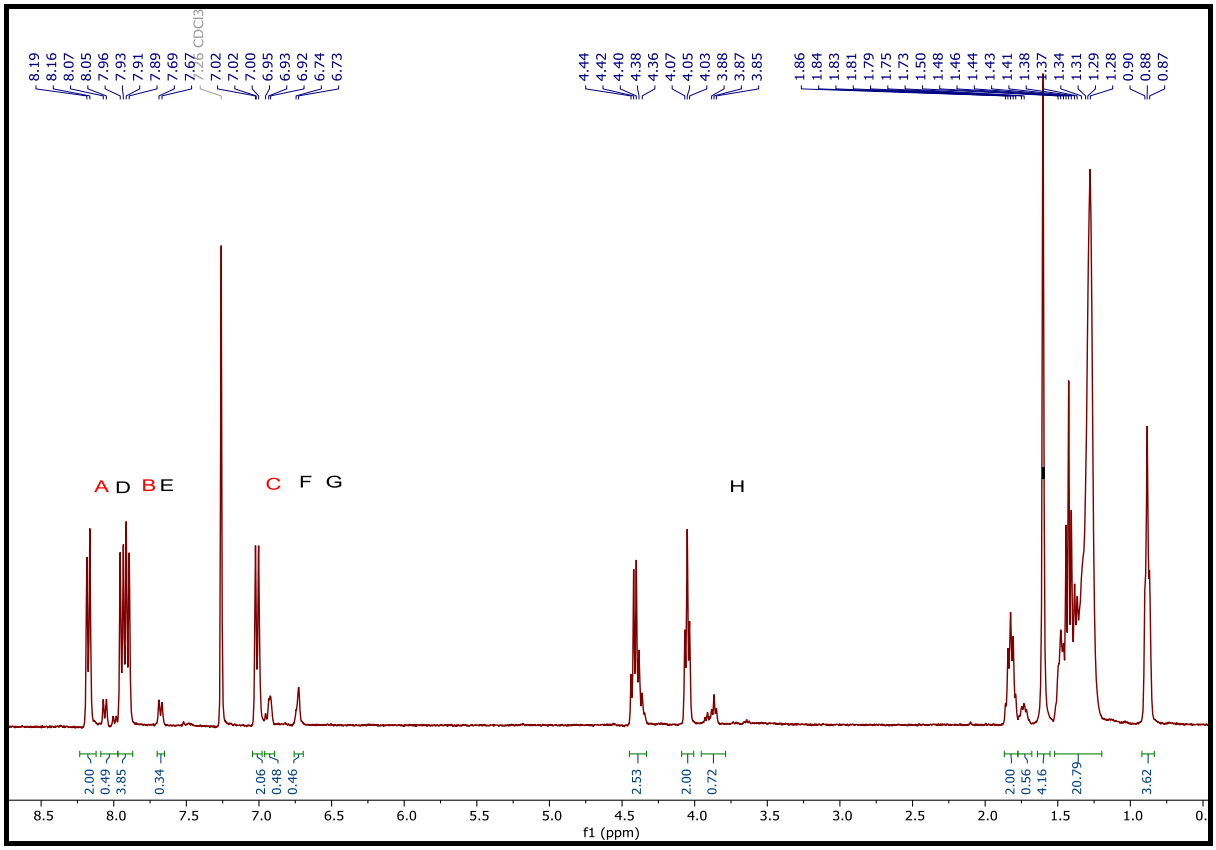

Figure 3.10: Expansion of the ^{1}H NMR spectra of compound 3a showing the integration of both the *trans* and *cis* isomers.

The *cis %* content was determined by ^{1}H NMR and calculated using the equation:[15] *Cis* % = $\frac{Acis}{Atrans+Acis} \times 100\%$ (**Equation 3.1**). The integration values were divided by the number of hydrogens that each signal was had (**Figure 3.10**). For example, peaks at A with a relative integration of 2.00 was divided by the 2 representing 2H per signal/peak, to give a value of 1H integration per H. These values were determined for all the signals associated with *trans* and *cis* isomers. The average intensity of a 1H signal for each isomer was determined in this way, this allowed all the available integration values to be used for the average without concern for having an equal amount of proton signals from the *trans* and *cis* isomers. From the two averages the ratio between the geometric forms or the percentage of either *cis* or *trans* isomer can easy be calculated. **Table 3.1** shows that after irradiation the *trans* isomer was determined to be 76.3% and the *cis* isomer was 23.7%. at room temperature.

Table 3.1: Calculation of the *trans* and *cis* isomer content from integration (%) after being exposed to UV light (365 nm) for 10 mins.

	***Trans* isomer**			***Cis* isomer**	
Peaks	Integration H per signal	Integration per H	peaks	Integration H per signal	Integration per H
A	2.00 (2H)	1.00	D	0.490 (4H)	0.123
B	3.85 (4H)	0.963	E	0.340 (2H)	0.170
C	2.06 (2H)	1.03	F	0.480 (1H)	0.480
			G	0.460 (1H)	0.480
average	Integration per H	0.998	average	Integration per H	0.310
	$\%trans$ $\frac{0.998}{0.998+0.310} \times 100$ =76.3%			$\%cis$ $\frac{0.310}{0.310+0.998} \times 100$ =23.7%	

All the synthesized molecules were calculated using the method in **Table 3.1** above. Each compound's isomers content (%) is shown in **Table 3.2** below. As mentioned above that all the synthesized compounds absorb at approximately the same wavelength therefore their photostability state and isomerization should be comparable. As shown in **Table 3.2**, looking at the trend from compound **3a** and **3b,** the *trans* isomer (%) decreased by approximately 3% meaning that as the chain increases, there is little to no significance on the *trans* to *cis* photoisomerization of the compound. However, the more conjugated the compound is, the more time it takes to isomerize as the compound is bulky and heavier as shown by the trend from compound **3a**, **5a** and **6a** respectively that there is approximately a 10% difference in the photoisomerization from *trans* to *cis* in 10 minutes of being exposed to UV light.

Table 3.2: *trans* and *cis* content (%) after UV irradiation from ^{1}H NMR integrals.

Compounds	***trans* isomer (%)**	***cis* isomer (%)**
3a	76. 3	27.7
3b	74.6	25.4
5a	86.2	13.8
5b	88.7	11.3
6a	95.3	4.7
6b	96.5	3.5

3.2.2 Kinetic parameters for the trans-cis isomerization

The more stable state thermodynamically for azobenzene is its *trans*-conformation. The absorption of light drives the *trans*-to-*cis* switching.[17] The *cis* isomer is more attractive for many applications due to its long-term stability.[9,18] The need for a more stable *cis* isomeric azobenzene has led to several approaches to prolong the *cis* lifespan. metal organic frameworks, crystalline material and azobenzene coordinated with metal centres are some of the approaches used to increase the life span of the *cis* isomer.[19,20] In this study, it has been shown that there is a decrease in the thermal isomerization for bulkier substituted azobenzene compounds by ^{1}H NMR spectroscopy. The lifetime of these compounds was studied by UV/Vis spectroscopy.

The thermal *trans* to *cis* isomerization kinetics of substituted azobenzene is not influenced by the *cis* isomer concentration, meaning that the amount of time the sample is exposed to radiation before the kinetics calculations does not have an impact.[13,21] Utilising Compound 3a (in chloroform), the kinetic parameters of the compounds were determined through plots of *trans*-*cis* isomerization, UV-Vis absorbance vs wavelength for *cis* forward reaction – formation of *cis* isomer (*trans*-to-*cis*) and reverse reaction – *cis* isomer reverting back to *trans* isomer (*cis*-to-*trans*) photoisomerization at 365 nm (**Figure 3.11a**), and pseudo kinetic first order plot for half-life determination against time (**Figure 3.11b**).

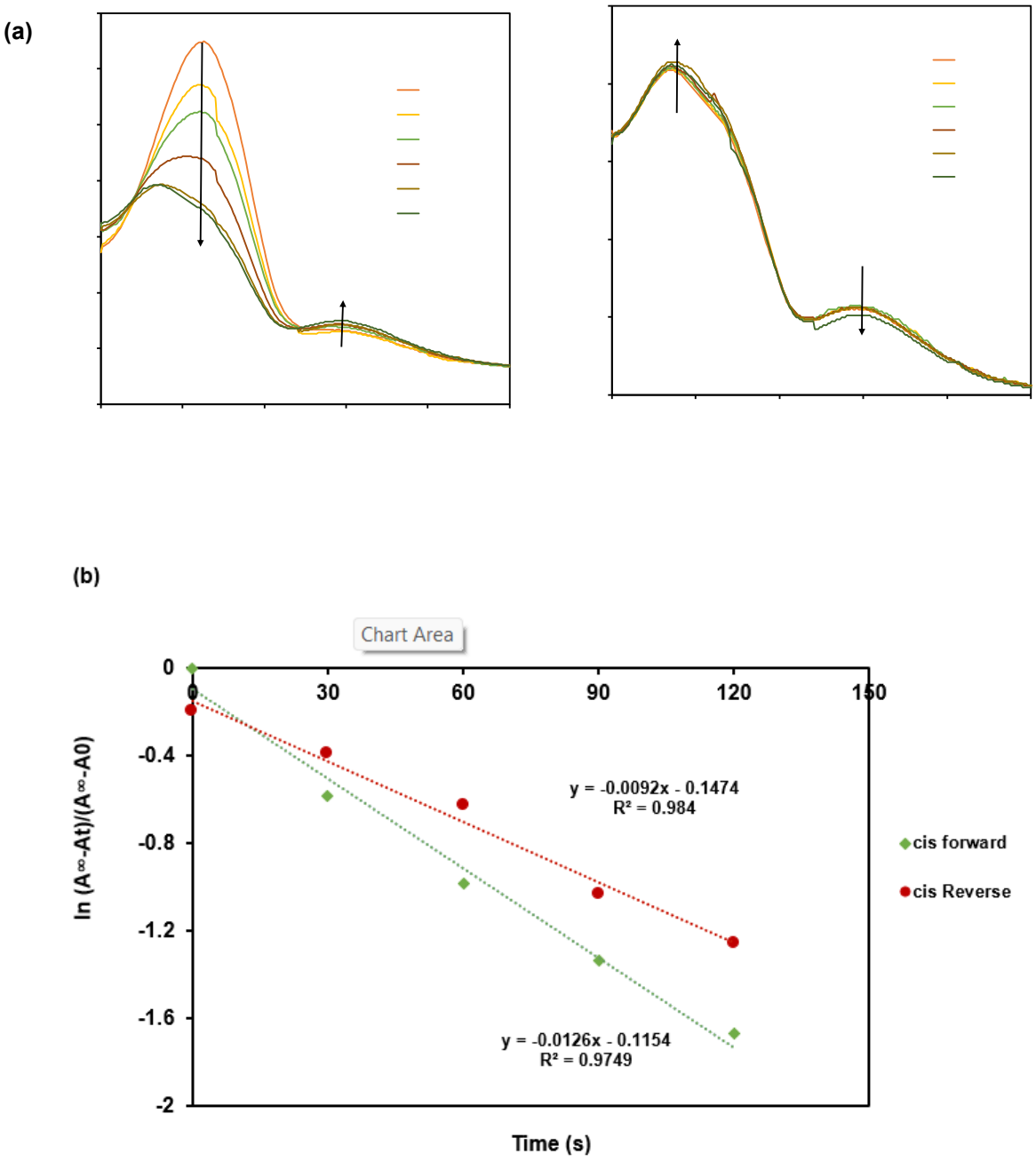

Figure 3.11: Compound 3b (in chloroform) plots of *trans-cis* isomerization, UV-Vis absorbance vs wavelength for (a) forward, (b) reverse photoisomerization at 365 nm (6W) and (c) pseudo kinetic first order plot for half-life determination.

The calculated half-life of *cis* isomers ranges from 49 to 63 seconds (forward – *trans* to *cis*) and 160 to 915 seconds (reverse – *cis* to *trans*) indicating stability over the long run, back-conversion from *cis* to *trans* was high enough to allow for long-term storage and the photoactive materials in this study exhibit cyclability (*trans-cis* and *cis-trans*) performance.[14] We have observed that increasing the alkyl chain has no significant impact on the isomerization of the compounds. The rate constants measured for all the compounds (**Figure 3.11b**) for the forward *cis* isomerization were slightly different (0.11 – 0.14 s^{-1}) and for the reverse *cis* isomerization, the average rate constant for the **3a**, **5a** and **6a** were 1.58 $\times 10^{-3}$ s^{-1}, 3.16 $\times$ 10^{-3} s^{-1} and 6.04 $\times$ 10^{-3} s^{-1}, respectively. This means that the *cis-trans* isomerization is slower that the *trans-cis* isomerization. The calculated activation energy for all the synthesized compounds ranges from approximately 33400 to 364500 J/mol for both the forward and reverse *cis* isomerization. The values obtained are smaller than 104600 J/mol obtained by Yu *et. al*.[22] This activation energy barrier is important as it separates the *trans* to the *cis* isomer. The half-life, isomerization rate constants and activation energy are summarised in **Table 3.3**.

Table 3.3: *cis* forward (*trans-to-cis*) and *cis* reverse(*cis-to-trans*) conversion rate constant (K_{obs} in s^{-1}) and half-life and the activation energy (ΔE_a in $J.mol^{-1}$) of all synthesized compounds.

compounds	***cis* forward (Kobs) s^{-1}**	***cis* reverse (Kobs) s^{-1}**	**$t_{1/2}$ (sec) *cis* forward**	**$t_{1/2}$ (sec) *cis* reverse**	**ΔEa (J/mol) *cis* forward**	**ΔEa (J/mol) *cis* reverse**
3a	0.014	1.64×10^{-3}	49.511	422.651	33560.93	35700.31
3b	0.014	1.64×10^{-3}	49.511	422.651	33560.93	35700.31
5a	0.012	7.58×10^{-4}	57.762	914.442	33714.71	36470.28
5b	0.013	7.58×10^{-3}	57.762	914.442	33714.71	36470.28
6a	0.011	2.0×10^{-3}	63.013	346.921	33801.52	35503.31
6b	0.011	2.0×10^{-3}	63013	346.921	33801.52	35503.31

3.2.3 Tauc plots and TD-DFT calculations

Band gap energies and optical properties are very important parameters for solar energy studies.[23] The band gap (E_g) has a direct correlation with the suitability of materials for use in optical, electronic, and energy applications.[24] Major parts of electronic, optoelectronic, and photovoltaic devices are semiconducting inorganic materials with band gaps ranging from 0 to 5 eV.[24,25] Large band-gap databases are helpful in choosing the best materials for each application because the band gap is the main material property that affects the device performance. Semiconductors with a band gap less than 3 eV are used in power electronics to maintain high electric fields.[24,25] The band gap energy of azobenzene is about 3 eV for the *trans* isomer and around 2 eV for the *cis* isomer.[13]

The band gap of all synthesized compounds (isomers) was obtained both experimentally by Tauc plots from the UV-Vis data (dissolved in $CHCl_3$) and theoretically by Time-dependent density functional theory (TD-DFT). The highest occupied molecular orbital (HOMO) and the lowest occupied molecular orbital (LUMO) energy values obtained by TD-DFT can be used to define a molecule's capacity to donate and receive electrons.[26–28]

The band gap energies of compounds **3**, **5** and **6** obtained experimentally by UV were similar at 3.57 eV for the *trans* isomers and around 2.4 eV for the *cis* isomers as shown in **Figure 3.12** showing compound **3** as an example. Many uses, including solar energy applications, can benefit from the notable variation in the band gap energies of the *cis* and *trans* isomers. The *cis* isomer is more energy-efficient than the *trans* isomer because it has a lower band gap energy. The bandgap of a material influences its energy efficiency by affecting how it interacts with light and how electrons move within the material. In solar thermal fuel cells, a smaller bandgap allows the material to absorb higher-energy photons (light particles). This means that materials with smaller band gaps can harness light from a broader spectrum, including ultraviolet and visible light, which can increase the efficiency of the solar cell.[29] The band gap energy of the *cis* isomer of a series of azobenzene derivatives was smaller than that of the *trans* isomer (**Table 3.4**). Furthermore, the TD-DFT calculated results using the basis set B3LYP/6-31G(d) shows that the electron densities from the HOMO and LUMO are localised upon the benzene rings and the azo linkage (**Figure 3.13a**). The DFT results shows that *trans* isomers of the ligands have band gap energies of around 3.5 eV and 2.4 eV for the *cis* isomers as shown by the molecular orbital diagram (**Figure 3.13b)** which is in agreement with the Tauc plots from UV-Vis experiments.

(a)

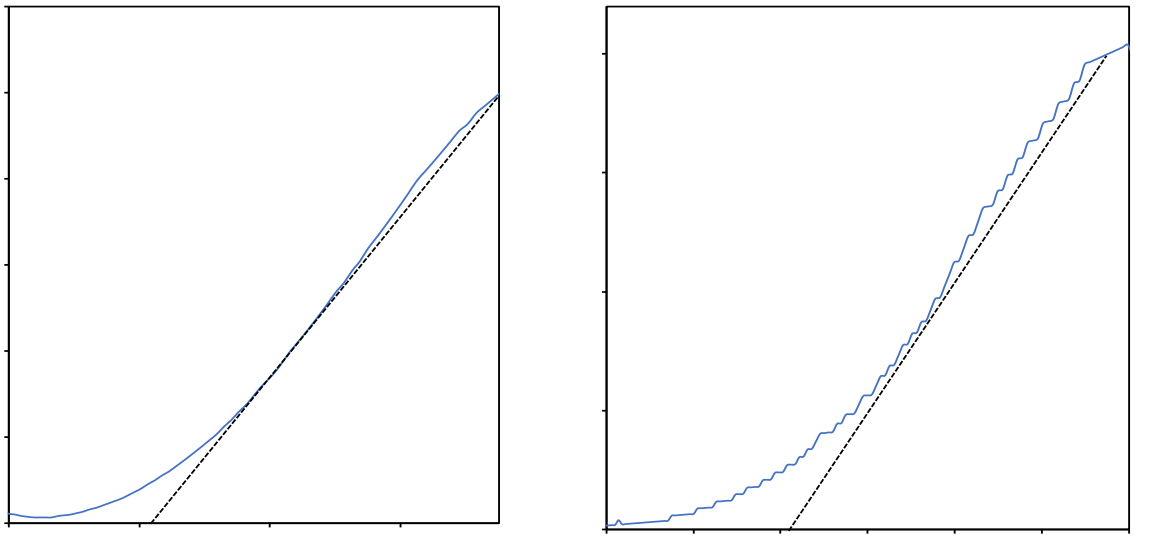

(b)

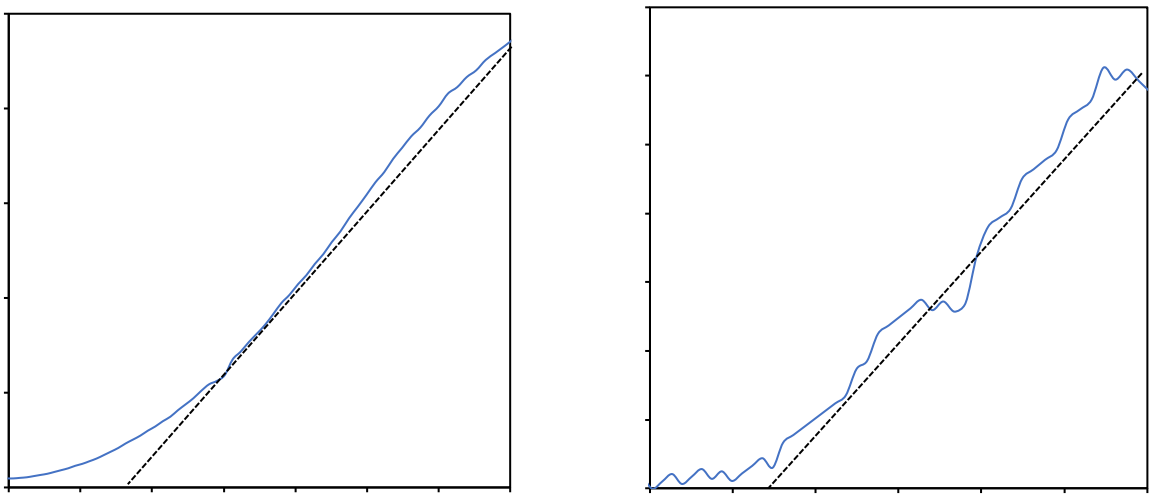

Figure 3.12: Determination of band gap energy of compound **3b** dissolved in $CHCl_3$ by Tauc plots from UV-Vis experiments (a) *cis* forward and (b) *cis* reverse reaction.

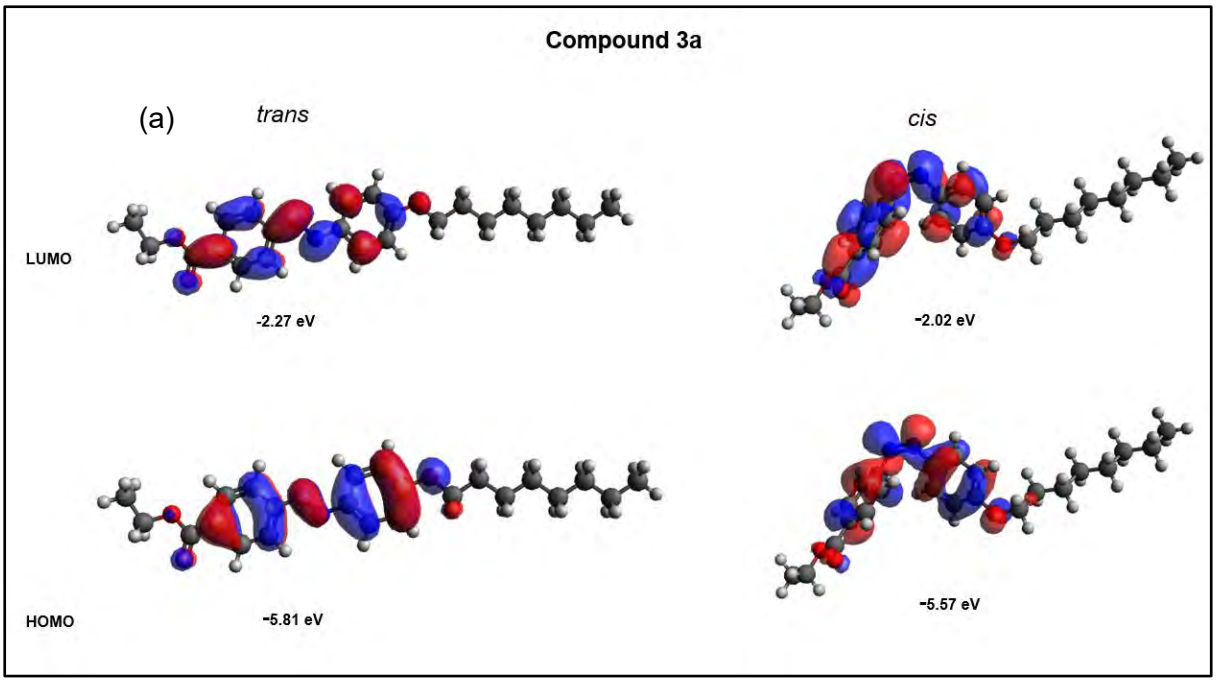
Compound 3a
(a)
trans
cis
LUMO
-2.27 eV
-2.02 eV
HOMO
-5.81 eV
-5.57 eV

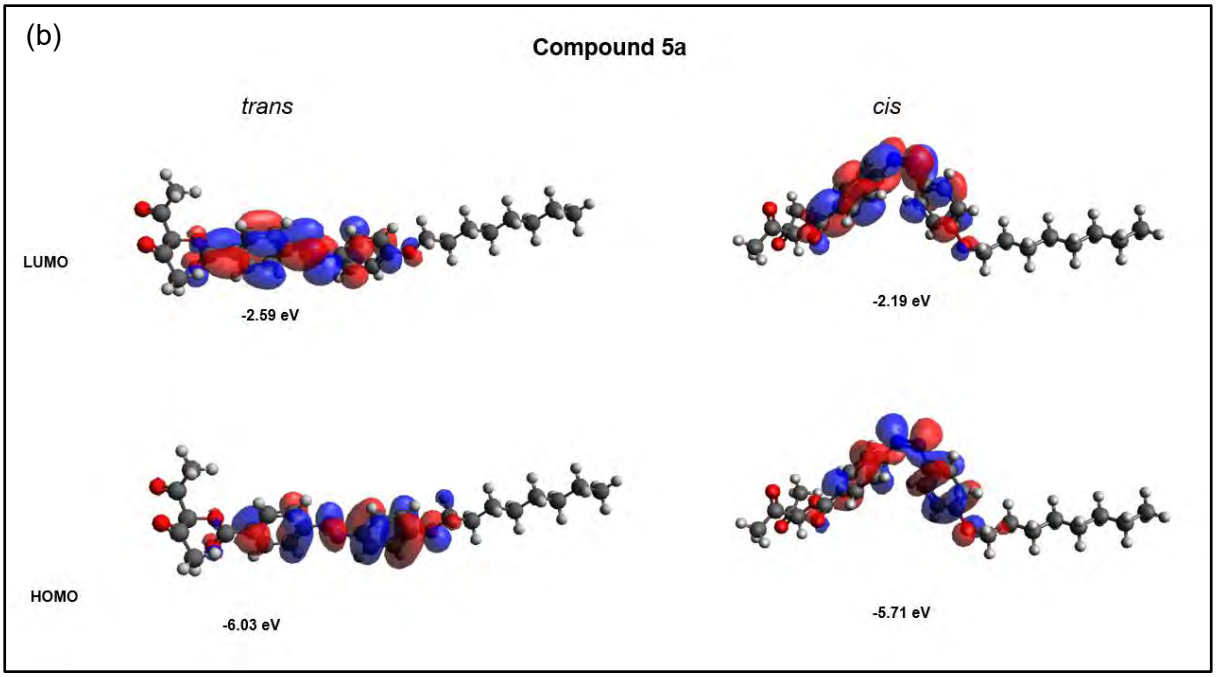
(b)
Compound 5a
trans
cis
LUMO
-2.59 eV
-2.19 eV
HOMO
-6.03 eV
-5.71 eV

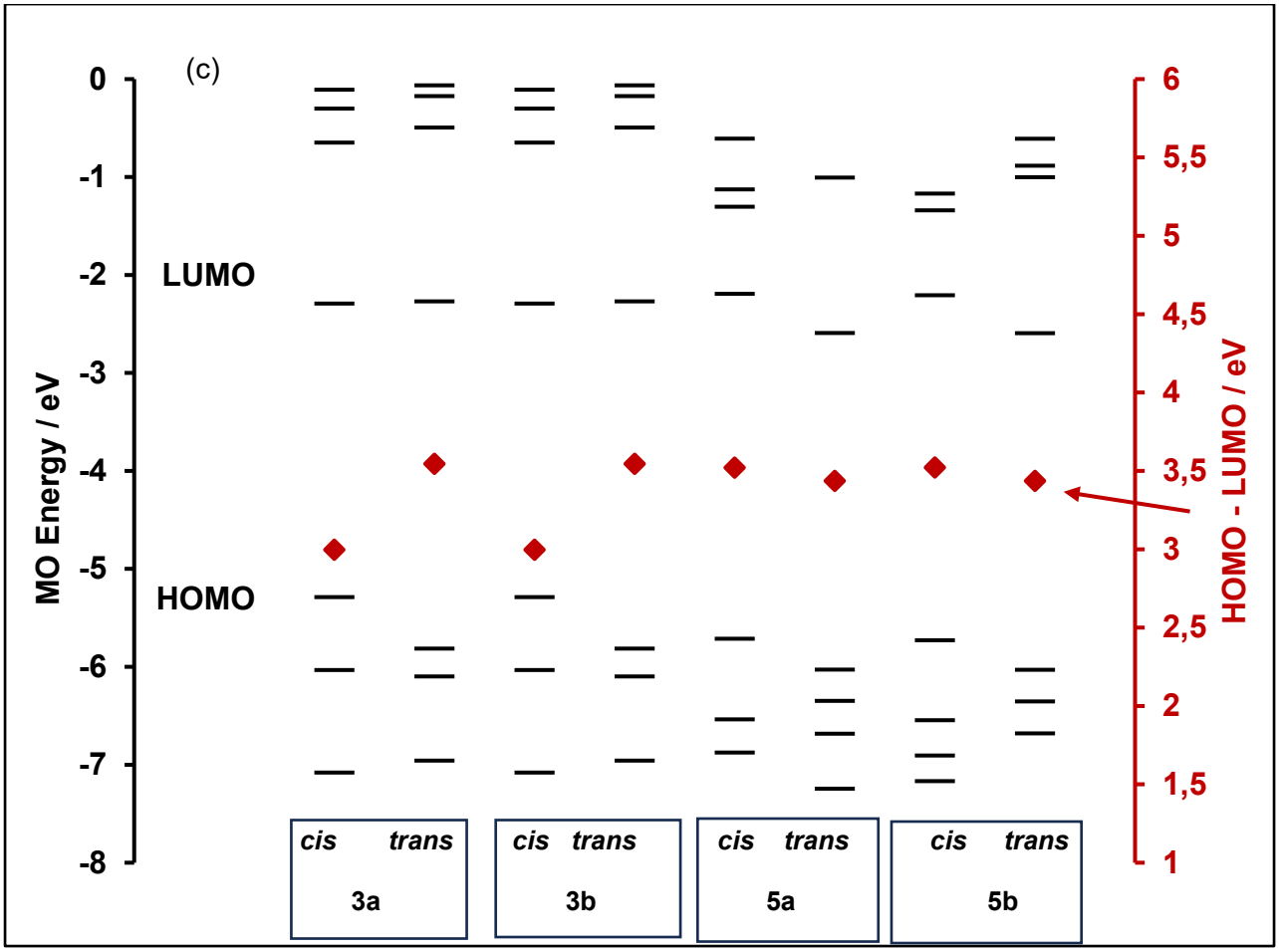

Figure 3.13: HOMO-LUMO for azobenzene ligands, showing the electron density between *cis* and *trans* isomers of (a) compound **3a** and (b) compound **5a**, and (c) MO energies at B3LYP/6-31G(d) level of theory. The HOMO and LUMO are highlighted with thick black lines, and the HOMO−LUMO gap values are highlighted with red diamonds and plotted against a secondary axis.

Attaching a metal has an impact on the band gap energies of the azobenzene. Because of their numerous intriguing features, copper oxides have been identified as possible materials for several uses in the last ten years.[30,31] Cupric (CuO) and cuprous (Cu2O) oxides are two stable forms of copper oxides that are abundant (natural abundance), stable, non-toxic, and affordable to produce. They have straight band gaps of 1.32 eV and 2.06 eV, respectively.[30,31] Applications for copper oxide films can be found in many areas, such as solar PV cells, energy, and magnetic storage media. Their high theoretical specific capacity, native p-type conductivity, and large hole mobility are the reasons for this. Additionally, they offer superior optical, thermal, electrical, and photocatalytic qualities.[30,31]

In this work, the TD-DFT calculated results of the -diketonato copper (II) metal complex, compound **6**, had band gap energies of around 1.78 eV for the *trans* isomer and 1.47 eV for the *cis* isomer. When comparing the HOMO and LUMO electron densities of the ligands

(compound **3** and **5**) to the complexes (compound **6**), we can observe that the electron density of both the ligands and the complexes is around the benzene rings and the azo linkage group. Nevertheless, the complexes show a push and pull of electrons on the benzene rings and azo linkage from the opposite sides of the copper metal. The general pull of electron clouds away from the ligand substituents (towards the copper atom center) is typical for transition metal complexes, the copper(II) complex is stabilized by synergic *sigma*- and *pi*-donation of electrons, from the ligand and metal, respectively.[6,7]

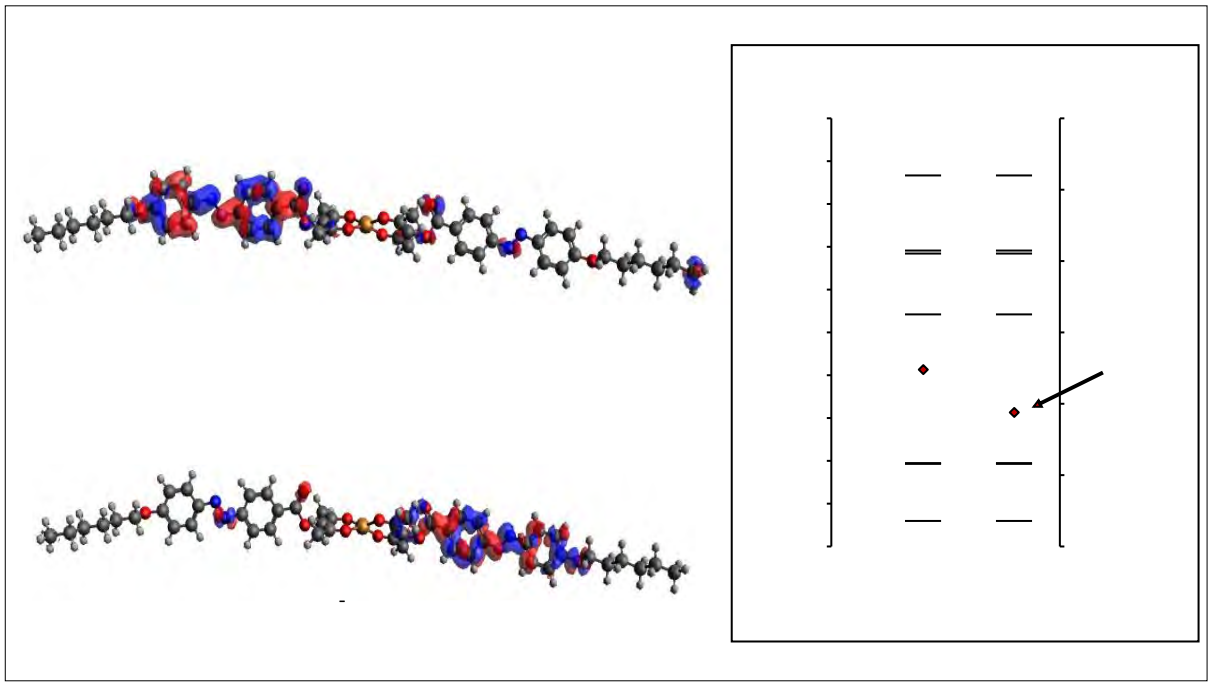

Figure 3.14: MO energies at B3LYP/6-31G(d) level of theory for synthesised azobenzene complex, compound 6a. The HOMO and LUMO are highlighted with thick black lines, and the HOMO−LUMO gap values are highlighted with red diamonds and plotted against a secondary axis.

Table 3.4: Band gap energies obtained by experimentally by Tauc plots for the synthesised compounds.

compounds	**Experimental (eV)**		**Theoretical (eV)**	
	trans	***cis***	***trans***	***cis***
3a	3.57	2.41	3.54	2.99
3b	3.55	2.42	3.55	2.97
5a	3.58	2.78	3.57	3.42
5b	3.54	2.78	3.56	3.42
6a	3.43	2.73	1.48	1.26

6b	3.54	2.75	1.47	1.26

In Summary, the synthesis of azobenzene precursors with different alkyl chain lengths was successfully achieved, with functionalization using β-diketone and β-diketonato copper (II) complex. The photophysical properties of the synthesized compounds were studied with UV-Vis spectroscopy determining *trans-cis* isomerization, ^{1}H NMR spectroscopy determining photostationery states, and UV-Vis spectroscopy determining kinetic properties.

3.3 References

1. Marturano, V., Ambrogi, V., Bandeira, N., Tylkowski, B., Giamberini, M. & Cerruti, P. Modelling of Azobenzene-Based Compounds. *Physical Sciences Reviews*, **2**, (2017).
2. Tiberio, G., Muccioli, L., Berardi, R., & Zannoni, C. How does the trans–cis photoisomerization of azobenzene take place in organic solvents? *ChemPhysChem,* **11**, 1018-1028 (2010).
3. Hanabusa, K., Isogai, T., Koyama, T. & Shirai, H. Synthesis and properties of thermotropic liquid-crystalline polymers linked through bis (P-diketonato) copper (II) complex. *Makromol. Chem* **210**, 197–210 (1993).
4. Han, J., Zhang, L. F. & Wan, W. Synthesis and liquid crystal behaviors of 2,4-dioxo-3-pentyl 4-decyloxy cinnamate rhodium(I) complexes. *Chin J Chem* **21**, 1521–1524 (2003).
5. Gimenez-Gomez, A. *et al.* A Photochemical Overview of Molecular Solar Thermal Energy Storage. *Photochem* **2**, 694–716 (2022).
6. Hu, J., Huang, S., Yu, M. & Yu, H. Flexible Solar Thermal Fuel Devices: Composites of Fabric and a Photoliquefiable Azobenzene Derivative. *Adv Energy Mater* **9**, (2019).
7. Huang, G., Curt, S. R., Wang, K. & Markides, C. N. Challenges and opportunities for nanomaterials in spectral splitting for high-performance hybrid solar photovoltaic-thermal applications: A review. *Nano Materials Science* **2**, 183–203 (2020).
8. Konieczkowska, J., Wasiak, A., Sobolewska, A., Bartkiewicz, S., Małecki, J. G., & Schab-Balcerzak, E. Kinetics of the dark cis–trans isomerization of azobenzene and azo pyridine derivatives in ethanol and chloroform solutions. *J Photochem Photobiol A Chem* **444**, (2023).
9. Konieczkowska, J. *et al.* Kinetics of the dark cis–trans isomerization of azobenzene and azo pyridine derivatives in ethanol and chloroform solutions. *J Photochem Photobiol A Chem* **444**, (2023).
10. Saydjari, A. K., Weis, P. & Wu, S. Spanning the Solar Spectrum: Azopolymer Solar Thermal Fuels for Simultaneous UV and Visible Light Storage. *Adv Energy Mater* **7**, (2017).
11. Purdes, A. J., Liu, Z. F., Morigaki, K., Enomoto, T., Hashimoto, K., & Fujishima, A. Kinetic studies on the thermal cis-trans isomerization of an azo compound in the assembled monolayer film. *The Journal of Physical Chemistry* **96**, 1875-1880 (1992).
12. Kucharski, T. J., Tian, Y., Akbulatov, S. & Boulatov, R. Chemical solutions for the closed-cycle storage of solar energy. *Energy and Environmental Science* vol. 4 4449–4472 Preprint at https://doi.org/10.1039/c1ee01861b (2011).

13. Mogale, R., Conradie, J., & Langner, E. H. Trans–cis kinetic study of azobenzene-4, 4′-dicarboxylic acid and aluminium and zirconium based azobenzene-4, 4′-dicarboxylate MOFs. *Molecules*, **27**, 1370 (2022).
14. Zhang, B., Feng, Y. & Feng, W. Azobenzene-Based Solar Thermal Fuels: A Review. *Nanomicro Lett* **14**, (2022).
15. Chen, H. *et al.* Water-Soluble Azobenzene-Based Solar Thermal Fuels with Improved Long-Term Energy Storage and Energy Density. *ACS Appl Mater Interfaces* (2023) doi:10.1021/acsami.3c12264.
16. Bandara, H. M. D. & Burdette, S. C. Photoisomerization in different classes of azobenzene. *Chem Soc Rev* **41**, 1809–1825 (2012).
17. Interfaces, F., Interfaces, F. & Chemistry, O. Cis -to- Trans Isomerization of Azobenzene Investigated by Using Thin Films of Metal- Organic Frameworks. (2015).
18. Kuroda, Y., Miyazaki, R., Shimonishi, D., Nakane, D. & Akitsu, T. Coordination and Photoisomerization of Azobenzene-Amino Acid Schiff Base Copper(II) Complexes to Lysozyme. *Journal of Materials Science and Chemical Engineering* **11**, 34–44 (2023).
19. Espinet, P., Esteruelas, M. A., Oro, L. A., Serrano, J. L. & Sola, E. Transition metal liquid crystals: advanced materials within the reach of the coordination chemist. *Coord Chem Rev* **117**, 215–274 (1992).
20. Serrano, J. L. (Ed.) Metallomesogens: synthesis, properties, and applications. *John Wiley & Sons*, (2008).
21. Han, M., Ishikawa, D., Honda, T., Ito, E., & Hara, M. Light-driven molecular switches in azobenzene self-assembled monolayers: effect of molecular structure on reversible photoisomerization and stable cis state. *Chemical Communications*, **20**, 3598-3600 (2010).
22. Yu, X., Wang, Z., Buchholz, M., Füllgrabe, N., Grosjean, S., Bebensee, F., & Heinke, L. cis-to-trans isomerization of azobenzene investigated by using thin films of metal–organic frameworks. *Physical Chemistry Chemical Physics*, **17**, 22721-22725 (2015).
23. Gomha, S. M. *et al.* New nematogenic conical-shaped supramolecular H-bonded complexes for solar energy investigations. *Sci Rep* **11**, (2021).
24. Gorai, P., McKinney, R. W., Haegel, N. M., Zakutayev, A. & Stevanovic, V. A computational survey of semiconductors for power electronics. *Energy Environ Sci* **12**, 3338–3347 (2019).
25. Kim, S. *et al.* A band-gap database for semiconducting inorganic materials calculated with hybrid functional. *Sci Data* **7**, 1–6 (2020).
26. Abdul, M., Kumar, T. & Alam, A. Since January 2020 Elsevier has created a COVID-19 resource centre with free information in English and Mandarin on the novel coronavirus

COVID- 19 . *The COVID-19 resource centre is hosted on Elsevier Connect , the company ' s public news and information* . (2020).

27. Beyramabadi, S. A. *et al.* Spectroscopic (Ft-Ir, Nmr, Uv-Vis, Fluorescence) and Dft Studies (Molecular Structure, Ir and Nmr Spectral Assignments, Nbo and Fukui Function) of Schiff Bases Derived from 2-Chloro-3-Quinolinecarboxaldehyde. *Journal of Structural Chemistry* **59**, 1342–1352 (2018).
28. Ebrahimi, H., Hadi, J. S. & Al-Ansari, H. S. A new series of Schiff bases derived from sulfa drugs and indole-3-carboxaldehyde: Synthesis, characterization, spectral and DFT computational studies. *J Mol Struct* **1039**, 37–45 (2013).
29. Hu, J., Huang, S., Yu, M. & Yu, H. Flexible Solar Thermal Fuel Devices: Composites of Fabric and a Photoliquefiable Azobenzene Derivative. *Adv Energy Mater* **9**, 1–10 (2019).
30. Bouachma, S. *et al.* Synthesis of PSi-n/CuO-p/Cu2O-n heterostructure for CO2 gas sensing at room temperature. *Appl Phys A Mater Sci Process* **128**, 1–13 (2022).
31. Lilova, V., Trifonova, Y., Stoilova, A., Georgieva, S. & Todorov, P. Optical Properties of Pazo Polymer Composite Films Doped with Particles of a Novel Copper Hydantoin Complex. *Journal of Chemical Technology and Metallurgy* **56**, 1192–1196 (2021).

Chapter 4: Thermal properties and liquid crystals studies

The thermal stability of azobenzene derivatives was studied using thermogravimetric analysis (TGA), differential scanning calorimeter (DSC) and polarizing optical microscopy (POM) equipped with a hot stage and a temperature regulator, have been used to study the mesogenic behaviour and thermal properties of compounds. Mesophases develop within a certain temperature range. The compound is be forced into the isotropic phase if the temperature is too high because the thermal motion obliterate the precise ordering of the liquid crystal phase.[1] Most liquid crystal materials produce a conventional crystal if the temperature is too low.[2,3] The aim of this section was to determine the thermal stability of the synthesized azobenzene derivatives by means of TGA, the liquid crystalline phases of the compounds by DSC and POM. The effect of liquid crystallinity by conjugation and metal-functionalisation to the compounds. The enthalpy and energy density stored in the chemical bonds of the compounds was determined by DSC.

4.3 Thermal stability by Thermogravimetric analysis (TGA)

Figure 4.2 below shows the TGA results of compounds **3a**, **5a** and **6a**. In compound **3a** (red line), a notable reduction in weight is noted, with the mass going from 100% to 91.53% at about 283.39 °C. The compound's water molecules are evaporating at the time of this event. This initial weight loss is caused by the elimination of water molecules from the compound, which are either chemically or physically bonded to it at high temperatures. This process is endothermic, which means that to help the liquid phase transition into vapour, it absorbs heat from the environment.[4] A second weight loss event is seen once the water evaporates. At 439 °C, this event results in the compound's full breakdown and a 100% reduction in weight. The chemical structure of the substance is broken down into its component parts or smaller compounds during this decomposition process. The breakdown temperature represents the compound's thermal stability limit, over which irreversible disintegration occurs. This breakdown process is frequently exothermic, which means it transfers heat into the environment.[4]

In compound **5a** (green line), The compound completely breaks down and loses all its weight at 510 °C. During this process of decomposition, the substance's chemical structure breaks down into its constituent parts or smaller compounds as the N=N of core (azo-rings) compound

gradually decreased, original azo and its derivatives typically thermally decompose by forming two free phenyl radicals and breaking the bonds next to N=N.[5,6] After 510 °C the β-diketones decomposed. The weight in compound **6a** (purple line), The loss of the core was observed between 314 °C and 597 °C. The decomposition of the β-diketone copper(II) metal bonds at 680 °C. As seen in **Figure 4.2**, as the azobenzene derivative (**3a**) is functionalized with a β-diketone (**5a**), its thermal stability increases but when coordinating with a metal (**6a**), the thermal stability decreases from above 800 °C to 680 °C. The compounds (**3a**,**5a** and **6a**) are capable of being used for most low and medium temperature solar energy applications as azobenzene derivatives since there is improvement in thermal stability from **3a** to **6a**, suggesting that these compounds are not appropriate for high temperature applications.[5]

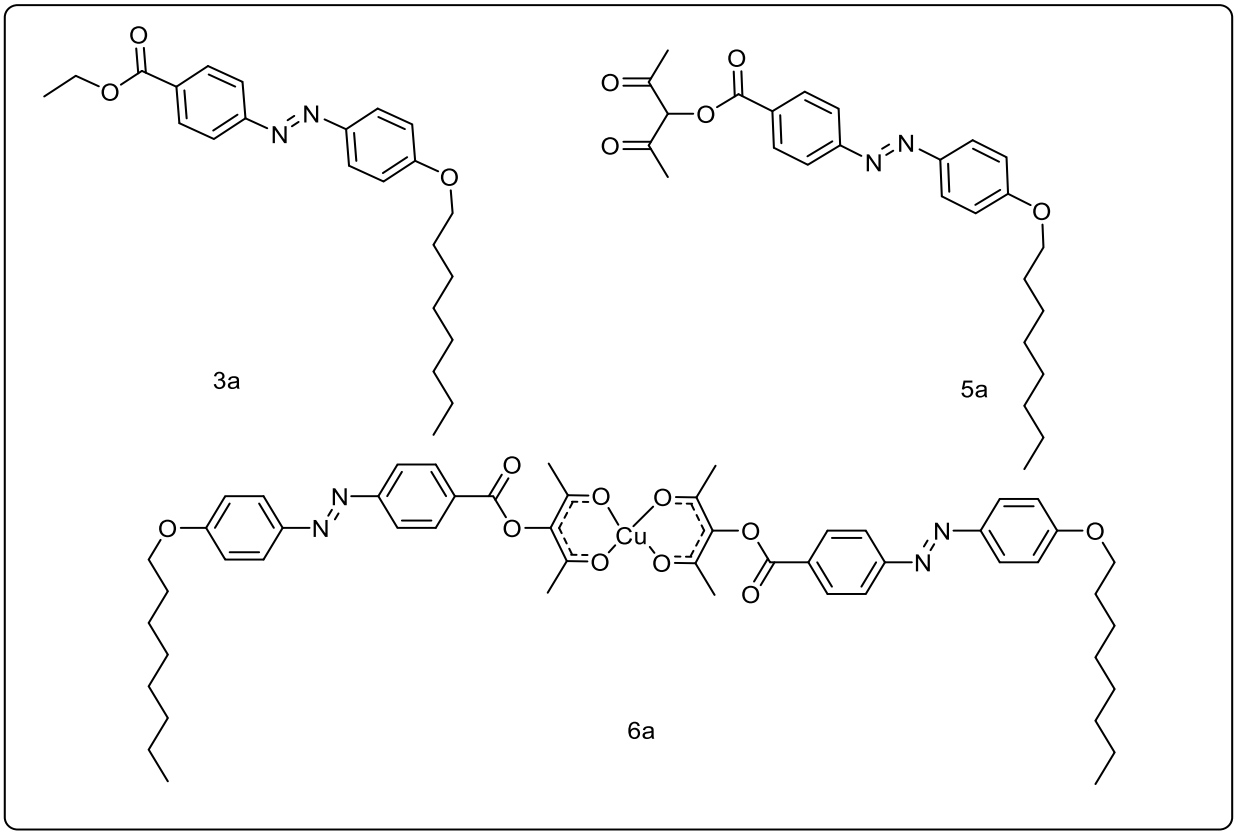

Figure 4. 1: Compounds **3a** (red), **5a** (green) and **6a** (purple) showing thermal decomposition.

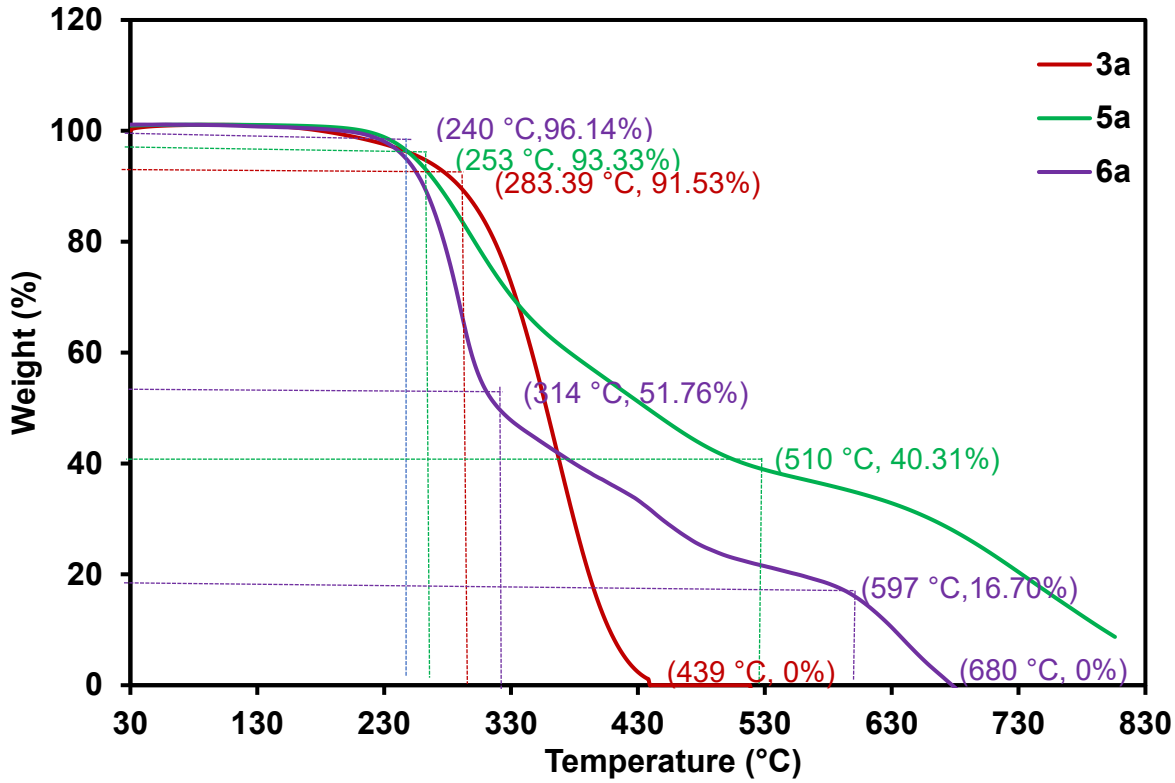

Figure 4.2: Thermal degradation (TGA) of compound **3a**, **5a** and **6a** between 30 °C–900 °C at 10 °C per minute under nitrogen atmosphere.

4.2 Thermal analysis by DSC and POM

4.2.1 Alkyl chains compounds

Figure 4.3 shows the DSC thermograms of compound **3a** and **3b** ligands, which were recorded at a heating and cooling rate of 10 °C min-1 (**3a** and **3b** correspondingly). These thermograms provide insight into the energy dynamics associated with heating and cooling processes, specifically pertaining to the compound's phase transitions. Examination of DSC shows two endothermic peaks and two exothermic peaks illustrating that compound **3a** and **3b** exhibit similar phase transition. **Figure 4.3** illustrates that as the alkyl chain length is increased, the stability of the phase transition is decreasing. For instance, in the DSC measurements of compound **3a**, A clear endothermic peak at 86°C signifies the phase change. This change indicates the compounds' transition from a crystal phase to a nematic liquid crystal phase. The peak's endothermic nature indicates that heat must be absorbed to break the ordered crystal lattice structure and cause molecular reorganisation into the less ordered but still anisotropic liquid crystalline phase. The compounds' reaction to heat energy is reflected in this transition, which frequently suggests modifications in molecule mobility and orientation.[7] A second thermal event with a smaller, more pronounced endothermic peak is seen at 104 °C. The

transition of the material from a nematic liquid crystalline phase to an isotropic liquid phase is represented by this peak. The endothermic nature of this transition denotes the absorption of heat required to break the orientational order in the nematic phase, which leads to the shift to a more disordered, isotropic state and the loss of long-range molecule alignment. At this transition, the material exhibits isotropic fluid characteristics and loses its directed molecular organisation.[8]

During cooling, the same phenomena was observed with the cooling peaks occurring at lower temperatures than during heating. The exothermic peaks at 100 °C indicates that the compounds were cooling from an isotropic liquid state to a nematic phase. A second event with a more pronounced exothermic peak is observed at 65 °C. Since the same phenomenon is observed in both heating and cooling, this means that the compounds are enantiotropic liquid crystals. [9]

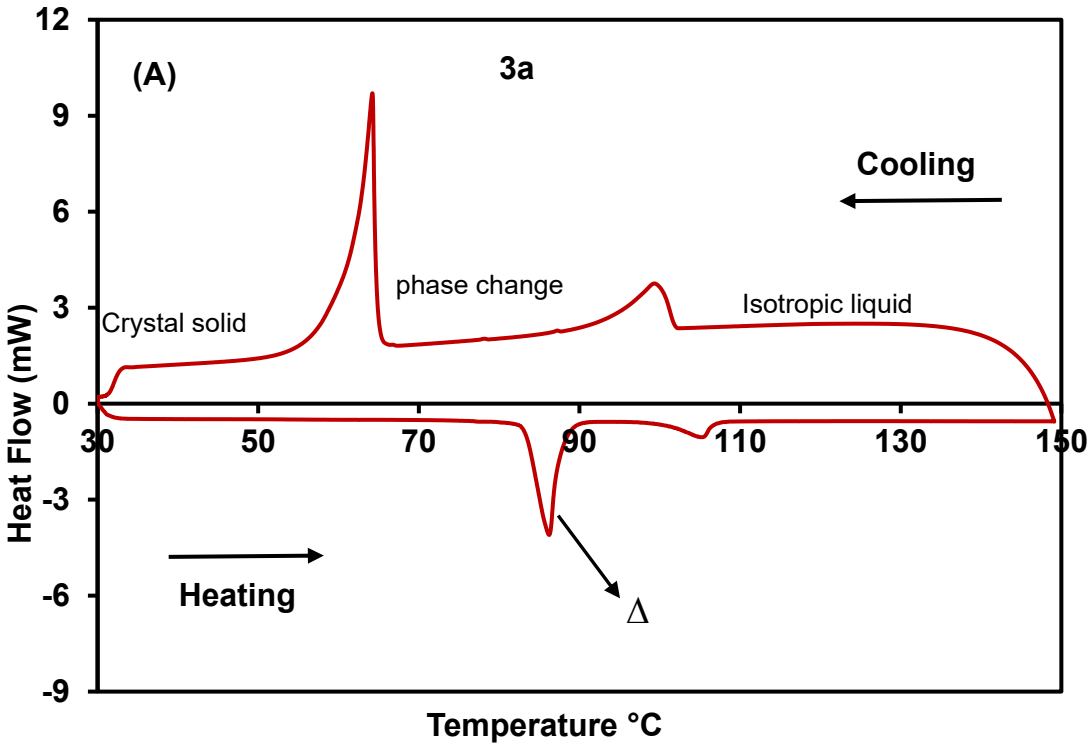

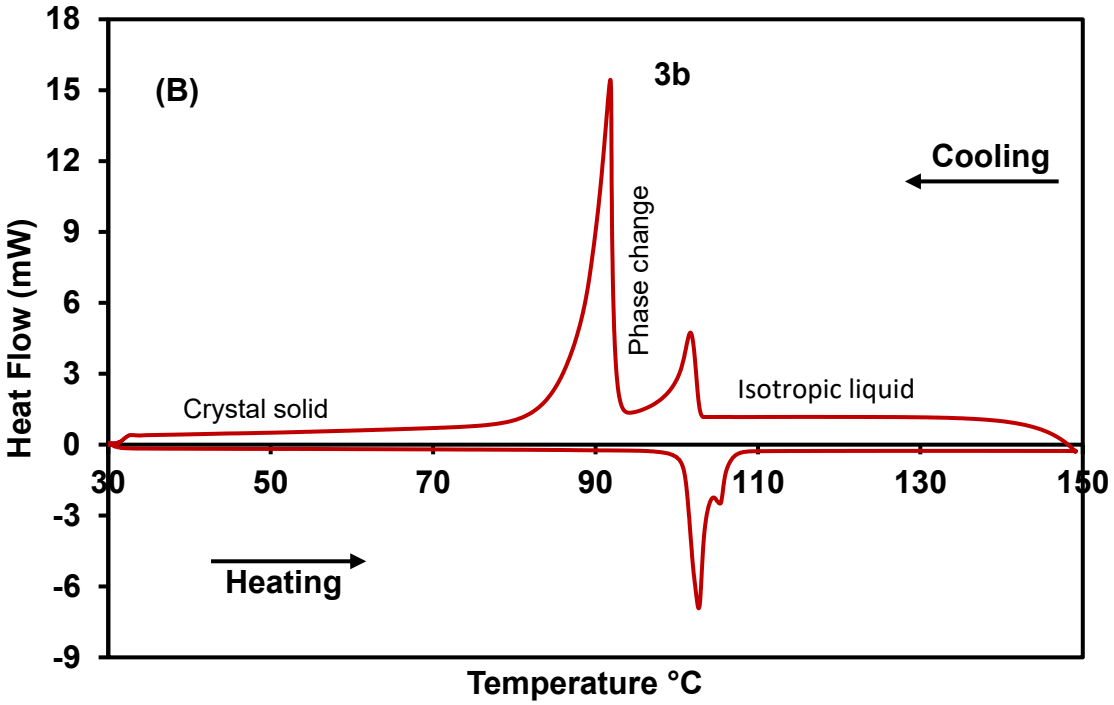

Figure 4.3: DSC thermogram showing phase transitions and enthalpy stored in each peak of (A) compound **3a** and (B) compound **3b** (10 °C.min^{-1}).

Differential scanning calorimetry (DSC) can be used to calculate the storage enthalpy (ΔH), which yields the maximum energy that each molecule can store. As a function of temperature and time, DSC calculates the heat flow through the sample because of variations in the loaded sample's physical and chemical characteristics. [10] The characterization of the first and second endothermic peaks reveals energy storage phenomena, wherein the compound absorbs 82.41 J/g and 16.52 J/g of energy, respectively. Conversely, the observation of two exothermic peaks denotes energy release during phase transitions, with the transitions from the isotropic liquid state to the crystal solid state resulting in the liberation of 16.56 J/g and 69.65 J/g of energy, respectively. The energy released is less than the energy stored due to the isomerization nature of the compounds. The DSC peaks provides information on how much energy is stored when heating and how much energy is released when cooling in which the sum of the enthalpy gives energy density (ED) for the exothermic peaks. Compound **3a** and **3b** have an energy density of 32.95 and 42.86 KJ/mol respectively.

DSC alone is not able to identify the different types of liquid crystalline phases, but the polarized optical microscope (POM) studies allow for the assignment of different phases. POM

Microphotographs of compound 3a shown in **Figure 4.4**, indicate the second heating cycle and the following textures that while heating:

(A) At 85 °C the compound is a crystal solid while melting is observed at 100 °C;

(B) Between 100 °C to 110 °C nematic phase is observed indicated by the development of droplets within the sample matrix;

(C) After 110 °C the compound is isotropic liquid, meaning the packing order of the crystals is completely destroyed;

During the cooling cycle, the same textures were observed as in the heating cycle, this means that the compounds are enantiotropic liquid crystals.[9]

(D) Above 105 °C, the compound was an isotropic liquid;

(E) Between 100 °C and 64 °C an overlap of a nematic and smectic phase indicated by the development of funnel shaped textures (red circle) is observed;

(F) At 64 °C the compound started to recrystallize and revert to its initial Crystal solid phase.

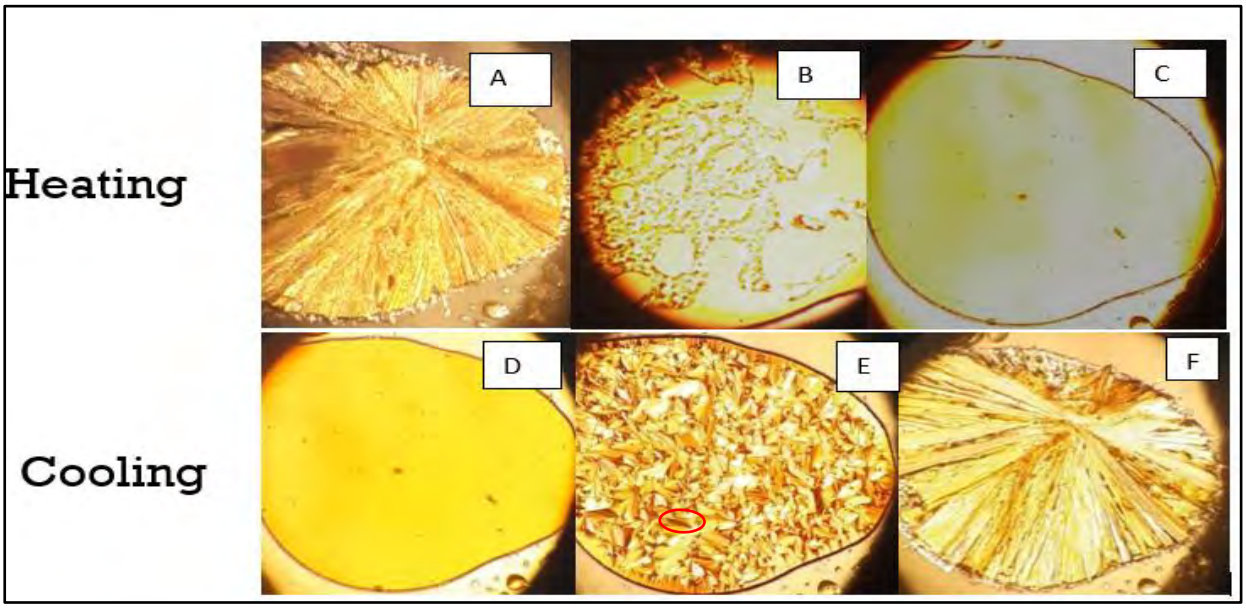

Figure 4.4: POM textures of compound **3a**: while heating, (A) below 100 °C, Crystal; (B) between 100 °C to 110 °C, smectic A phase; and (C) after 110 °C, isotropic liquid; and when cooling (D) above 105 °C, isotropic liquid; (E) between 100 °C and 64 °C, nematic phase; and (F) below 64 °C, Crystal (10X magnification).

Table 4. 1: Summary of compound **3a** and **3b** phase transitions and peak enthalpy and energy density from DSC and POM at 10 °C min^{-1}.

Heating							
Compounds	**T_{Cr-Sm} (°C)**	**ΔH_{Cr-Sm} (j/g)**	**T_{Sm-I} (°C)**	**ΔH_{Sm-I} (j/g)**	**T_{Cr-I} (°C)**	**ΔH_{Cr-N} (j/g)**	**ED (kj/mol)**
3a	85.81	82.44	104.52	16.52			18.91
3b					102.71	114.1	46.85
Cooling							
Compounds	**T_{I-Sm} (°C)**	**ΔH_{I-Sm} (j/g)**	**T_{Sm-Cr} (°C)**	**ΔH_{Sm-Cr} (j/g)**			**ED (kj/mol)**
3a	100.91	16.56	60.2	69.65			16.48
3b	101.71	13.95	91.82	90.45			21.43

Cr = Crystalline solid phase, N = Nematic, I = Isotropic liquid and T = Temperature.

4.2.2 β-diketonato-compounds

The DSC thermograms of compound **5a** ligand measured at a heating and cooling rate of 10 °C min^{-1} is displayed in **Figure 4.5**. During the first heating process, the compounds are melting from the initial crystal phase (Cr) to the liquid crystal phase (Nematic (N)) at72.55 °C and melting from N to an isotropic liquid phase (I) at 138.55 °C. During cooling, there are two observed phase transitions: one from isotropic liquid to a nematic phase at 50.69 °C and another from nematic to crystal solid at 48.14 °C as an intermediate supercooled crystalline phase. Glass transition (T_g) was also observed during cooling at 33 °C. The second heating cycle involved recrystallization (also known as cold crystallization) at 71.30 °C. A rare event known as "cold crystallisation" happens when a material is heated below its melting point, causing crystallisation to accompany an exothermal anomaly.[11] The liquid state gives way to a deep supercooled state without crystallisation during cooling, and cold crystallisation occurs via glass transition on subsequent heating, according to differential scanning calorimetry (DSC) analysis of crystalline materials that exhibit cold crystallisation. Thus, the material is storing extra thermal energy in its pre-cold crystallisation condition.[11,12]

This was followed by the crystal to nematic phase at 76.15 °C then from nematic to isotropic at 139.15 °C. During the second heating, the cold crystal was 1.25 °C lower than that of the initial crystal meaning that the cold crystal was thermodynamically less stable (easy to decompose) than the initial crystal. During cooling, the same phenomenon was observed, the nematic phase overlapped with the crystal phase at 49°C.

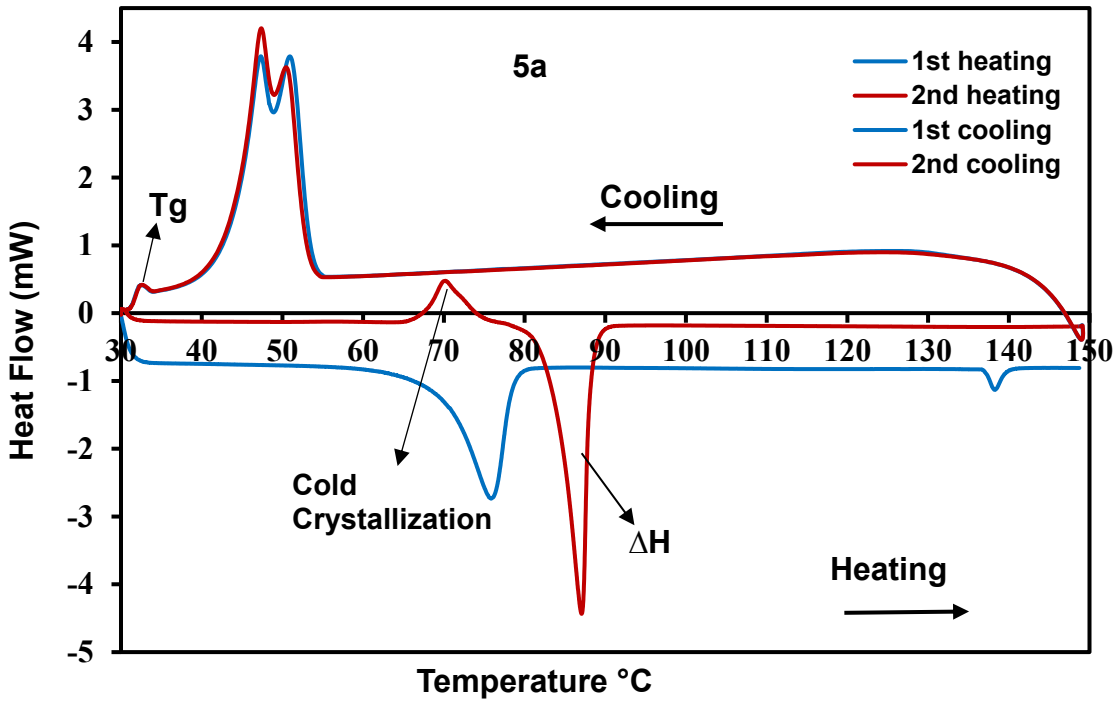

Figure 4.5: DSC thermogram showing phase transitions and enthalpy stored in each peak of compound **5a** (10 °C.min^{-1}).

At 73°C in **Figure 4.6** (compound **5b**) shows a distinct endothermic peak which indicates the occurrence of a phase transition. This transition signifies the transformation of the material from a crystal phase to a nematic liquid crystalline phase. At 139°C, another thermal event is observed, characterized by a lesser distinct endothermic peak. This peak corresponds to the transition of the material from the nematic liquid crystalline phase to an isotropic liquid phase. During cooling, the same phenomenon is observed, the crystal phase occurred immediately after the nematic phase at 37°C. Compound **5b** shows more stability than **5a** as it shows no significant differences during the 1st and the 2nd cycle. It has also a broad nematic range of

about 60 °C, an indication of a stable nematic phase during heating. While during cooling this phase is less stable indicated by a very small temperature range to a crystal. There is a clear enantiotropic phenomenon shown by both compounds where both transitions during cooling occur far below the melting points which are around 85 and 73 °C respectively.

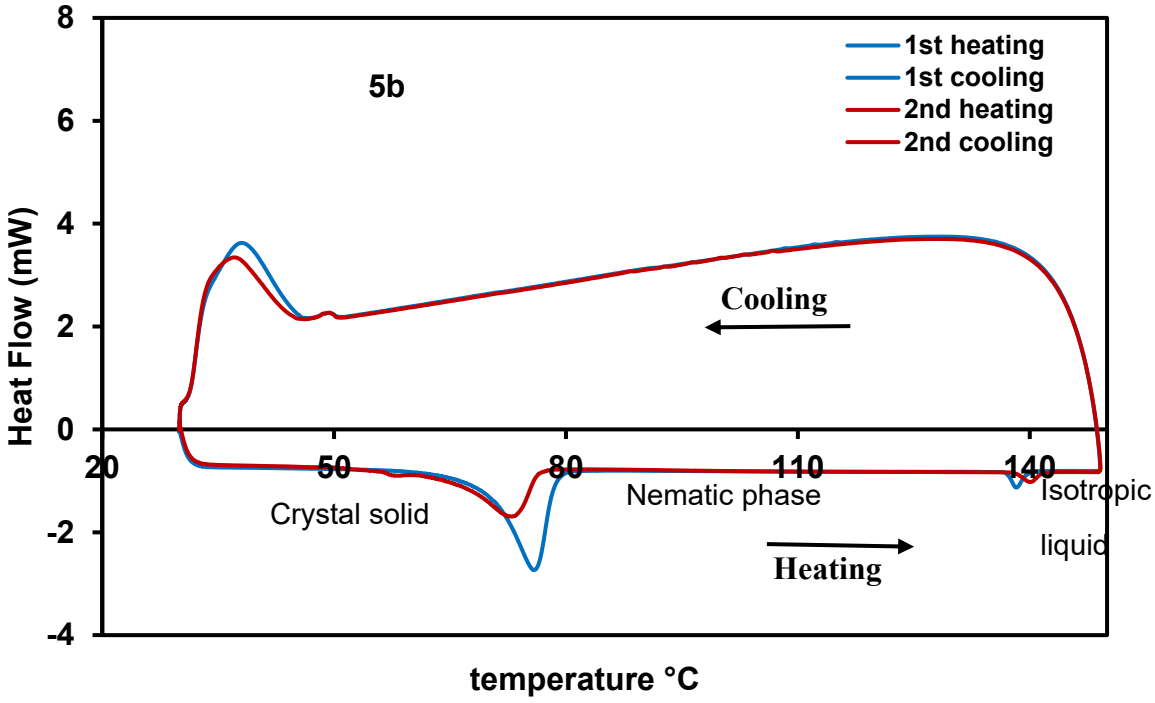

Figure 4.6: DSC thermogram showing phase transitions and enthalpy stored in each peak of compound **5b** (10 °C.min^{-1}).

The DSC peaks also provides information on how much energy is store when heating and how much energy is released when cooling. For example, in compound **5a**, during the first heating, the first and second endothermic peak stored an energy of 59.37 and 3.70 J/g respectively. During the first and the second cooling, two exothermic peaks, from the isotropic liquid state to the crystal solid state released a combined energy of 75.2 J/g . During the second heating, the cold crystal has an energy of 15.65 J/g and the second peak has an energy of 66.99 J/g. Compound **5a** and **5b** have an energy density of 34.03 and 20.20 KJ/mol respectively for the exothermic peaks.

Phase transitions were observed while cooling because during the heating cycle, the phase changes were not clear, for example, in compound **5b**, and confirmed by POM (**Figure 4.7**). The POM macrophotographs shows that the compounds exhibit both smectic A and nematic phases, which the smectic phase peak is not shown on DSC. In **Figure 4.7** a texture labelled A show the presents of a nematic phase at 135 °C indicated by the presence of nematic threads while B show the development of nematic droplets at 110 °C and 135 °C, crystal solid at 80 °C.

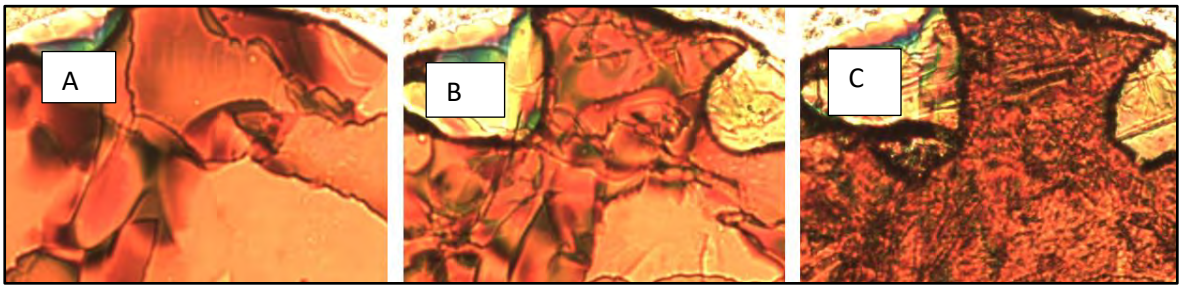

Figure 4.7: POM textures of compound **5b**: while cooling, (a) after 140 °C, Crystal; (b) between 110 °C to 135 °C, a mixture of smectic A and a nematic phase; and (c) below 80 °C, nematic phase (50X magnification).

Table 4. 2: Summary of compound **5a** and **5b** phase transitions and peak enthalpy and energy density from DSC (for the first cycle) and POM at 10 °C min^{-1}.

Heating							
Compound	**T_{Cr-N} (°C)**	**ΔH_{Cr-N} (J/g)**	**T_{N-I} (°C)**	**ΔH_{N-I} (J/g)**			**ED (kj/mol)**
5a	79,35	66,99	140,97	3,69			15.99
5b	75,87	64,63	138,28	3,28			16.32
Cooling							
Compound	**T_{I-N} (°C)**	**ΔH_{I-N} (J/g)**	**T_{N-Cr} (°C)**	**ΔH_{N-Cr} (J/g)**	**T_{I-Cr} (°C)**	**ΔH_{I-Cr} (J/g)**	**ED (kj/mol)**
5a					71,3	75.2	34.03
5b	46,76	0,35	37,53	41,67			20.20

Cr = Crystalline solid phase, N = Nematic phase, Sm = Smectic phase, I = Isotropic liquid and T = Temperature

4.2.3 β-diketonato-Copper (II) complexes

The DSC thermograms of compound **6a** and **6b** ligands measured at a heating and cooling rate of 10 °C min^{-1} are displayed in **Figure 4.8** (**6a** and **6b** respectively). Phase transitions were observed, for example, in compound **6a**, and confirmed by POM. A look at the first and second heating, a shift of the first three-finger like peak showing the melting point at around 68.61 °C (first heating) and 72.08 °C (second heating) with an assumed. It is challenging to assign and analyse the heating curves for this compound however the cooling curves give clear observations. Transformation to an isotropic liquid phase is observed at the same temperature (88.47 °C) for both cycles. Looking at the first and second cooling, a consistent trend of an isotropic liquid to nematic-smectic A to crystal solid phase transitions are observed. The nematic-smectic A thermal transition is observed at 73 °C (second cycle), this transition is short lived as another small peak at is observed shortly at 78 °C.The small peak at 88 °C is assumed to be a transition from a nematic to a smectic phase due the smallest thermal energy it released.[13] The smectic phase is stable up to 49.07 °C where the compound transitions to a crystal solid phase.

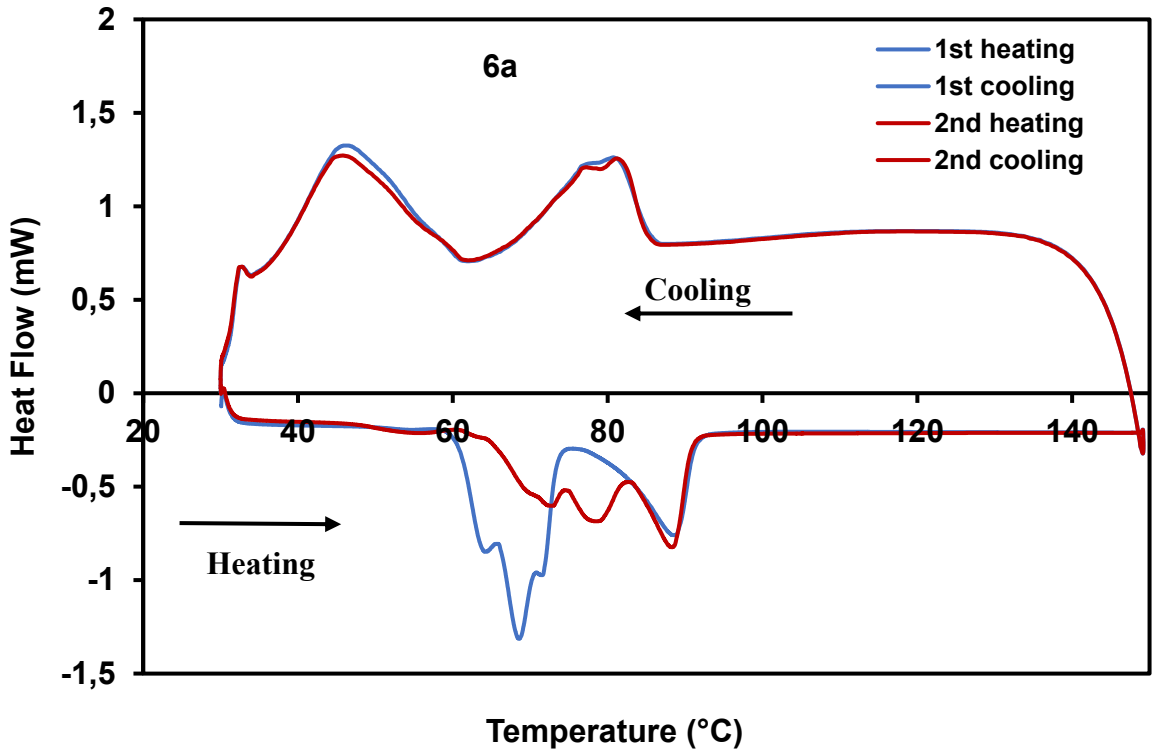

Figure 4.8: DSC thermogram showing phase transitions and enthalpy stored in each peak of compound **6a** (10 °C.min^{-1}).

The POM micrographs (**Figure 4.9**) below shows that the compound was a solid crystal until 49.09 °C where there is an overlap of both smectic A and nematic phase (red circle, showing the line defects). The liquid crystalline phases were stable until 100 °C where the phase changed to an isotropic liquid. The same phenomenon was observed during both heating and cooling cycles. [13]

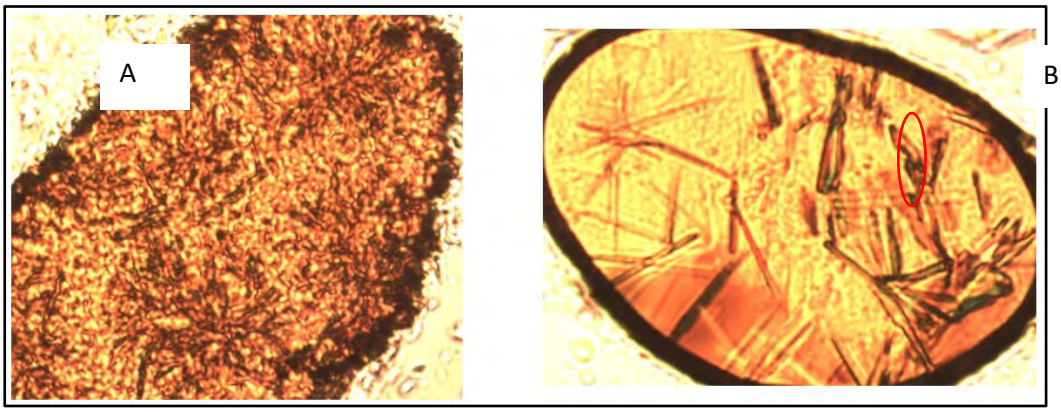

Figure 4. 9: POM textures of compound **6a**: while cooling, (A) below 49.07 °C, crystal solid phase and (B) above 79.77 °C, a mixture of smectic A and a nematic phase (50X magnification).

Compound **6b** does not show any liquid crystalline properties both by DSC and POM. DSC thermograms show only one transition from a crystalline solid to an isotropic liquid at 71.38 °C while an isotropic liquid to crystal solid is observed during cooling at 48.18 °C (**Figure 10**). For metallic compounds **6a** and **6b** is observed that the liquid crystalline properties for the compound with a longer chain were destroyed. This implies that the presence of the copper metal and a longer alkyl chain (n=10) stabilized the crystal structure of the compound.

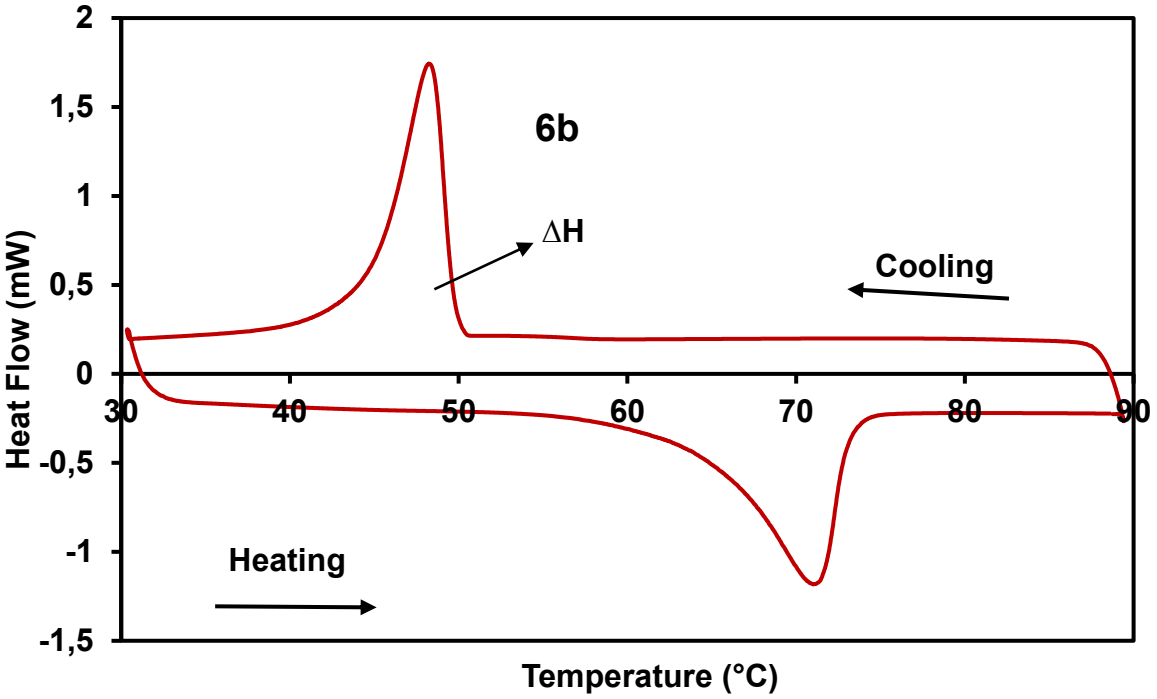

Figure 4.10: DSC thermogram showing phase transitions and enthalpy stored in each peak of compound **6b** (10 °C.min^{-1}).

Compound 6**b** shown in **Figure 4.11** below shows that despite the compound not showing any liquid crystallinity phase changes in DSC, there are nematic droplets forming at a temperature of about 79.77 °C just before the compound transitioned to an isotropic liquid. Because both the side chains and the metal centre phase transitions are involved in the enthalpy shift, the DSC signals are broad showing an overlap of the nematic phase change and the transition to an isotropic liquid. Moreover, the transition is made more difficult by the main chain's molecular weight dispersion within the polymer.[14]

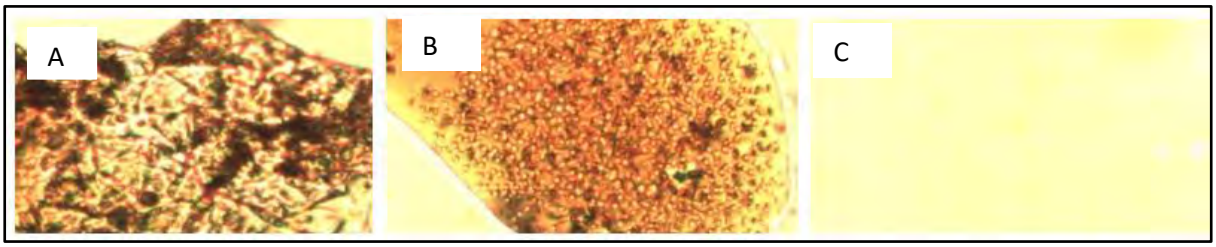

Figure 4. 11: POM textures of compound **6b**: while cooling, (A) below 70.01 °C, crystal solid phase, (B) above 79.77 °C nematic droplets and (C) At 85.77 °C, an isotropic liquid was observed (50X magnification).

As mentioned above, the DSC peaks also provides information on how much energy is store when heating and how much energy is released when cooling. For example, in compound 6**a**,the endothermic peaks store an enthalpy of 27.91 J/g and released an energy of 19.62 J/g. while compound **6b** stored an enthalpy of 33.54 J/g and released 32.43 J/g which is a good property meaning that it has good cyclability as compared to **6a.** Compound 6**a** and **6b** have an energy density of 26.80 and 33.17 kJ/mol respectively for the exothermic peaks, this shows that compound 6b has a good storage capacity.

Table 4. 3: Summary of compound **6a** and **6b** phase transitions and peak enthalpy and energy density from DSC (for the second cycle for 6a) and POM at 10 °C min^{-1}.

Heating							
Compounds	**T_{Cr-Sm} (°C)**	**ΔH_{Cr-Sm} (J/g)**	**T_{Sm-N} (°C)**	**ΔH_{Sm-N} (J/g)**	**T_{N-I} (°C)**	**ΔH_{N-I} (J/g)**	**ED (kj/mol)**
6a	72,16	3,29	78,85	4,82	88,5	11,51	9.22
	T_{Cr-I} (°C)	**ΔH_{Cr-I} (J/g)**					
6b	71,02	33,54					34.30
Cooling							
Compounds	**T_{I-N} (°C)**	**ΔH_{I-N} (J/g)**	**T_{N-Cr} (°C)**	**ΔH_{N-Cr} (J/g)**			**ED (kj/mol)**
6a	80,71	9,43	45,84	18,48			26.80
	T_{Cr-I} (°C)	**ΔH_{Cr-I} (J/g)**					
6b	48,25	32,43					33.17

To sum up, the following goals were accomplished: TGA was used to determine the thermal stability of the synthesised azobenzene derivatives, and the β-diketones compounds (**5a** and **5b**) were more stable; DSC and POM were used to confirm the compounds' liquid crystalline phases and the all the synthesized compounds are enantiotropic liquid crystals. The impact of conjugation and metal-functionalization on the compounds' liquid crystallinity was investigated. DSC was used to calculate the enthalpy and energy density that were stored in the compounds' chemical bonds and compound **6a** and **6b** shows to have more storage capacity.

4.3 References

1. Gharanjig, H., Gharanjig, K., Hosseinnezhad, M. & Jafari, S. M. Differential scanning calorimetry (DSC) of nanoencapsulated food ingredients. in *Characterization of Nanoencapsulated Food Ingredients* 295–346 (Elsevier, 2020). doi:10.1016/B978-0-12-815667-4.00010-9.

2. Pijpers, M. F. J. & Mathot, V. B. F. Optimization of instrument response and resolution of standard- and high-speed power compensation DSC: Benefits for the study of crystallization, melting and thermal fractionation. *J Therm Anal Calorim* **93**, 319–327 (2008).

3. Chiyindiko, E., Stuurman, N. F., Langner, E. H. G. & Conradie, J. Electrochemical behaviour of bis(β-diketonato)copper(II) complexes containing γ-substituted β-diketones. *Journal of Electroanalytical Chemistry* **860**, (2020).

4. Löwen, H. A phase-field-crystal model for liquid crystals. *Journal of Physics Condensed Matter* **22**, (2010).

5. Simula, T. "Liquid Time Crystals." *arXiv preprint arXiv:2202.05407* (2022).

6. Lisetski, L., Bulavin, L. & Lebovka, N. Effects of Dispersed Carbon Nanotubes and Emerging Supramolecular Structures on Phase Transitions in Liquid Crystals: Physico-Chemical Aspects. *Liquids* **3**, 246–277 (2023).

7. Han, J., Zhang, L. F. & Wan, W. Synthesis and liquid crystal behaviours of 2,4-dioxo-3-pentyl 4-decyloxy cinnamate rhodium(I) complexes. *Chin J Chem* **21**, 1521–1524 (2003).

8. Purdes, A. J., Liu, Z. F., Morigaki, K., Enomoto, T., Hashimoto, K., & Fujishima, A. Kinetic studies on the thermal cis-trans isomerization of an azo compound in the assembled monolayer film. *The Journal of Physical Chemistry* **96**, 1875-1880 (1992).

9. Frandsen, A. F. *NASA Work Experience* (No. KSC-E-DAA-TN24465) (2015).

10. Corradini, M. G. & Julian McClements, D. Microscopy | Food applications. in *Encyclopedia of Analytical Science* 47–56 (Elsevier, 2019). doi:10.1016/B978-0-12-409547-2.14314-8.

11. Frandsen, A. F. *Polarized light microscopy* (No. KSC-E-DAA-TN37401) (2016).

12. Levit, S. L. *et al.* Color Space Transformation-Based Algorithm for Evaluation of Thermochromic Behavior of Cholesteric Liquid Crystals Using Polarized Light Microscopy. *ACS Omega* **5**, 7149–7157 (2020).

13. Andrienko, D. Introduction to liquid crystals. *Journal of Molecular Liquids*, *267*, 520-541 (2018).

14. Collings, P. J., & Goodby, J. W. Introduction to liquid crystals: chemistry and physics. *Crc Press* (2019).

15. Moussout, H., Ahlafi, H., Aazza, M. & Bourakhouadar, M. Kinetics and mechanism of the thermal degradation of biopolymers chitin and chitosan using thermogravimetric analysis. *Polym Degrad Stab* **130**, 1–9 (2016).

16. Nguyen, T. L. & Saleh, M. A. Thermal degradation of azobenzene dyes. *Results Chem* **2**, 100085 (2020).

17. Guo, S., Zhang, Y., Xiong, R. & Singh, A. K. Thermal stability improvement of azobenzene for the integration of photochemical and solar thermochemical energy conversion. *Case Studies in Thermal Engineering* **52**, 103774 (2023).

18. Jesionek, P. *et al.* Studies on the nature and pressure evolution of phase transitions in 1-adamantylamine and 1-adamantanol. *Spectrochim Acta A Mol Biomol Spectrosc* **299**, (2023).

19. Kumar, M., Gowda, A. & Kumar, S. Discotic Liquid Crystals with Graphene: Supramolecular Self-assembly to Applications. *Particle and Particle Systems Characterization* **34**, (2017).

20. Jamain, Z., Azman, A. N. A., Razali, N. A. & Makmud, M. Z. H. A Review on Mesophase and Physical Properties of Cyclotriphosphazene Derivatives with Schiff Base Linkage. *Crystals* vol. 12 Preprint at https://doi.org/10.3390/cryst12081174 (2022).

21. Zhang, B., Feng, Y. & Feng, W. Azobenzene-Based Solar Thermal Fuels: A Review. *Nanomicro Lett* **14**, (2022).

22. Honda, A., Kakihara, S., Kawai, M., Takahashi, T. & Miyamura, K. Cold Crystallization and Polymorphism Triggered by the Mobility of the Phenyl Group in Alkyl Azo Dye Molecules. *Cryst Growth Des* **21**, 6223–6229 (2021).

23. Rudzki, A., Chruściel, J., Zalewski, S. & Zając, W. Thermal analysis and FTIR study of 4-n-hexadecyloxybenzoic acid (16OB). *J Therm Anal Calorim* **148**, 10663–10677 (2023).

24. Bailly-Reyre, A. & Diep, H. T. Nematic and smectic phases: Dynamics and phase transition. *Symmetry (Basel)* **12**, 1–13 (2020).

25. Ohkawa, S., Ohta, R., Kawabata, K. & Goto, H. Polymerization in liquid crystal medium: Preparation of polythiophene derivatives bearing a bulky pyrimidine substituent. *Polymers (Basel)* **2**, 393–406 (2010).

Chapter 5: Experimental

5.1 Material

All solid and liquid reagents for the synthesis were purchased from Merck, Sigma Aldrich, and used without further purification. The preparation, purification, and reactions described were carried out under an atmosphere of Argon and Nitrogen gas respectively.

5. 2 Techniques and apparatus

5.2.1 Fourier Transform Infrared (FT-IR) spectroscopy.

Infrared spectroscopy was performed on a PerkinElmer Spectrum FT-IR spectrophotometer over the range 4000 – 600 cm^{-1}.

5.2.2 Nuclear Magnetic Resonance (NMR) spectroscopy

Infrared Nuclear magnetic resonance (NMR) spectra were recorded on Bruker Advance Ultrashield 400 MHz and, Bruker Advance Ultrashield 600 MHz spectrometers. The chemical shifts of the compounds in each experiment were reported in parts per million (ppm) and proton and carbon spectra were calibrated to the residual protonated solvent signals and deuterated solvent signals respectively. All NMR experiments were performed in deuterated solvents (DMSO and $CDCl_3$) and the coupling constants (J) are reported in hertz (Hz) and the peak multiplicities are abbreviated as follows: s = singlet, d =doublet, dd = doublet of doublets, ddd = doublet of doublets of doublets, t = triplet, q =quartet and m = multiplet. The NMR spectra were analysed using MestReNova software.

5.2.3 Mass Spectrometry

Mass spectral analyses were performed on a Bruker Compact Q-TOF mass spectrometer (Bruker Daltonics, Bremen, Germany) with a positive electron spray as the ionization technique by direct infusion at 0.3 mL min^{-1}. The m/z values were measured in the range of 50 – 1000 in acetonitrile. Prior to analysis, the instrument was calibrated with sodium formate (5 mM) in resolution mode.

5.2.4 UV – Visible Spectroscopy

UV-Vis spectroscopy was obtained from OPTIZEN POP UV-Vis Spectrophotometer. A blank Macro cuvette Quartz glass with a 1 cm path-length containing the exact solvent (Chloroform and THF). The measurements were carried out from 200 nm to 700 nm with medium scan rate.

5.2.5 TD – DFT calculations

Density functional theory (DFT) and time-dependent density functional theory (TD-DFT) were carried out by using the B3LYP exchange-correlation functional of the Gaussian 09 software package (version E01). Geometry optimisations were performed at the B3LYP/6-31G(d) level of theory. The optimised B3LYP geometries were used to carry out excited state TD-DFT calculations. The visualisation of the generated MOs was carried out with Chemcraft.

5.2.6 Thermogravimetric analysis

Thermogravimetric analyses were performed on Perkin Elmer TGA 4000 equipment, the samples were placed in aluminium containers and heated from the temperature of 30-900°C, at a heating rate of 10 ºC minute^{-1} in an atmosphere of nitrogen and the thermogravimetric curves were processed with Microsoft excel.

5.2.7 Melting point (M.p) and liquid crystals studies

Melting points and liquid crystals transition temperatures were determined by Differential Scanning Calorimetry (DSC) and the mesophase morphologies were determined by Polarized Optical Microscopy (POM) and all the temperature quoted are the onset values from the transitions. DSC results were obtained using TA instrument, TRIOS DSC – 01360 (192.168.0.2) mounted in Tzero aluminium pans at 10 °C/minute and POM results were obtained using a microscope with a LINKAM, TMS 94 hot stage.

5.3 Synthesis and Identification of all compounds

The Azobenzene precursor, compound 1, and the hydrolysis of esters to carboxylic acid, compound 4a, 4b and were synthesized using a procedure published by Niezgoda et. al.[1] The addition of alkyl chains, compound 3a and 3b (n = 8 and 10), were synthesized using a method published by Yang et al.[2] The procedure followed to synthesise γ-substituted β-diketones (compound 5a and 5b) was adapted from Wan et.al.[3,4] The gamma-substituted beta-diketonato-Cu (II) complex (compound 6a and 6b) were synthesized using the procedure from Hanabusa et.al.[5]

5.3.1 Synthesis of ethyl (*trans*)-4-((4-hydroxyphenyl) diazenyl) benzoate

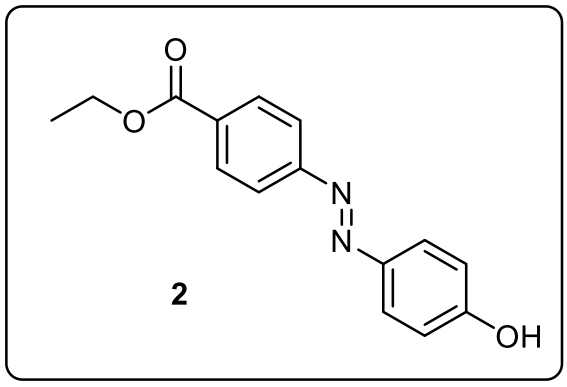

2

Ethyl 4-aminobenzoate (50 g, 0.303 mol) was dissolved in 1 M aqueous HCl (200 ml) and kept in the ice bath at 0–5 ˚C. $NaNO_2$ (20.9 g, 0.303 mol) was dissolved in a minimum amount of water, which was added dropwise to the ethyl 4-aminobenzoate and HCl mixture to produce a diazonium salt solution. Sodium carbonate (53 g, 0.500 mol) and phenol (28.5g, 0.303 mol) were dissolved in 200 ml water cooled to less than 5 ˚ C and then added to the earlier prepared cooled diazonium salt solution dropwise. The resulting mixture was stirred for 3 hours at 0–5 ˚C and next neutralized with diluted HCl resulting in a yellow crude product which was filtered off and air-dried. Yield: 66.70 g (76.89%). M.p: 146 - 148 ºC. ^{1}H NMR (400 MHz, $CDCl_3$) δ (ppm) 1.39–1.42 (t, 3H, CH_3), 4.37–4.42 (q, 2H, CH_2), 6.94–6.96 (d, 2H, Ar-H), 7.87–7.91 (q, 4H, Ar-H), 8.15–8.17 (d, 2H, Ar-H). FTIR (cm $^{-1}$): 3455 (ArOH), 1688 (C=O), 1590 (N=N). UV/Vis (λ max) (nm): 360 ($CDCl_3$) and 364 (THF).

5.3.2 Synthesis of Ethyl (*trans*)-4-((4-(alykloxy) phenyl) diazenyl) benzoate

Compounds **3a** and **3b** were synthesized using compound **2** (15 g, 0.052 mol), anhydrous K_2CO_3 (15.2 g, 0.110 mol) and KI (0.3 g, 0.00181 mol) dissolved in 200 mL of acetone, under an argon atmosphere. After 10 min stirring, 1-bromoalkyl (8.9 g, 0.054 mol) was added dropwise via syringe while the solution was refluxing. The mixture was stirred overnight under reflux. After cooling down to room temperature, 200 mL of water was added. The product was extracted with dichloromethane. The organic layer was dried with $MgSO_4$ and filtered, and then the solvent was evaporated. The product was recrystallized with ethanol. The product was orange powder.

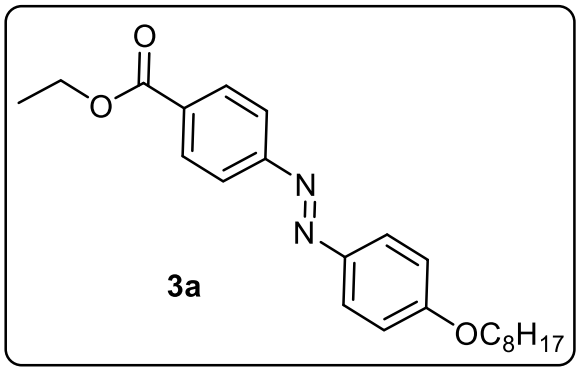

Compound 3a: Yield: 9.13g (49.57%). M.p: 86 – 88 ° C. ^{1}H NMR (600 MHz, $CDCl_3$) δ (ppm): 0.86–0.89 (t, 3H, CH_3), 1.28–1.52 (m, 13H, CH_2, CH_3), 1.78–1.84 (quint, 2H, CH_2), 4.02–4.05 (t, 2H, OCH_2), 4.36–4.42 (q, 2H,$COOCH_2$), 6.98–7.00 (d, 2H, Ar-H), 7.87–7.92 (q, 4H, Ar-H), 8.15–8.17 (d, 2H, Ar-H). FTIR (cm $^{-1}$): 2918 – 2850 (CH_2), 1715 (C = O) and 1602 (N = N). UV/Vis (λ max) (nm): 363 ($CDCl_3$) and 365 (THF).

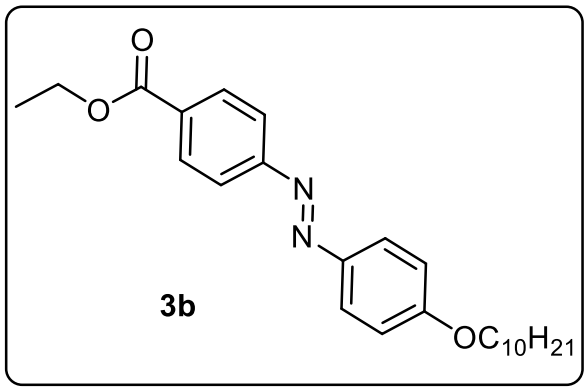

Compound 3b: Yield: 10.34g (48.34%). M.p: 102 - 104 ° C. ^{1}H NMR (600 MHz, $CDCl_3$) δ (ppm): 0.86–0.89 (t, 3H, CH_3), 1.28–1.52 (m, 17H, CH_2, CH_3), 1.78–1.84 (quint, 2H, CH_2), 4.02–4.05 (t, 2H, OCH_2), 4.36–4.42 (q, 2H,$COOCH_2$), 6.98–7.00 (d, 2H, Ar-H), 7.87–7.92 (q, 4H, Ar-H), 8.15–8.17 (d, 2H, Ar-H). FTIR (cm $^{-1}$): 2918 – 2850 (CH_2), 1715 (C = O) and 1602 (N = N). UV/Vis (λ max) (nm): 363 ($CDCl_3$) and 364 (THF).

5.3.3 Synthesis of (*trans*)-4-((4-(alkyloxy) phenyl) diazenyl) benzoic acid

Compound **4a** and **4b** were synthesized using compound **3** (3 g, 0.018 mol) dissolved in EtOH and NaOH (1 g, 0.025 mol) was added. Mixture was refluxed for 24 h and after cooling to room temperature was acidified with diluted HCl. After vacuum filtration the crude product was twice recrystallized from acetic acid. An orange powder was collected.

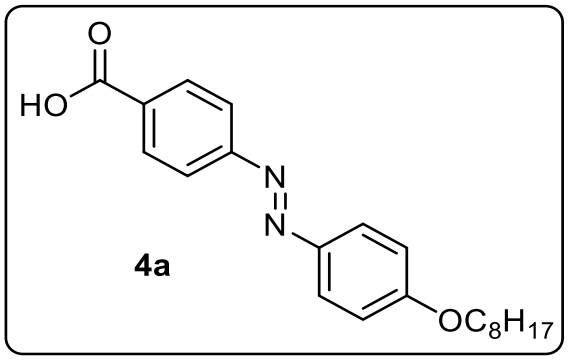

Compound 4a: Yield: 2.04 g (32%). M.p >230 ° C. ^{1}H NMR (600 MHz, $CDCl_3$) δ (ppm): 0.86–0.89 (t, 3H, CH_3), 1.28–1.52 (m, 10H, CH_2, CH_3), 1.78–1.84 (quint, 2H, CH_2), 4.02–4.05 (t, 2H, OCH_2), 6.98–7.00 (d, 2H, Ar-H), 7.87–7.92 (q, 4H, Ar-H), 8.15–8.17 (d, 2H, Ar-H), 13.23 (s, OH). FTIR (cm $^{-1}$): 3658 (OH), 2918 – 2850 (CH_2), 1715 (C = O) and 1602 (N = N). UV/Vis (λ max) (nm): 357 ($CDCl_3$) and 362 (THF).

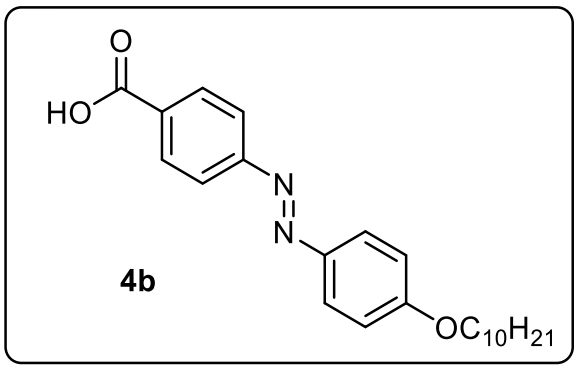

Compound 4b: Yield: 2.15 g (31.25%).M.p: >230 ° C ^{1}H NMR (600 MHz, $CDCl_3$) δ (ppm): 0.86–0.89 (t, 3H, CH_3), 1.28–1.52 (m, 14H, CH_2, CH_3), 1.78–1.84 (quint, 2H, CH_2), 4.02–4.05 (t, 2H, OCH_2), 6.98–7.00 (d, 2H, Ar-H), 7.87–7.92 (q, 4H, Ar-H), 8.15–8.17 (d, 2H, Ar-H), 13.23 (s, OH). FTIR (cm $^{-1}$): 3658 (OH), 2918 – 2850 (CH_2), 1715 (C = O) and 1602 (N = N). UV/Vis (λ max) (nm): 362 ($CDCl_3$) and 361 (THF).

5.3.4 Synthesis of 2,4-dioxopentan-3-yl (*E*)-4-((4-(alkyloxy) phenyl) diazenyl) benzoate

Compounds 5a and 5b were synthesized by mixing compound 4 (0.5 g, 0.00208 mol.) and KOH (0.12 g, 0.0089 mol.) in anhydrous DMF (6.25 ml), stirred under nitrogen gas at 80 °C for 3 h, 3-chloro-2,4-pentanedione (0.26 ml, 0.004 mol.) was added. The reaction mixture was then stirred over night at 50 °C under reflux. After cooling to ambient temperature, water (20 ml) was added to the reaction mixture and the mixture was extracted three times with chloroform. The combined extracts were washed three times with water and then dried with anhydrous sodium sulphate. The solvent was partly removed under reduced pressure. The product was recrystallized with methanol to give a brown- orange crystalline product.

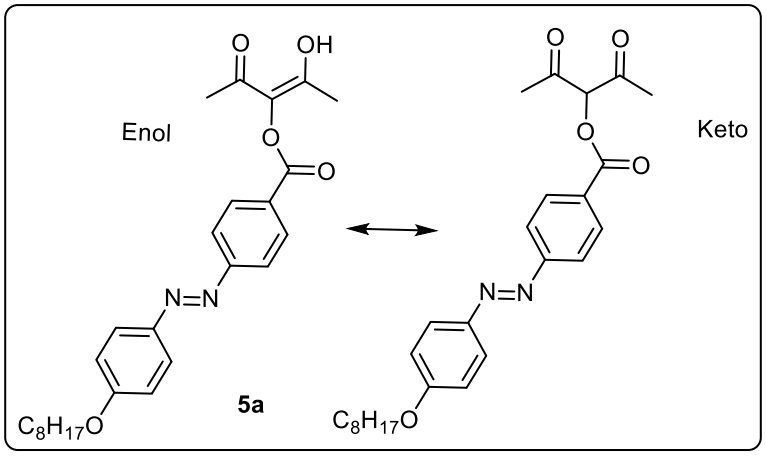

Compound 5a: Yield: 0.26 g (30%). M.p: 78 - 80 ° C. ^{1}H NMR (600 MHz, $CDCl_3$) δ ppm: 0.86 –0.90 (t, 4 × CH_3), 1.25 – 1.50 (m, 2 × 10H, CH_2, CH_3), 1.80 – 1.85 (quint, 2 × 2H, CH_2) 2.3 (m, 12H, enol and keto overlap, 4 × CH_3), 4.04 – 4.07 (s, 1H, overlap between enol CH and –OCH_2)), 5.75 (s, 1H, keto CH), 7.01 – 8.31 (m, 16H, Ar keto-enol forms), 14.54 (s, 1H, OH of γ-substituents). ^{13}C NMR (600Hz, $CDCl_3$) δ ppm: 29.17 – 31.84 (enol and keto overlap, 4 × CH_3), 122.64 – 164.51 (m, keto-enol Ar-carbons), 129,23 (=C-O-C), 184.96 (s, enol, C-OH), 191.93 (keto C=O). FTIR (cm $^{-1}$): 3662 (OH), 2981 – 2920 (CH_2), 1723 (C = O), 1598 (N = N) and 1252 (C-O-C). UV/Vis (λ max) (nm): 367 ($CDCl_3$) and 365 (THF).

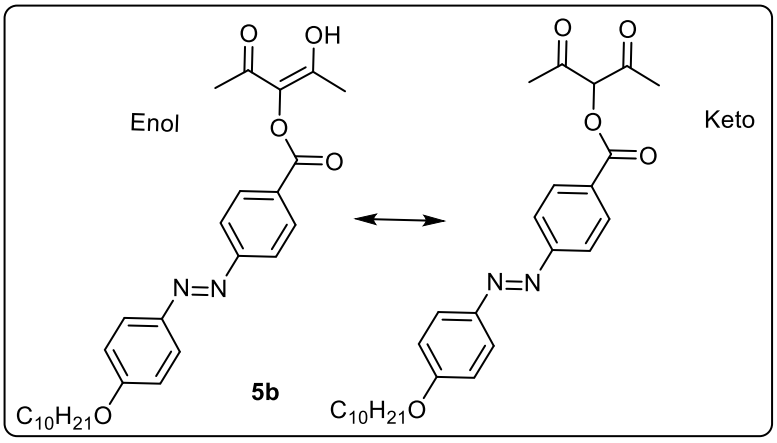

Compound 5b: Yield: 0.28 g (32.31%). M.p: 68 - 70 ° C. ^{1}H NMR (600 MHz, $CDCl_3$) δ ppm: 0.86–0.89 (t, 4 × CH_3), 1.19–1.47 (m, 2 × 14H, CH_2, CH_3), 1.78–1.84 (quint, 2 × 2H, CH_2) 2.3 (m, 12H, enol and keto overlap, 4 × CH_3), 4.1 (s, 1H, overlap between enol CH and –OCH_2)), 5.9 (s, 1H, keto CH), 7.1 – 8.2 (m, 16H, Ar keto-enol forms), 13.2 (s, 1H, OH of γ-substituents). ^{13}C NMR (600Hz, $CDCl_3$) δ ppm: 29.17 – 31.84 (enol and keto overlap, 4 × CH_3), 122.64 – 164.51 (m, keto-enol Ar-carbons), 129,23 (=C-O-C), 184.96 (s, enol, C-OH), 191.93 (keto C=O). FTIR (cm $^{-1}$): 3649 (OH), 2978 – 2853 (CH_2), 1715 (C = O), 1598 (N = N) and 1246 (C-O-C). UV/Vis (λ max) (nm): 362 ($CDCl_3$) and 362 (THF).

5.3.5 Synthesis of *para*-substituted *β*-Cu (II)

Compound 5 (0.2 g, 0.00041 mol.) in 1,4-dioxane (44 ml) was added in triethanolamine (TEA) (2.5 ml) followed by methanolic solution (1.4 ml) containing $CuCl_2 \cdot 2H_2O$ (0.045 mg, 0.012 mol). The mixture was stirred at room temperature for 1 hour and then refluxed for 30 minutes. The solvent was evaporated, and then the residue was washed with methanol, water and methanol successively resulting in the formation of crude product. The product was dissolved in THF (3.9 ml) and poured into methanol (100 ml). Precipitate was filtered off and dried. Green-brown powder was collected.

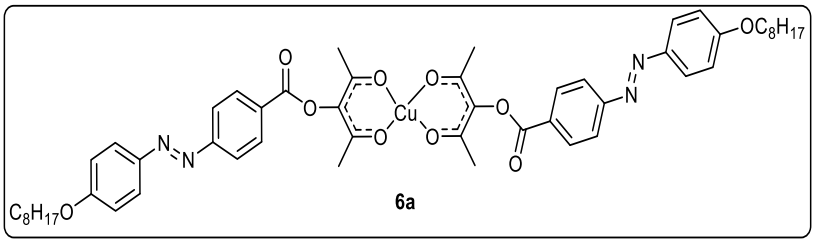

6a

Compound 6a: Yield: 0.15 g (32.54%). M.p: 60 - 62 ° C. ^{1}H NMR (400 MHz, DMSO) δ ppm: 0.84 – 0.91 (m, 3H), 1.28 (s, 4H), 1.44 (s, 1H), 1.76 (t, J = 7.3 Hz, 2H), 2.19 (s, 1H), 2.37 (s, 3H), 4.11 (t, J = 6.6 Hz, 2H), 5.08 (s, 1H), 5.98 (s, 0H), 7.16 (d, J = 8.5 Hz, 2H), 7.97 (dd, J = 16.9, 9.0 Hz, 3H), 8.23 (dd, J = 35.3, 8.2 Hz, 2H). MS (m/z): 965.51. FTIR (cm $^{-1}$): 2921 – 2854 (CH_2), 1718 (C = O), 1601 (C = C), 1503 (N = N) and 1263 (C-O-C). UV/Vis (λ max) (nm): 369 ($CDCl_3$) and 363 (THF).

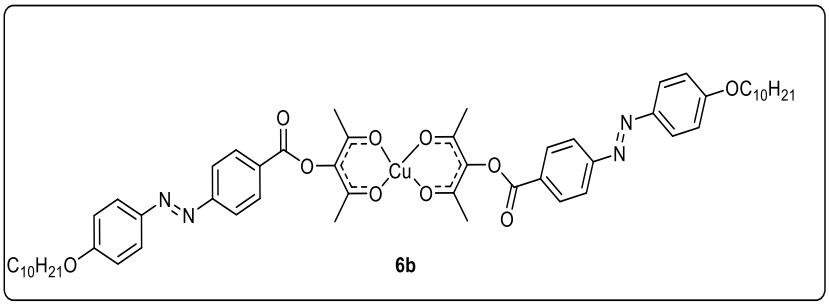

6b

Compound 6b: Yield: 0.16 g (37,34%). M. p: 54 - 56 ° C. ^{1}H NMR (400 MHz, DMSO) δ ppm: 0.84 – 0.91 (m, 3H), 1.28 (s, 6H), 1.44 (s, 1H), 1.76 (t, J = 7.3 Hz, 2H), 2.19 (s, 1H), 2.37 (s, 3H), 4.11 (t, J = 6.6 Hz, 2H), 5.08 (s, 1H), 5.98 (s, 0H), 7.16 (d, J = 8.5 Hz, 2H), 7.97 (dd, J = 16.9, 9.0 Hz, 3H), 8.23 (dd, J = 35.3, 8.2 Hz, 2H). MS (m/z): 1021.65. FTIR (cm $^{-1}$): 2918 – 2850 (CH_2), 1715 (C = O), 1602 (C = C), 1500 (N = N) and 1252 (C-O-C). UV/Vis (λ max) (nm): 361 ($CDCl_3$) and 363 (THF).

5.4 References

1. Niezgoda, I., Jaworska, J. & Galewski, Z. Mesogenic properties and studies of the photoisomerization process in solutions of branched azobenzene derivatives with ester group. *J. Mol. Liq.* **222**, 571–575 (2016).

2. Yang, R., Zhao, D., Dong, G., Liu, Y. & Wang, D. Synthesis and characterization of photo-responsive thermotropic liquid crystals based on azobenzene. *Crystals* **8**, (2018).

3. Chiyindiko, E., Stuurman, N. F., Langner, E. H. G. & Conradie, J. Electrochemical behaviour of bis(β-diketonato)copper(II) complexes containing γ-substituted β-diketones. *J. Electroanal. Chem.* **860**, (2020).

4. Han, J., Zhang, L. F. & Wan, W. Synthesis and liquid crystal behaviors of 2,4-dioxo-3-pentyl 4-decyloxy cinnamate rhodium(I) complexes. *Chinese J. Chem.* **21**, 1521–1524 (2003).

5. Hanabusa, K., Isogai, T., Koyama, T. & Shirai, H. Synthesis and properties of thermotropic liquid-crystalline polymers linked through bis (P-diketonato) copper (II) complex. *Makromol. Chem*. **210**, 197–210 (1993).

Chapter 6: Conclusion

The aim of this work was to synthesise and characterise liquid crystalline azobenzene derivatives with alkyl chain length (n) where n=8 and 10, coordinated with a β-diketonato-copper(II) metal as efficient solar thermal fuel cells that can capture, convert, store, and release solar energy.

The azobenzene precursor selected absorb at the wavelength of the sun's spectrum that is between 280-700 nm (UV-Vis). The synthesised compounds were dissolved in chloroform to observe their photoresponsive nature. The N=N bond is the most active, allowing free rotation of the molecule for isomerization to occur hence the wavelength absorption of the compounds shown no significant difference. When the kinetic parameters of the compounds were compared, the *cis-to-trans* isomerisation was found to have a longer half-life than the *trans-to-cis* isomerisation indicating long-term photoswitching cyclability. The *para*-substituted-β-diketonato copper(II) complexes (**6**) were found to have high activation energy that compound azobenzene ligands (**5** and **6**) meaning it has long-term stability for backward conversion of the isomers.

Band gap energies are very important parameters for solar energy studies. When the band gap of the compounds is compared between the experimental (Tauc plots) and the theoretical (TD-DFT) we found that there is no significant difference in the values as the electron density is around the rings and the N=N bond. The band gap differ from the isomers as the *trans*-isomer is around 3.5 eV and the *cis* isomer is around 2.4 eV which is within the range of semiconducting inorganic materials. The *para*-substituted-β-diketonato copper (II) complex had a very small band gap energy of 1.7 eV showing to be more suitable to be a semiconductor than the ligands.

The thermal stability of the compounds was studied by TGA. All the compounds decomposed after 400 $^{\circ}C$, with the β-diketone substituted ligand (**5**) found to be more stable. These compounds are suitable for low- and medium-temperature solar energy applications due to their improved thermal stability, but not suitable for high-temperature applications.

The DSC thermograms of the alkyl chain ligands (**3**) show a similar phase transition, with stability decreasing as the alkyl chain increases. Polarized optical microscope (POM) studies allow for the assignment of different phases, with the alkyl chain ligands (**3**) exhibiting a smectic A liquid crystalline phase. The DSC thermograms of compound the β-diketone

substituted ligand **(5)** ligands show phase transitions during heating and cooling at 10°C min^{-1}. The compounds exhibit both smectic and nematic phases, with the smectic phase not shown on DSC. The first heating process involved melting from the initial crystal phase to the liquid crystal phase and an isotropic liquid phase. After cooling, two phase transitions were observed, including a glass transition and a cold crystal. Cold crystallization occurs when a material is heated below its melting point, causing crystallization to accompany an exothermal anomaly. The DSC thermograms of the *para*-substituted-β-diketonato copper (II) complexes (**6**) show phase transitions, with the smectic phase being less stable than the nematic phase. POM macrophotographs show a consistent trend of an isotropic liquid to nematic-smectic A to crystal solid phase transition. The *para*-substituted-β-diketonato copper (II) complexes (**6**) appears less stable, with no liquid crystalline phase. As the alkyl chain increases, the molecule loses order and liquid crystallinity during the cooling cycle.

The DSC peaks also provides information on how much energy is store when heating and how much energy is released when cooling. We found that the alkyl chain ligands (**3)** stored more energy as compared to the β-diketone substituted ligand **(5)** and the *para*-substituted-β-diketonato copper (II) complexes (**6**) This is because compound **5** and **6** needs more UV-Vis exposure as the compounds are bulky and isomerises slowly.

Energy storage density (ED) is a crucial indicator of energy storage capacity in solar thermal fuels based on azobenzene photoswitches. DSC peaks provide information on energy storage and release during heating and cooling, with the sum of enthalpy determining energy density for exothermic peaks. The energy density of compounds decreases from compound **3** to compound **5** and increases as metalation of the *para*-substituted-β-diketonato copper (II) complexes (**6**) occurs, indicating the metal's effect on energy storage.

In summary, the more functionalised azobenzene derivatives are, or the bulkier the become, the more time they need to be exposed to UV-Vis to absorb more solar energy. Also, the bulkier they are, the more time they take to isomerise, meaning the energy stored in the chemical bonds will take time to be depleted. We also noticed that with more functionalisation, the liquid crystallinity of the compounds is destroyed.

Nevertheless, there is still more analysis to be carried out to qualify these synthesised compounds as materials for solar thermal fuels. To be specific, the following modifications are recommended:

- Exposed the compounds to a stronger UV light (as in this work a 6 W light was used) to obtain 100% *cis* isomer.
- Preform quantum yield analysis to see if the high-energy isomer performs with high efficiency.
- Synthesise a series of alkyl chain, from 1 to 15 carbon chains to study the chain effect in the azobenzene derivatives.
- Compare the beta-diketonato-copper (II) complexes with Nickel and zinc metals to study the difference in energy and liquid crystalline properties.

Appendix

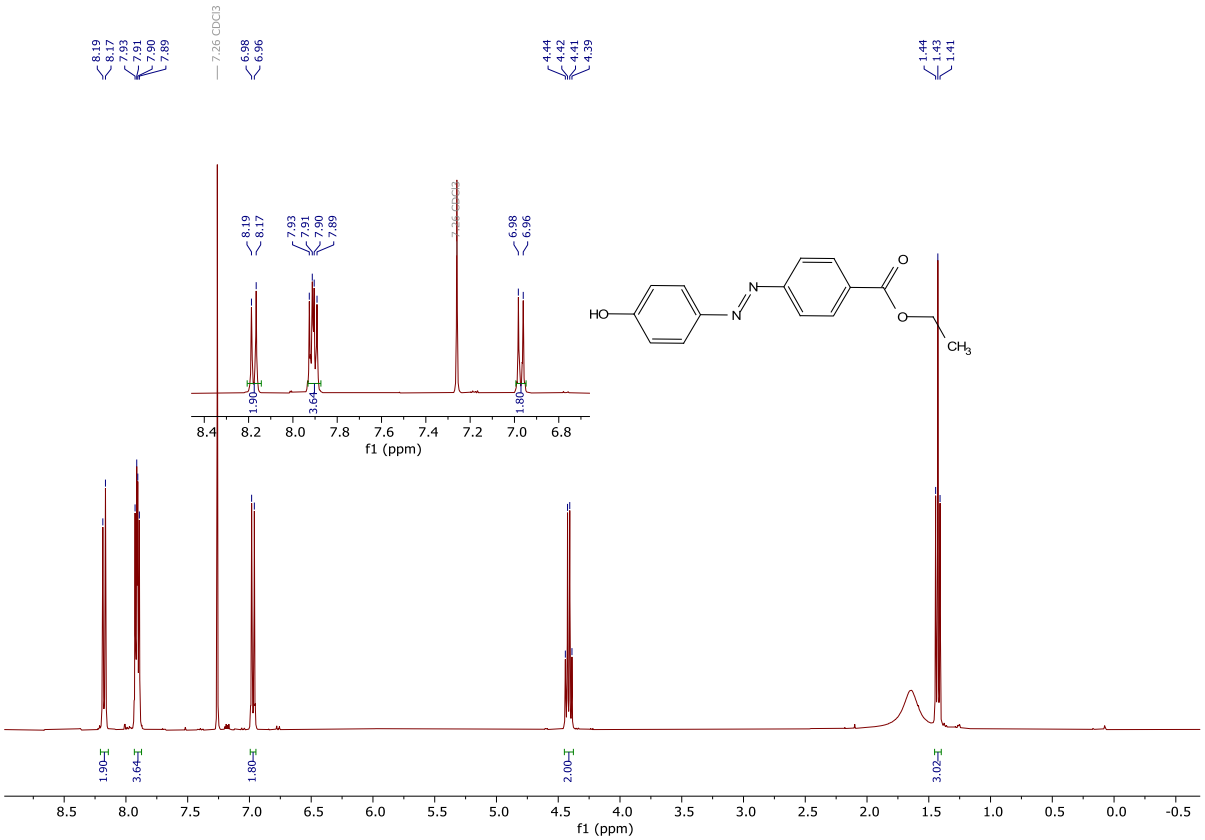

Figure 1: ^{1}H Spectrum of starting material, **2**.

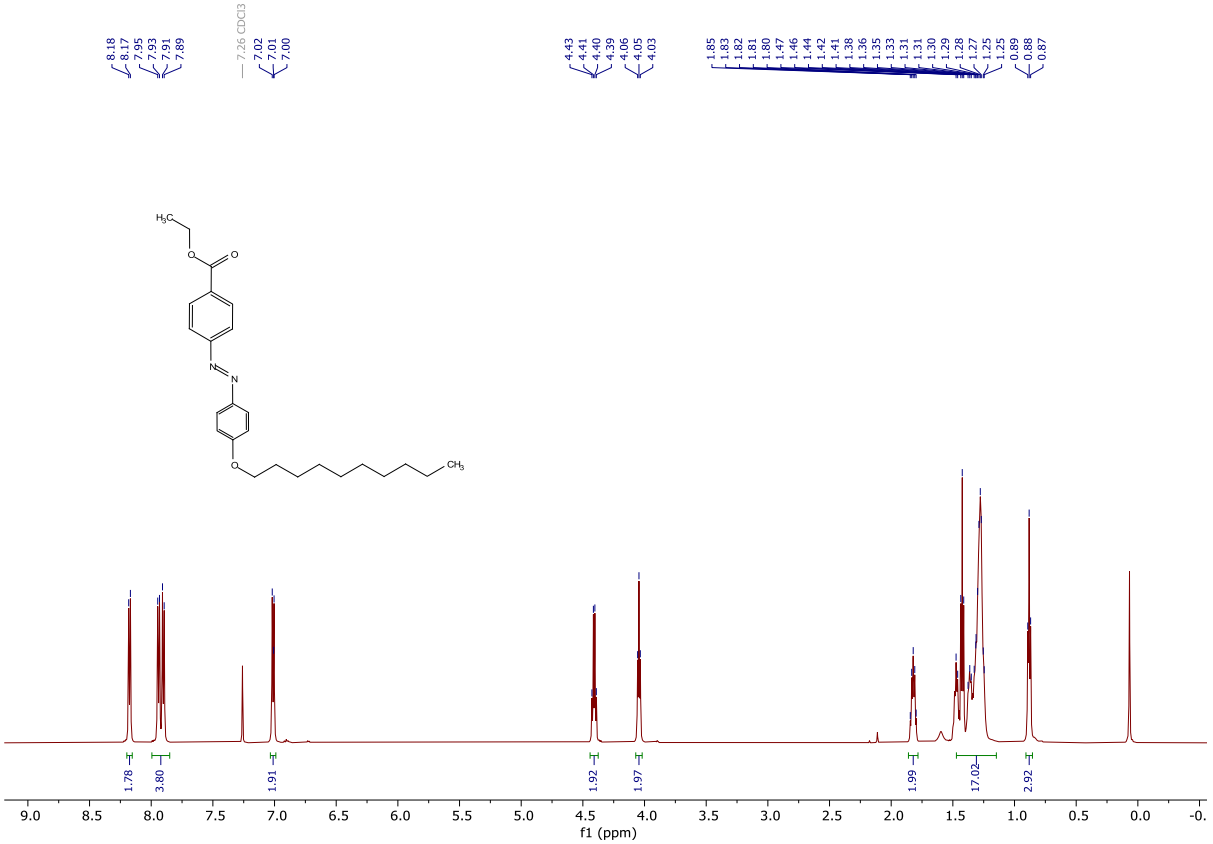

Figure 2: [1]H Spectrum of compound **3b**.

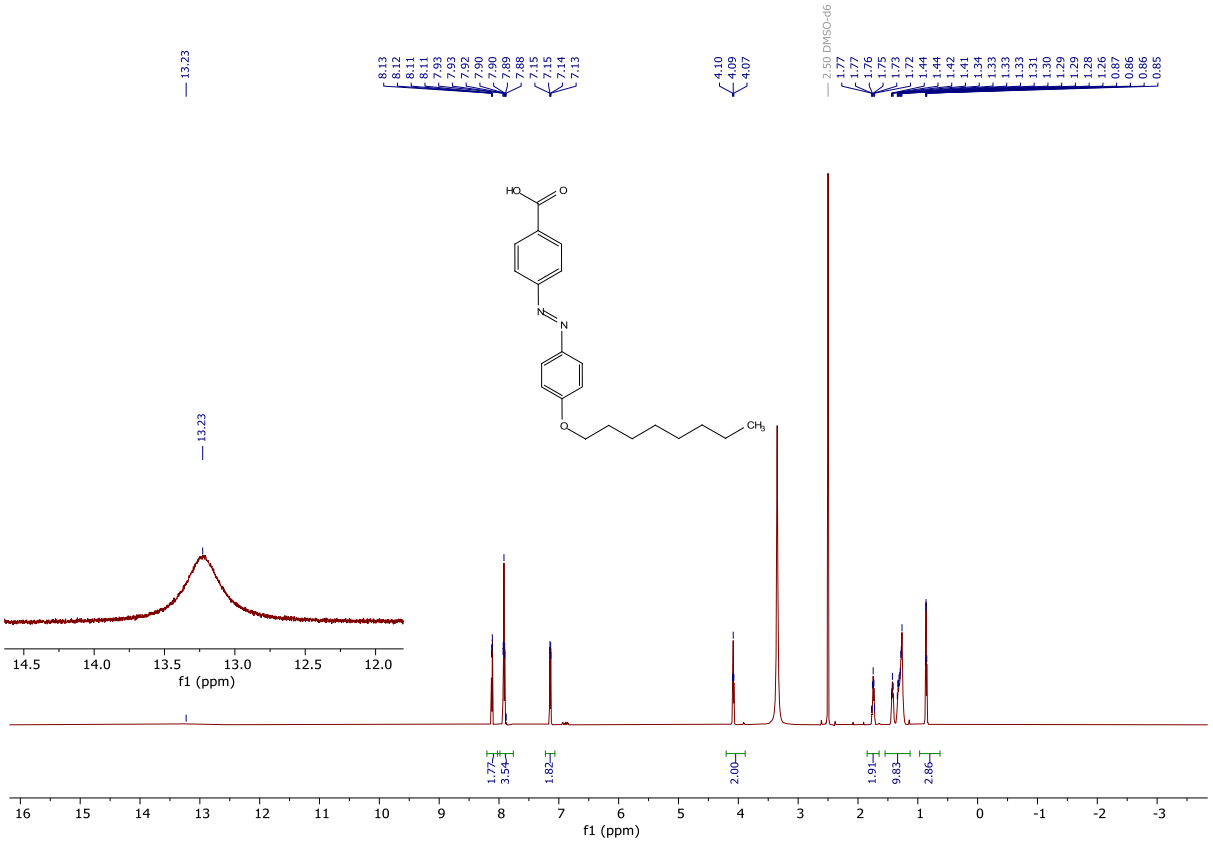

Figure 3: [1]H Spectrum of compound **4a**.

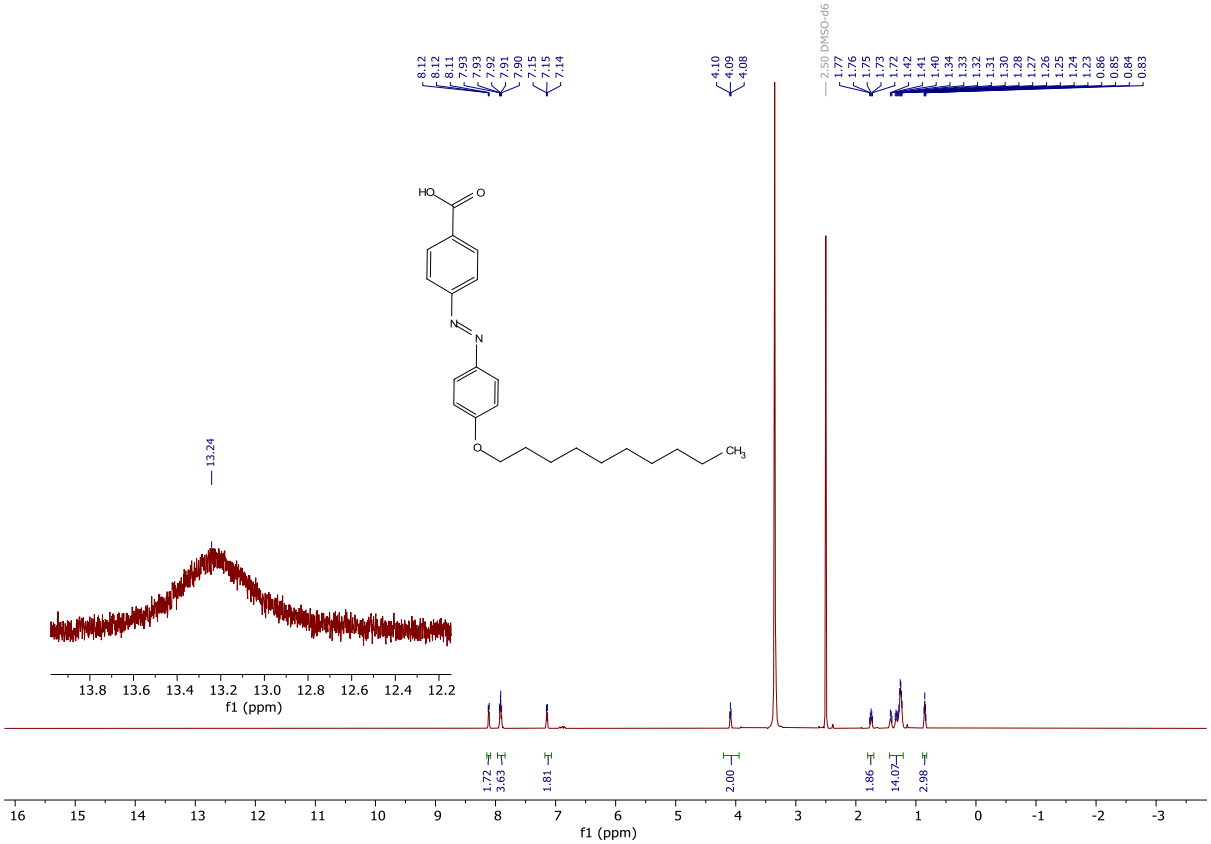

Figure 4: [1]H Spectrum of compound **4b**.

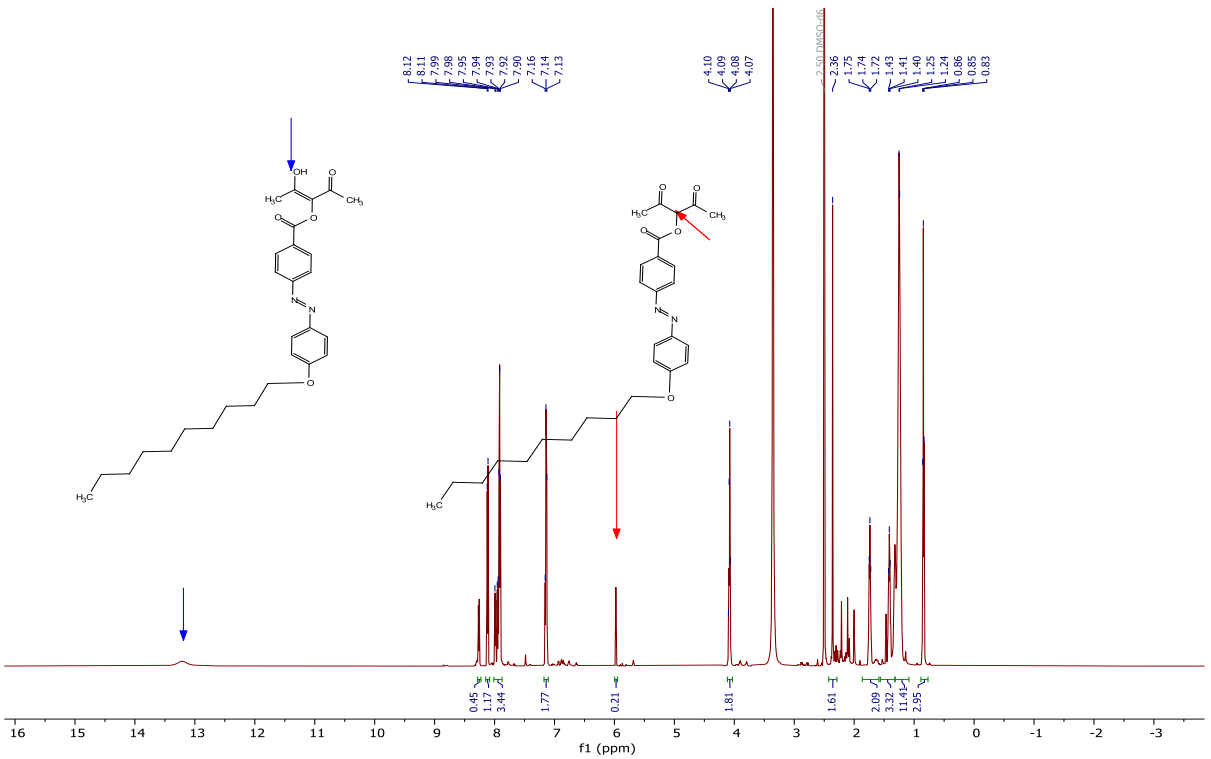

Figure 5: [1]H spectrum of compound **5b**.

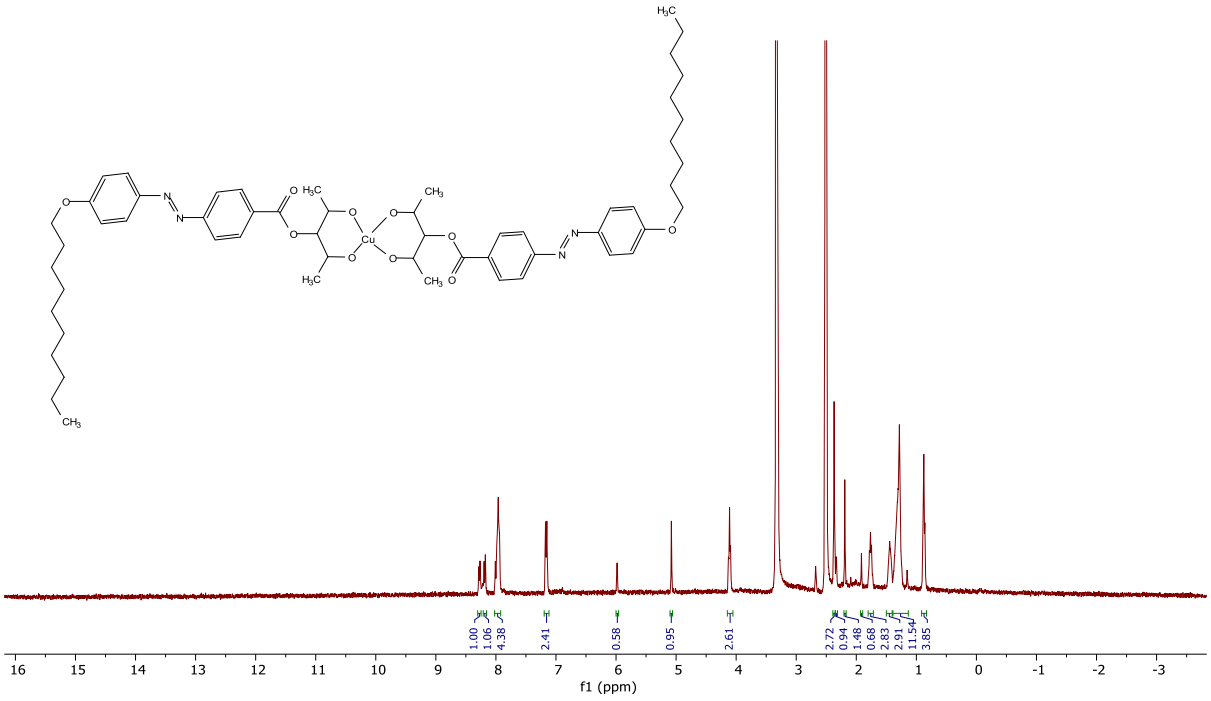

Figure 6: ^{1}H Spectrum of compound **6a**.

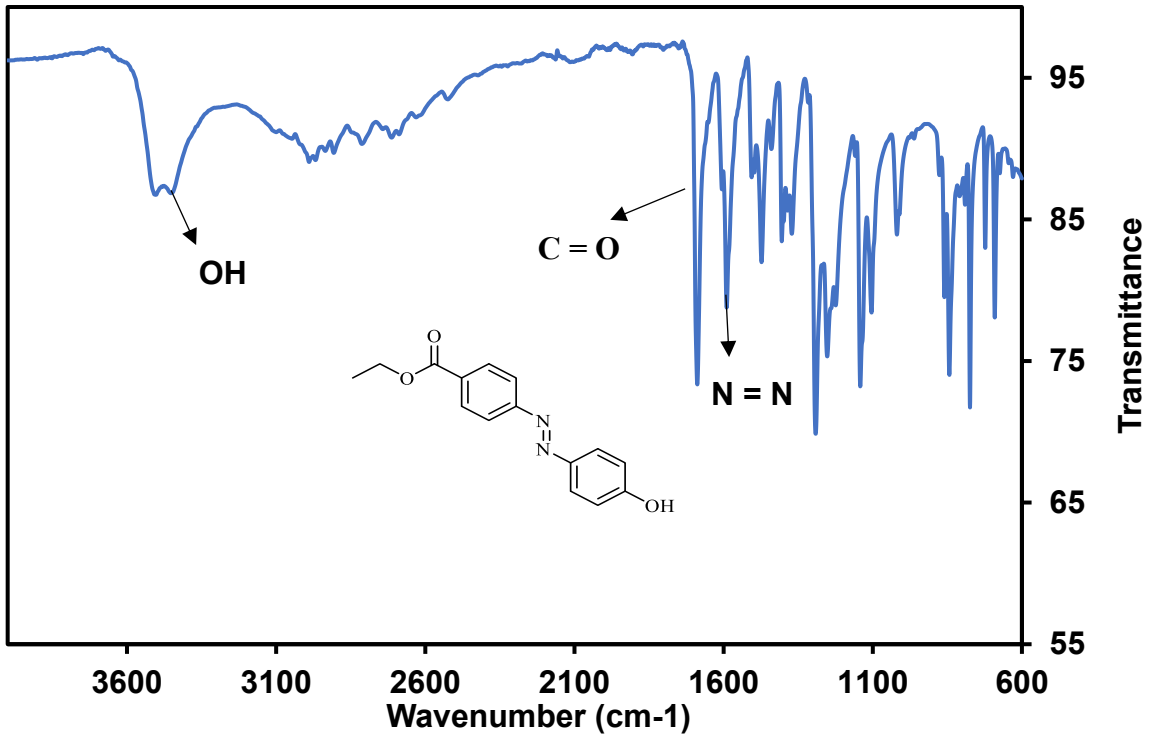

Figure 7: FTIR Spectrum of compound **2**.

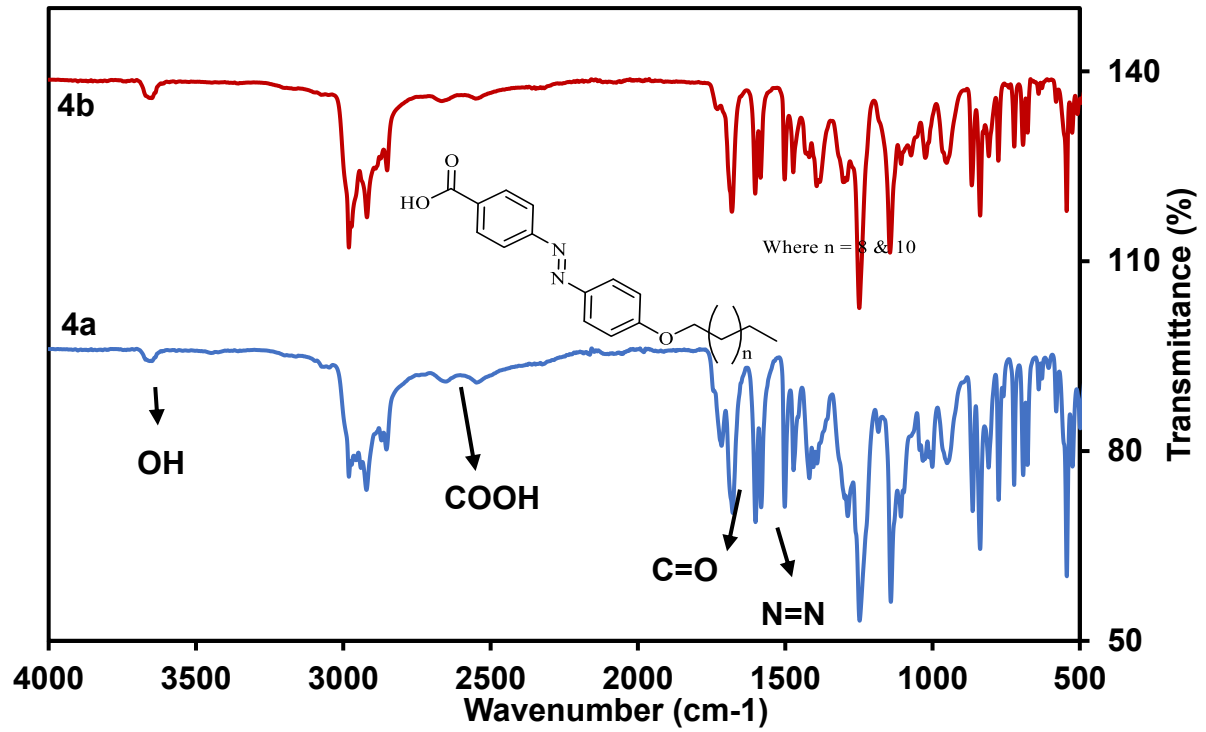

Figure 8: FTIR Spectra of compound **4a & 4b**.

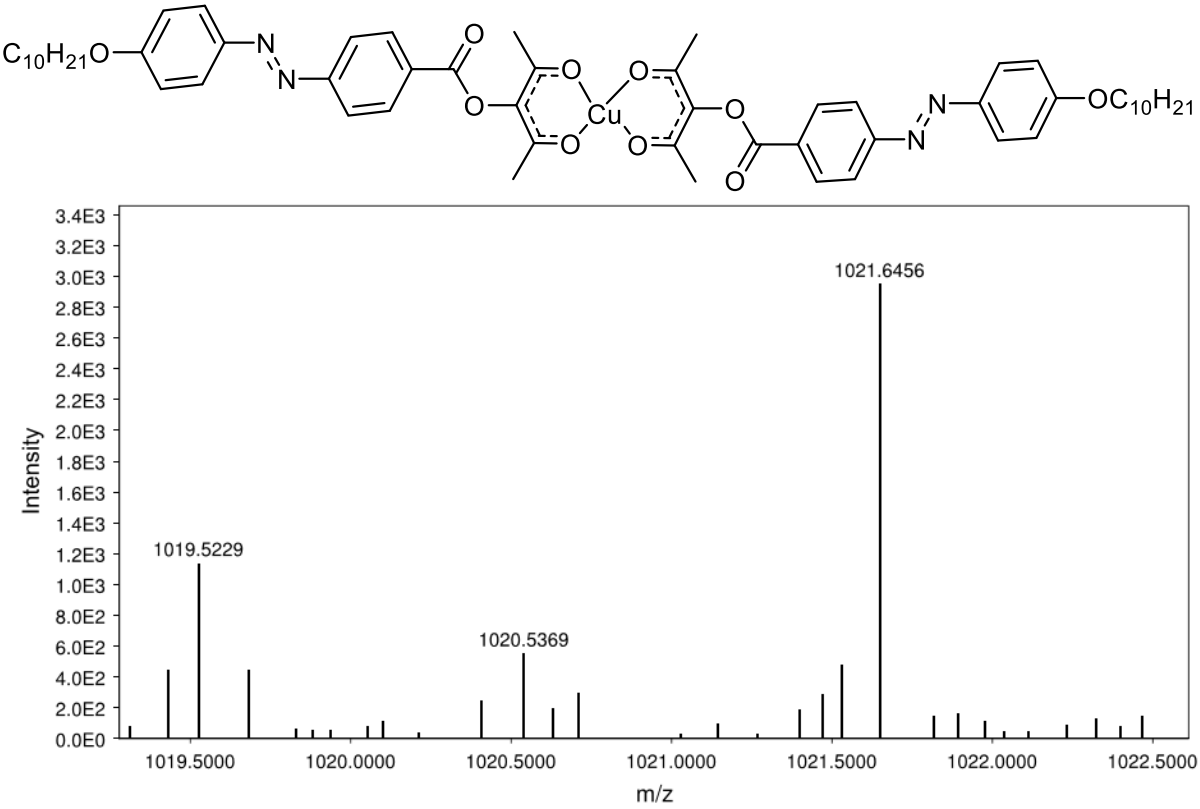

Figure 9: Mass Spectrum of compound **6b**.

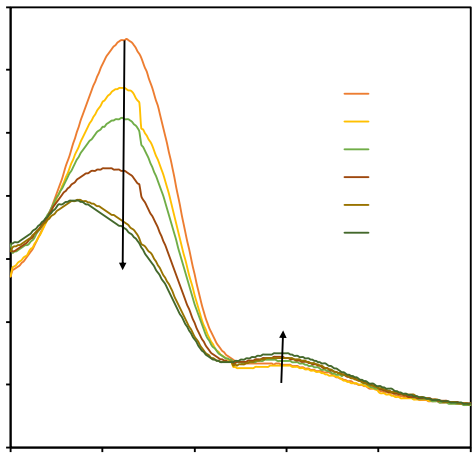

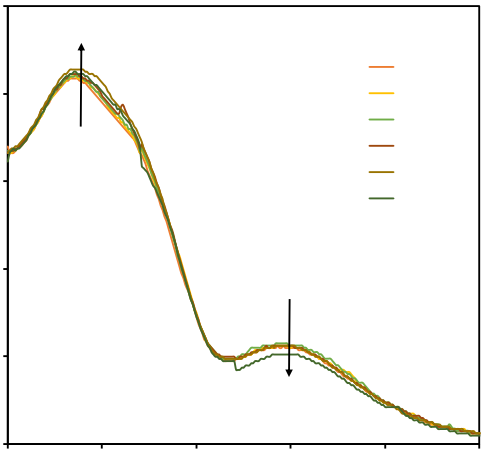

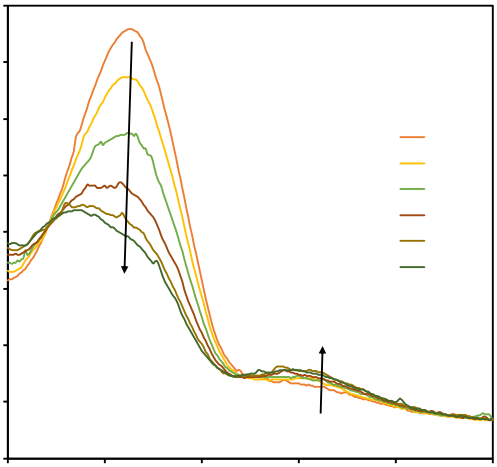

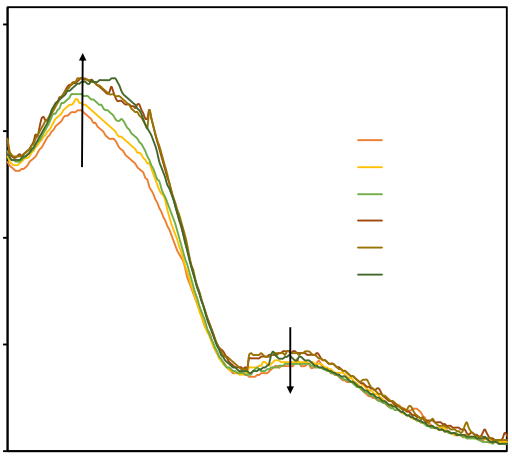

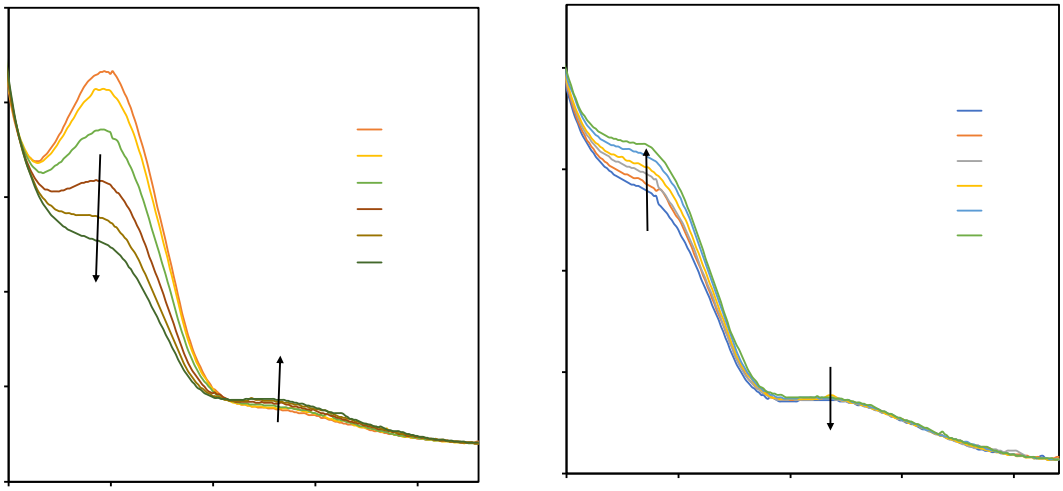

Figure 10: Compound **3a**, **5a** and **6a** (in chloroform) plots of *trans-cis* isomerization, UV-Vis absorbance vs wavelength for *cis* forward and reverse photoisomerization at365 nm (6W).

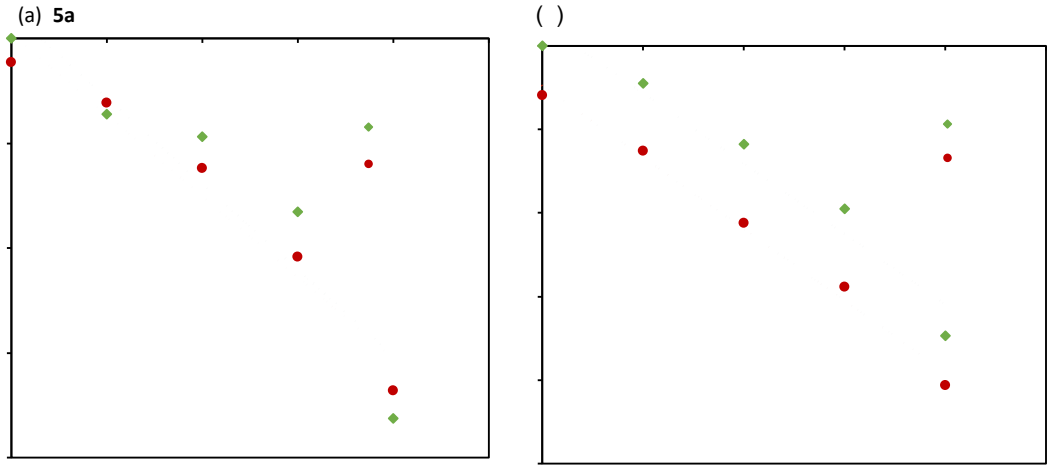

Figure 11: Pseudo kinetic first order plot for half-life determination against time (sec).

Appendix

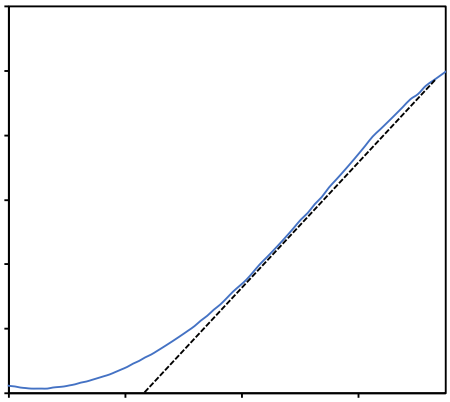

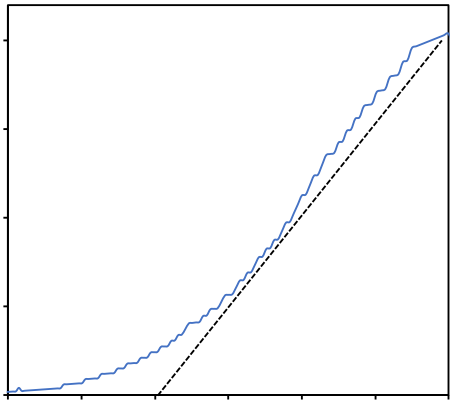

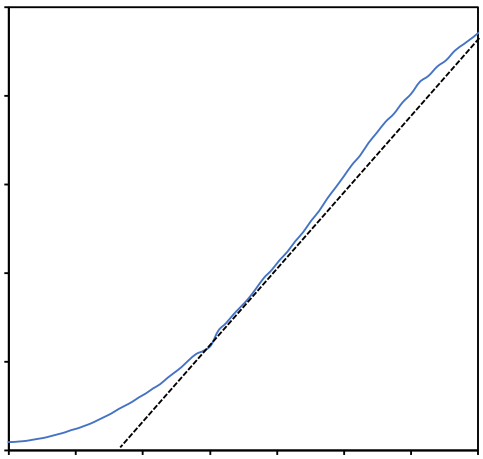

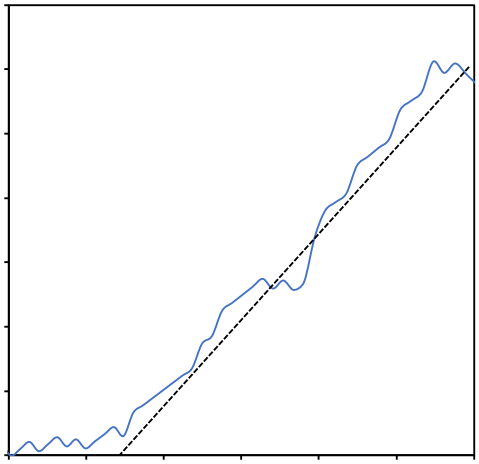

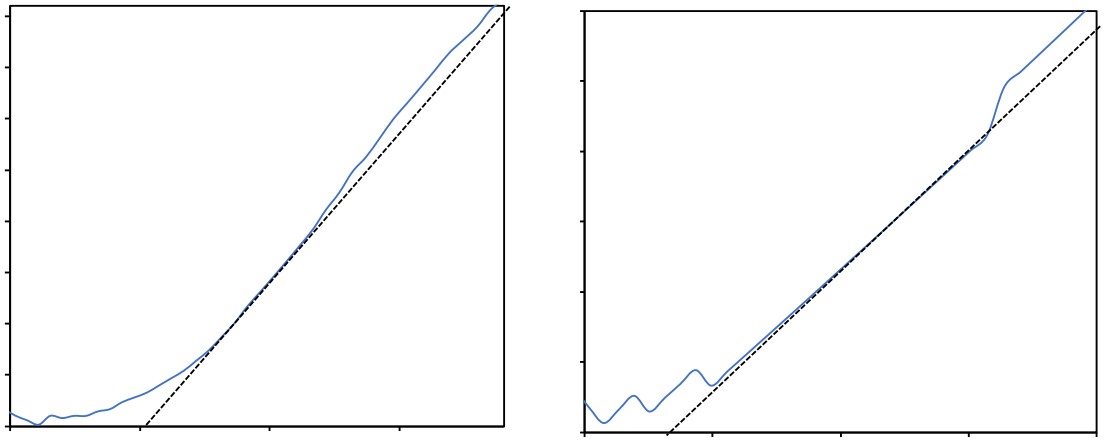

Figure 12: Determination of band gap energy of compound 3a dissolved in $CHCl_3$ by Tauc plots from UV-Vis experiments using compound **3b, 5b & 6b** as an example.